Exploring the role of substantia nigra dopaminergic neurons in the initiation of self paced actions

Joaquim Alves da Silva

Tese para obtenção do grau de Doutor em Medicina

na Especialidade em Saúde Mental

na NOVA Medical School | Faculdade de Ciências Médicas

Setembro, 2017

Exploring the role of substantia nigra dopaminergic neurons in the initiation of self paced actions

Joaquim Alves da Silva

Orientadores: Rui M. Costa, Professor Associado Convidado

Carlos Filipe, Professor Auxiliar com Agregação

Tese para obtenção do grau de Doutor em Medicina

na Especialidade em Saúde Mental

Setembro, 2017

The content of this thesis is partially published in:

Alves da Silva, J, Tecuapetla, F, Paixão, V, Costa, R. M. Dopamine neuron activity before action initiation gates and invigorates future movements. *Nature*, Accepted for publication, 2017

The work developed in this thesis was carried out under the Gulbenkian Program for Advanced Medical Education. It was supported by by an MD PhD fellowship attributed to Joaquim Alves da Silva by the Gulbenkian Foundation and grants from ERA-NET, European Research Council (COG 617142), and HHMI (IEC 55007415) to Rui M. Costa.

The work presented in this thesis was developed in the Neurobiology of Action Lab at the Champalimaud Neuroscience Program, in the Champalimaud Centre for the Unknown

To my parents Joaquim and Eugénia that got me started and to Ana, Maria and Manuel that keep me going.

To my grandfather Henrique, the first person to tell me that I should do a PhD, even before I knew what a PhD was.

To Fatuel Tecuapetla, for the wisdom and friendship, for the questions answered, and most of all, for the questions you taught me to make.

To my Neurobiology of Lab colleagues, thank you for creating such an amazing working environment, for all the discussions and challenging questions

To Rui, 'oh Captain my Captain', for making me better and believe that there are no impossible experiments

"One kid says to me, "See that bird? What kind of bird is that?" I said, "I haven't the slightest idea what kind of a bird it is." He says, "It's a brown-throated thrush. Your father doesn't teach you anything!" But it was the opposite. He had already taught me: "See that bird?" he says. "It's a Spencer's warbler." (I knew he didn't know the real name.) "Well, in Italian, it's a Chutto Lapittid. In Chinese, it's a Chung-long-tah, and in Japanese, it's a Katano Tekeda. You can know the name of that bird in all the languages of the world, but when you're finished, you'll know absolutely nothing whatever about the bird. […]

I learned very early the difference between knowing the name of something and knowing something."

Richard Feynman

RESUMO

Decidir quando nos movemos é essencial para a nossa sobrevivência. A perda de neurónios dopaminérgicos (DANs) na substantia nigra pars compacta (SNc), a alteração patológica característica da doença de Parkinson (PD), causa deficits na iniciação do movimento e lentificação do movimento. A teoria dominante é que o papel dos DANs da SNc no movimento deve-se a mudanças mantidas da atividade destes neurónios (atividade tónica) enquanto as alterações fásicas da atividade estão envolvidas na aprendizagem baseada na recompensa. No entanto, foi demonstrado que a atividade fásica dos DANs da SNc se correlaciona com o início e terminação de uma sequência de ações aprendida. Contudo, continua por esclarecer se esta atividade é ou não necessária para a iniciação 'self-paced' de sequências de ações. A maioria dos estudos anteriores que incidiram sobre movimento ou iniciação de ações utilizaram lesões crónicas ou fármacos para manipular a via nigro-estriada. Estes métodos não são ideais para estudar o papel de populações neuronais específicas devido a limitações tais como a baixa resolução temporal e a baixa especificidade destas manipulações. Devido a isto, o papel dos DANs da SNc na iniciação de movimentos/ações 'self-paced' continua a ser pouco claro.

Para resolver esta questão nós utilizámos uma abordagem optogenética para gravar, visualizar e manipular a atividade de DANs da SNc com uma elevada especificidade neuronal e resolução temporal.

Descobrimos que quando murganhos se movimentavam livremente num 'open field', os DANs da SNc aumentavam a sua atividade de forma transitória, antes do início do movimento. Para testar se este aumento de atividade era ou não necessário para a iniciação do movimento, expressámos uma opsina inibitória (ArchT) nos DANs da SNc dos murganhos. Utilizando esta estratégia foto-inibimos estes neurónios transitoriamente e descobrimos que conseguíamos perturbar a probabilidade e o vigor das iniciações de movimento mas não conseguíamos modificar a aceleração dos

animais quando estes já se encontravam em movimento. Em seguida quisemos saber se uma breve activação destes neurónios era suficiente para promover a iniciação de movimento. Para conseguirmos isto expressámos ChR2 nos DANs da SNc e ativámos transitoriamente estes neurónios enquanto os murganhos se moviam livremente. Ao contrário da experiência de inibição, esta breve ativação promoveu a iniciação do movimento quando os murganhos se encontravam imóveis, e de uma forma semelhante não modificou a aceleração dos murganhos quando estes já se encontravam em movimento.

Quando treinámos os murganhos para realizarem uma sequência de acções (recompensando-os se eles pressionassem uma alavanca 8 vezes) descobrimos que os DANs da SNc aumentavam a sua actividade transitoriamente imediatamente antes do início e o final da sequência. Para além disto, estes neurónios na sua maioria correspondiam a uma população que não respondia à recompensa. Quando inibimos transitoriamente os DANs da SNC imediatamente antes do inicio da sequência os murganhos exibiram um aumento da latência para iniciarem a sequência. Contudo, não conseguimos perturbar a execução da sequência quando fizemos a mesma inibição após a sequência ter sido iniciada.

Os nossos resultados demonstram que a actividade dos DANs da SNc modulam não apenas a probabilidade mas também o vigor dos movimentos futuros mas não modula o movimento durante a sua execução. Isto sugere que o 'gating' de iniciações 'self-paced' acontece através de efeitos permissivos da dopamina nos circuitos estriatais que por sua vez recebem a informação relativa a que ações iniciar de outros 'inputs'.

A depleção de dopamina na PD é crónica. Os estudos sobre o papel da dopamina no movimento utilizando modelos animais de depleção crónica são bastante importantes mas têm uma utilidade limitada para a compreensão do papel dinâmico dos DANs da SNc nos circuitos para os quais projetam. O nosso trabalho, ao demonstrar a relevância da atividade transitória destes neurónios imediatamente antes do início de movimentos 'self-paced', sugere que poderá ser benéfico desenvolver terapêuticas que providenciem modulações transitórias dos circuitos dos gânglios da base quando os doentes com PD querem iniciar uma ação (e.g. estimulação cerebral profunda em 'closed–loop' despoletada por atividade cortical nas áreas relacionadas com o planeamento motor).

ABSTRACT

Deciding if and when to move is critical for survival. Loss of dopamine neurons (DANs) in substantia nigra pars compacta (SNc), the pathological hallmark of Parkinson's disease (PD), causes deficits in movement initiation and slowness of movement. The dominant theory is that the role of SNc DANs in movement is mainly due to sustained changes in their firing (tonic changes) while phasic changes are involved in reward-based learning. Nevertheless, phasic activity of SNc DANs has been found to correlate with the start and finish of a learned action sequence. However, it remains unclear whether this activity is necessary for self-paced action initiation. The majority of previous studies on movement/action initiation have used chronic lesions or drugs to manipulate the nigrostriatal pathway. These methods are not ideal to study the role of specific neuron populations due to constraints such as temporal resolution and/or specificity of the manipulations. Thus, the role of SNc DANs in self-paced movement/action initiation remains unsettled.

To tackle this question we used an optogenetic approach to record, image and manipulate the activity of genetically identified SNc DANs with high specificity and temporal resolution.

We found that when mice were freely moving in an open field SNc DANs transiently increased their activity just before self-paced movements were initiated. To test whether this transient increase in activity was necessary for movement initiation we expressed an inhibitory opsin (ArchT) in SNc DANs of mice. We proceeded to briefly photoinhibit these neurons and found that we could disturb the probability and vigor of movement initiations but we could not change mice's acceleration when they were already moving. Next we wanted to know whether brief activation of SNc DANs was sufficient to promote movement initiation. To achieve this we expressed ChR2 in mice's SNc DANs and briefly activated these neurons while mice were freely moving. Contrary to the inhibition experiment, this brief activation promoted movement initiation when

mice were immobile and in a similar way it did not change significantly mice's acceleration when they were already moving.

When we trained mice to perform a learned action sequence (by rewarding them if they pressed a lever 8 times) we found that SNc DANs increased their activity transiently just before the start and finish of the action sequence. Furthermore, these neurons were largely non-overlapping with reward related DANs. When we briefly inhibited SNc DANs just before the action sequence, mice increased their latency to initiate the sequence. However, inhibition of these neurons when mice had already started the action sequence did not change their performance.

Our results show that the activity of SNc DANs modulates not only the probability but also the vigor of future movements but that it does not modulate movements once they have been initiated. This suggests that the gating of self-paced initiation happens by permissive effects of dopamine on downstream striatal circuits that would receive information about which plans to execute from other inputs.

Dopamine depletion in PD is chronic. Studies of the role of dopamine in movement in chronic models of depletion are very valuable, but have limited our understanding of the dynamic role of SNc DAN activity in downstream circuits. Our work, by highlighting the relevance of transient activity of these neurons before self-paced movement initiation, suggests that it could be beneficial to pursue treatments aimed at providing transient modulations of basal ganglia circuitry when patients initiate movements, e.g. via closed-loop deep brain stimulation triggered by activity in cortical areas related to motor planning.

CONTENTS

Chapter 1 | INTRODUCTION

PRIMUM MOVENS

Deciding if and when to move is one of the most important functions of the brain. Actions can be triggered by particular stimuli, or initiated in a self-paced manner without explicit external triggers. The appropriate initiation of movements in response to changes in internal state (e.g. low energy reserves) is crucial for the adoption of behaviours aimed at homeostasis (e.g. finding a food source and consuming it). Thus, the regulation of self-paced movement initiation is essential for survival. This regulation can be even subtler as for example the decision to explore or not a certain environment and to what extent to explore it. Although several brain structures have been implicated in the generation and regulation of self-paced movements, the loop formed by the cortex, basal ganglia and thalamus seems to be one of the most important brain circuits involved in the selection and initiation of self-paced movements. Within this circuit, the nigrostriatal system has attracted most attention since it was discovered that Parkinson's disease (PD) was caused by the loss of neurons that project from the substantia nigra compacta to the dorso-lateral striatum.

The work presented in this thesis focuses on understanding the role of substantia nigra DANs in self-paced movement initiation. To provide an adequate introduction to a thesis involving DANs is almost as daunting as trying to tackle this question.

We will start with a brief overview of basal ganglia organization, followed by the account of the discovery that positioned the nigrostriatal system as one of the most important systems in the regulation of self-paced movement. Next we will follow with a description of the evolution of research regarding the role of midbrain DANs in the functioning of basal ganglia, highlighting the current views and controversies on the role of these neurons in self-paced movement, and we will finish by trying to convince you that this is a thesis worth reading.

THE NIGROSTRIATAL SYSTEM

Brief description of basal ganglia organization

The basal ganglia (BG) are a group of subcortical nuclei which are part of the forebrain circuitry involved in action selection (Gerfen & Surmeier 2011). The cortex, the thalamus and the basal ganglia form a loop. Cortex (more specifically layer V) and thalamus send glutamatergic projections to the striatum which is the largest nuclei in the BG. In primates it is possible to differentiate two distinct structures within the striatum: The caudate and the putamen. However in rodents these structures are not easily distinguished. Ninety-five percent of striatal neurons are medium sized GABAergic neurons, termed medium spiny neurons (MSNs) due to their large and spine rich dendritic tree. The other 5% are composed of four classes of interneurons (cholinergic and parvalbumin, calretinin and NPY GABAergic interneurons). MSNs are anatomically organized in two pathways: A direct pathway, composed of neurons that project directly to output nuclei of the basal ganglia (substantia nigra pars reticulata and internal globus pallidus) and an indirect pathway that projects to the external globus pallidus, a nucleus in-between the striatum and the output nuclei of the basal ganglia. Finally the output nuclei project to the thalamus which projects back to the cortex and striatum completing the loop. The output nuclei also project to the superior colliculus and brainstem nuclei (e.g. pedunculopontine nucleus).

One interesting property of the BG is the dense and widespread innervation of the striatum by dopaminergic terminals (Matsuda et al. 2009). The history of the discovery of the dopaminergic neurons that project to the striatum goes hand in hand with the history of PD and its treatment and it is a good starting point to discuss the role of dopamine in movement initiation.

The discovery of dopamine and its relation to movement

DANs are present in different regions of the brain. From the mesencephalon to the olfactory bulb, DANs can be found in 9 distinctive cell groups (A 8-16) (Björklund & Dunnett 2007). Substantia nigra compacta neurons (A9 cell group) became the focus of researchers' attention when it was described that the loss of these neurons was the pathological hallmark of PD (Foix & Nicolesco 1925; Hassler 1938). However, this happened decades before it was realized that dopamine was a neurotransmitter on its own and not just an intermediate product of the noradrenaline pathway (Carlsson et al.

1958). In part this was shown by using reserpine to deplete dopamine brain levels and restoring them again using L-DOPA (a precursor of dopamine and noradrenaline). This depletion of dopamine led to a PD like phenotype which was alleviated by L-DOPA infusion. Following this finding, it was shown that PD patients had a severe loss of dopamine in the caudate and putamen (Ehringer & Hornykiewicz 1960). This discovery was quickly followed by a therapeutic breakthrough: the use of L-DOPA to treat the symptoms of PD (Birkmayer & Hornykiewicz 1961). The following quote exemplifies the excitement of the first report:

> *'Bed-ridden patients who were unable to sit up, patients who could not stand up when seated, and patients who when standing could not start walking performed all these activities with ease after L-DOPA [levodopa]. They walked around with normal associated movements and they could even run and jump. The voiceless, aphonic speech, blurred by pallilalia and unclear articulation, became forceful and clear as in a normal person.'* (Birkmayer & Hornykiewicz 1961)

In fact, to this day, L-DOPA therapy is the cornerstone of PD treatment (Muzerengi & Clarke 2015). Interestingly it still took two years from the first successful use of L-DOPA to the discovery that SNc neurons were in fact dopaminergic neurons (Hornykiewicz 1963). From this point on it became evident that it was mainly the mesostriatal projection that was progressively lost in PD and not the striato-nigral projections (Hornykiewicz 2006). The specificity of the loss of midbrain DANs captured also the attention of researchers who realized that the ventral lateral SNc neurons were more susceptible to being lost in PD while the more medial VTA neurons were more spared (Hassler 1938; German et al. 1989). This pattern also suggested that midbrain DAN loss in PD was higher for neurons that project to the striatum (mesostriatal projection) than for neurons projecting to cortical or limbic structures (German et al. 1989). Given the striking movement related symptoms of PD, an association between the mesostriatal projection and movement emerged. Why does dopamine loss in the striatum produce such debilitating symptoms? Or from another perspective, what is the role of dopamine in the functioning of the basal ganglia?

Dopamine function in the basal ganglia

An important breakthrough came from the discovery that the direct and indirect pathway could be segregated not only based on their anatomical properties but also on

their dopamine receptor expression profile. Direct pathway neurons express D1 receptors and indirect pathway express D2 receptors (Gerfen et al. 1990; Gong et al. 2003). Both D1 and D2 are G-protein coupled receptors. However, while D1 receptors are coupled to G_s and G_{olf} proteins, D2 receptors are coupled to G_o and G_i proteins.

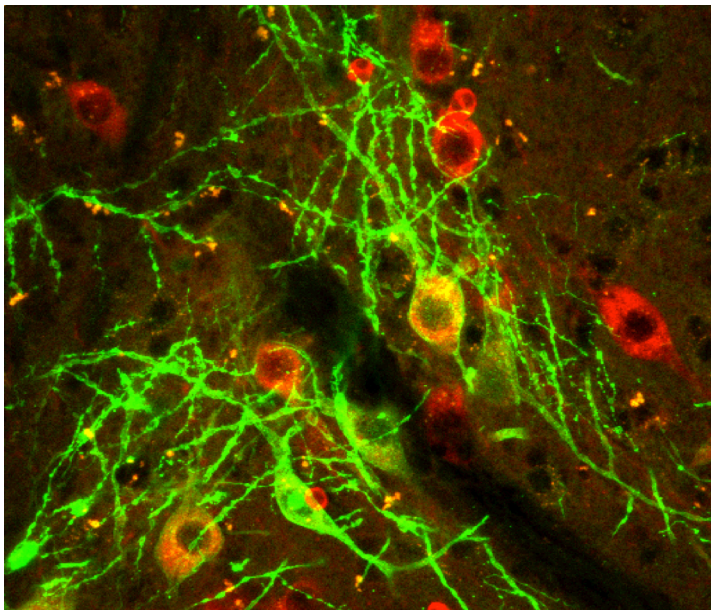

Figure 1.1 | Example of substantia nigra DANs (red). Some of the DANs are expressing ChR2 (green).

This difference dictates a signaling cascade that has opposite effects. In a simplistic way dopamine through D2 receptors leads to a decreased responsiveness of striatopallidal neurons postsynaptically and a decreased release of glutamate through its presynaptical effects. On the other hand, D1 receptors seem to depress weak, asynchronous stimuli but increase the sensitivity to strong coordinated glutamatergic input (Surmeier et al. 2007). These findings and earlier observations led to the consolidation of the classical model of striatal dopamine modulation (Albin et al. 1989). This model states that dopamine release in the striatum facilitates the activation of direct pathway neurons and concomitantly decreases the activation of indirect pathway neurons. This leads to a decrease in the activity of the output nuclei of the basal ganglia with disinhibition of thalamo-cortical projections, resulting in the facilitation of movement. Conversely, decreased release of dopamine would shift the balance of activation towards the indirect pathway neurons, thus increasing the activity of the output nuclei resulting in the inhibition of movement. However, this model was based mostly on indirect, *in vitro* or *in vivo* anesthetized animal data (Surmeier et al. 2007). Although *in vitro* experiments allow for greater experimental control and more specific manipulations, it needs to be kept in mind that the system is in a very artificial state,

and thus the measurements and principles found may not generalize to the *in vivo* state. One such example is the up and down states of MSNs found in *in vitro* experiments. In the absence of convergent glutamatergic input, the MSNs membrane potential is ~-85 mV mainly due to a rectifying inward potassium current. On the other hand, in the presence of convergent glutamatergic input, MSNs can enter an up-state with a membrane potential at ~-55mV, closer to the spiking threshold. It was thought that these up-states were facilitated by the action of dopamine on D1 receptors (Surmeier et al. 2007). However, when intracellular recordings of MSN were performed *in vivo*, it was found that clear bistable up and down-states were only apparent during slow wave sleep while a much more irregular membrane potential pattern was observed during wakefulness (Mahon et al. 2006). The recent findings supporting a co-activation of D1 and D2 MSNs when actions are initiated (Cui et al. 2013; Jin et al. 2014) are also examples of *in vivo* data contradictory to the classical model.

When it became possible to do external recordings of single neurons in behaving animals, researchers tried to identify DANs and record their activity as movement happened. However, to do this, some form of identification was necessary to distinguish SNc DANs from other neurons in the substantia nigra (e.g. GABAergic neurons). Based on experiments in anesthetized or paralyzed rats using selective lesions of dopaminergic neurons (using 6-OHDOPA) or dopaminergic pharmacologic manipulations (e.g. apomorphine and haloperidol) and histological verification, a set of criteria were found to distinguish putative DANs from other neurons present in SNc (Benjamin S Bunney et al. 1973; Guyenet & Aghajanian 1978; Ungless & Grace 2012):

- Slow firing rate (2-10Hz)
- Large (>2.2 ms overall) biphasic action potential (if not high pass filtered)
- Inhibition by low dose dopamine or apomorphine (dopamine receptor agonist)
- Antidromic activation from the striatum with slow conduction velocity (0.5 m/s)

After confirming that these criteria also identified DANs in behaving animals (Steinfels et al. 1981), researchers used them to record putative DANs and correlate their activity with movements (Trulson et al. 1981; Schultz et al. 1983; Trulson 1985). The first reports did not reveal a clear relation between DAN activity and movement kinematics (Steinfels et al. 1981; Trulson et al. 1981; Schultz et al. 1983). In cats putative DAN activity was slightly increased (≈20%) when quiet awakening was compared with movement periods (Trulson et al. 1981; Trulson 1985). Nevertheless, dopamine concentration in the striatum in the same animals increased 50% during

periods of movement (Trulson 1985). In spite of this, the authors stated that they saw 'no relationship to phasic movement' although it is not clear what they meant by phasic movement or how they were measuring it. In a primate study Schultz et al (Schultz et al. 1983) found that the majority of DANs recorded were modulated by the onset of a reaching movement (determined by EMG), independently of it being trained or untrained. However they reported that the modulation preceded movement onset for only a minority of these neurons. They did not find modulations for more subtle movements. It is important to note that although these recordings were done in behaving primates, the animals were restrained to a chair when they were performing the arm reaching task.

Given the dramatic motor phenotype observed when DANs are lost, these first results were puzzling. The lack of clear correlation between the activity of DANs and movement kinematics while still having a moderate modulation of these neurons during active periods, led researchers to the hypothesis that DANs worked more like a level setting mechanism necessary for the motor acts while not encoding any characteristics of the motor act *per se* (Schultz et al. 1983).

DOPAMINE, REINFORCEMENT LEARNING AND MOTIVATION

DAN researched was led in a completely different direction by a seminal finding by Wolfram Schultz who discovered that midbrain DANs are phasically[1] activated by rewarding stimuli or reward predicting stimuli (Schultz 1986). Moreover, this activation is dependent on the unpredictability of the stimuli. For example, initially DANs are activated by a food reward that is preceded by a stimulus that fully predicts it. However, with training and consolidation of this conditioning, DANs are no longer activated by the reward and start responding to the stimulus that predicts it (Schultz et al. 1997) according to the following equation (Schultz 1998):

DA neuron activation = appetitive stimulus occurred - appetitive stimulus predicted

[1] Midbrain DANs are known to have two modes of firing: Tonic firing which is sustained, slow and irregular single or double spikes firing; and burst firing which is a transient rapid succession of spikes of progressively decreasing amplitude and increasing duration (Benjamin S Bunney et al. 1973; Grace & Bunney 1983).

This equation also matches what is observed when a reward is predicted and does not happen: a negative dopamine activation (i.e. a decrease in DAN activity).

In this way, DANs are reporting an error or deviation between the animal prediction and the actual outcome (Schultz 1997) and not just the occurrence of appetitive events (**Fig. 1.2a**). This became specially significant when a parallel was established between this property and the learning from discrepancy described by the Rescorla-Wagner model (Rescorla & Wagner 1972) and the temporal difference algorithm (Sutton & Barto 1981), a method by which artificial systems can learn to predict. DANs were now seen as a neural substrate for prediction and reward (Schultz 1997). With this finding, DANs research moved from the domain of movement to the domain of reinforcement learning.

The error prediction hypothesis quickly captured the attention of neuroscientists. It is an elegant theory, built on solid data, which provided a bridge between neuroscience and computer science.

However, several observations demonstrated that phasic activation of DANs is diverse and not fully explained by the error prediction paradigm. For example, DANs have been shown to be phasically activated by both appetitive and aversive events, responding in a way that reflects the salience but not the value of the events (Matsumoto & Hikosaka 2009). Furthermore, value or salience coding DANs also respond to alerting events (Bromberg-Martin et al. 2010; Schultz 2010; Nomoto et al. 2010)[2]. These responses depend on salience, surprise, novelty, arousal and attention and they are attenuated if the alerting stimuli are repeated in a predictable way (Bromberg-Martin et al. 2010). More recently, it was shown that when a conditioned stimulus (CS) signals a reward only if a rat stays immobile for a certain amount of time, the transient increase of dopamine only happens when the rat initiates the movement to collect the reward and not when the CS appears (Syed et al. 2015).

These data highlight that the function of phasic DAN activity cannot just be the reinforcement of previous actions, otherwise DANs that encode salience would be reinforcing actions that lead to both reward and punishment. An alternative could be

[2] Here we use the term alerting similarly to the definition used by Bromberg-Martin and Hikosaka (Bromberg-Martin et al. 2010): An unexpected sensory cue that captures the attention of the animal and often leads to behavioral reactions.

that phasic dopamine activity is also important for preparing or motivating actions which is consistent with its association with rewarding, aversive or alerting stimuli.

DANs, MOTIVATION, MOVEMENT INITIATION AND VIGOR

What do we mean by motivation? Motivation and movement share the same etymology: Motivation derives from the latin word *moti,* the past participle of movere (*to move*). Motivation can be defined as the process by which animals become energized to initiate goal-directed behaviors (Palmiter 2008). Thus there is a close relation between movement initiation and motivation.

There is extensive evidence suggesting a role of DANs in the modulation of motivation in both rodents and humans. For example, although transgenic mice with dopamine depletion can move sufficiently to find and consume food, they do not eat enough to survive (Palmiter 2008). This happens in spite of intact perception of the metabolic/hormonal changes associated with food deprivation and is restored by rescuing dopamine production in the neurons that project to the dorsal striatum. This has been interpreted as dopamine being necessary for mice to engage in goal-directed behaviors. Accordingly, inhibition of D2 receptors (Salamone et al. 1991) decreases the effort mice are willing to spend working for a food reward, while blocking dopamine re-uptake as the opposite effect (Yohn et al. 2016). Patients with PD have a tendency to select less vigorous reaching movements in spite of being able to perform those movements faster without increased accuracy/speed trade-off. Based on this, it has been argued that 'motor motivation' is the fundamental role of the dopaminergic projection to the striatum (Mazzoni et al. 2007).

While researchers have used motivation and overlapping concepts to highlight dopamine's energizing function of goal-directed behaviors, the way this 'energization' is measured has differed from study to study. Movement initiation can be broken into subcomponents that can be modulated by motivation. One approach to this dissection of motivation processes has been the distinction between 'response vigor' (rate of movement/action initiations) and 'movement vigor' (energy expenditure of the movement/action initiated, Panigrahi et al. 2015). Bradykinesia of PD patients seems to be a combination of deficits both in movement initiation and a tendency to select less vigorous movements (Berardelli et al. 2001; Mazzoni et al. 2007), with similar

observations in animal models where the nigrostriatal pathway is perturbed (Zweifel et al. 2009; Panigrahi et al. 2015).

It is very challenging to discriminate what is a motor effect mediated by a change in motivation and what is purely a change in motor execution. In the case of the experiments involving the dopamine system, experimenters have argued that different dosages of drugs that modulate dopamine activity can achieve this dissociation (Wise 2004). However, the lack of specificity of such drugs, especially the lack of temporal

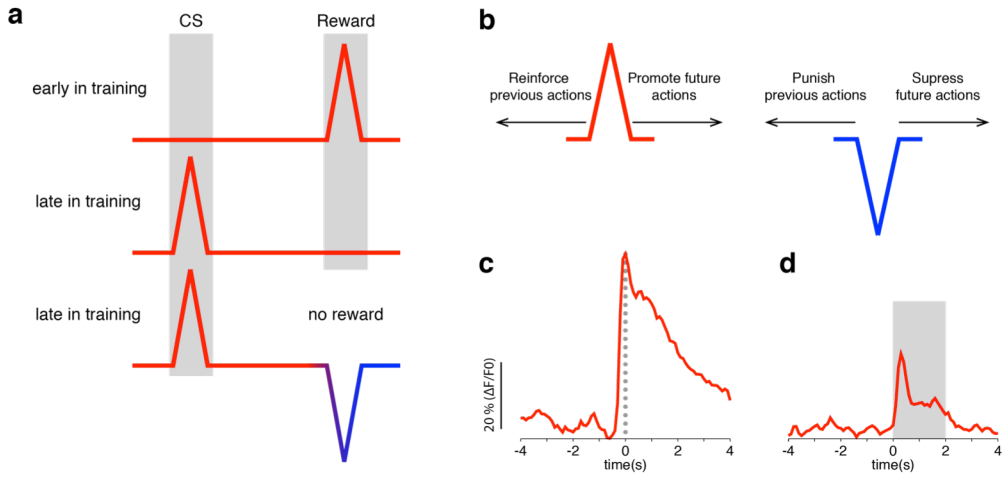

Figure 1.2 I Error prediction hypothesis

a, Error prediction in DANs. In the beginning of conditioning DANs are activated by the delivery of reward. After several sessions pairing the conditioned stimulus (CS) with reward delivery, DANs are phasically activated by the CS but not by reward delivery. At this point in training, if the reward is withheld after the presentation of the CS, there is a decrease in the activity of DANs at the predicted time of reward delivery. **b**, Conventional theory for DANs error prediction. Phasic increases of dopamine lead to the reinforcement of previous actions that led to the unexpected reward or reward predicting stimuli and can modulate neural activity to promote immediate reward seeking actions. Sudden decrease of DANs activity would have the opposite effects; decreasing the probability of repeating previous actions and suppressing immediate actions (adapted from Bromberg-Martin et al. 2010). **c** and **d**, However DANs are not only phasically activated according to the error prediction theory. The activity of a genetically identified neuron is phasically increased after reward delivery (c) but it is also phasically increased after the presentation of a salient stimulus (light flash) that did not predict a reward (d). Despite the latter having a smaller magnitude than the former, this type of phasic activation is not directly explained by the conventional theory of error prediction (average neuron response obtain by calcium imaging of SNc DANs in freely moving mouse).

specificity weakens this argumentation. For example, drug effects are present before a movement is selected, when in fact motivation plays a role in the decision of how much effort to put into the movement, but also during the execution of the movement itself.

Even a subtle difficulty in executing movements could change the motivation of mice to initiate movement. The same applies for experiments that have used lesions or genetic manipulations to change dopamine neurotransmission. These experimental challenges have contributed to the role of DANs still being considered 'mysterious' (Salamone & Correa 2012).

Part of this 'mystery' is also driven by the challenge of understanding the function of neurons that seem to be important for distinct processes such as reward learning, motivation and self-paced movement (even though the last two are tightly linked). The widely accepted view is that the role of DANs in motivation and movement is supported by their tonic or sustained activity, while their role in reward prediction is mostly attributed to phasic changes in activity (Niv et al. 2005; Schultz 2007). However this view has been challenged recently (Jin & Costa 2010; Wang & Tsien 2011; Barter et al. 2015; Dodson et al. 2016; Howe & Dombeck 2016). In fact most of this work was published during the development of this thesis.

WHY YOU SHOULD KEEP READING THIS THESIS

One thing is conspicuous from the introduction above: In spite of the striking motor phenotype seen in PD patients, our understanding of how SNc DANs modulate movement remains limited. Our goal with this study was to understand the role of substantia nigra DANs in self-paced movement initiation.

To achieve this we used high-resolution motion sensors to characterize in detail spontaneous mouse movement. Concomitantly we employed optogenetically-aided recordings to monitor the activity of DANs, with no food deprivation, reinforcement, or salient cue delivery. Furthermore, we used temporal and state-specific optogenetic manipulations to examine the role of dopamine activity in gating the initiation of spontaneous self-paced movements. Also, we imaged and manipulated the activity of SNc DANs while mice performed a learned action sequence.

The combination of detailed characterization of movement and action execution with high temporal resolution neuronal manipulations allowed us to dissect the behaviour into three components: The probability of initiating a movement, the latency to initiate a movement and the vigor of the movement once initiated. Through our neuron-specific and high temporal resolution manipulations we were able to interrogate the role of DANs in each of them.

Chapter 2 | TRANSIENT INCREASE IN SNc DAN ACTIVITY PRECEDES THE INITIATION OF MOVEMENTS

SUMMARY

The ability to initiate self-paced movements is necessary for the exploration of our environment, to navigate to relevant locations, the execution of learned actions and even the acquisition of new actions. It is vital to our survival. In this chapter we used high-resolution motion sensors to characterize mouse spontaneous movement initiations. At the same time we employed optogenetically-aided recordings to monitor the activity of DANs while mice freely explored an open field, with no food deprivation, reinforcement, or salient cue delivery. Our main aim in this chapter was to evaluate whether there were significant changes in the activity of SNc DANs in relation to movement initiation. Indeed we found that the activity of most SNc DANs is modulated by movement initiation. However, some neurons were positively and others negatively modulated. Moreover, positively modulated neurons were heterogeneous with different profiles that clustered into three different groups. While all positively modulated neurons were changing significantly before movement initiation, most negatively modulated neurons were changing significantly at movement initiation or after. Interestingly, some but not all of positively modulated neurons were vigor related (i.e. their activity was predictive of the vigor of future movement initiations). This result suggests that quick variations (subsecond) and not only slow tonic changes of DAN activity might be relevant for movement initiation.

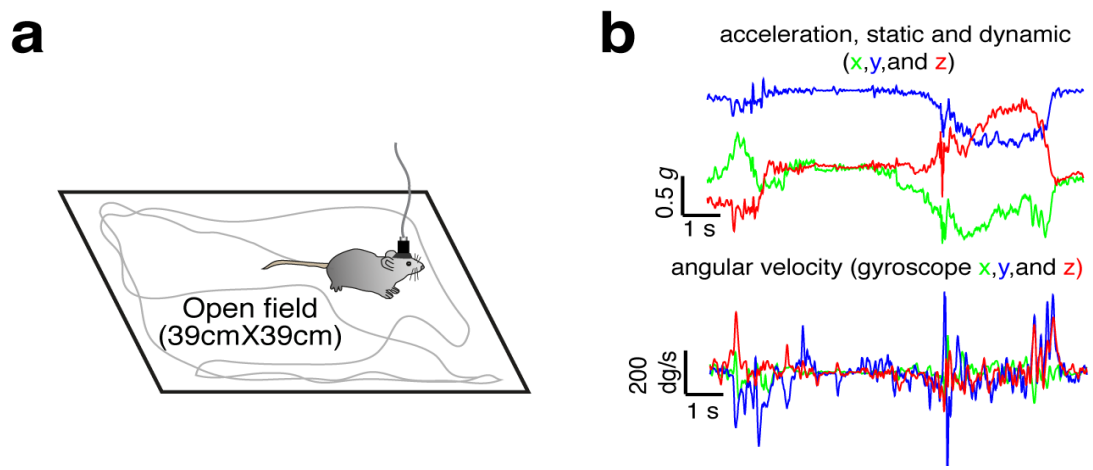

Figure 1.3 I Characterization of mice spontaneous movement initiation

a, Behavioural set-up. **b**, Example of raw acceleration (gravitational and dynamic acceleration) and angular velocity collected using 6-axis inertial sensor.

RESULTS

High-resolution motion sensors discriminate movement states

We used head-mounted motion sensors to measure acceleration and angular velocity of spontaneous movement in mice freely moving in an open field (**Fig. 2.1a,b**). This allowed us to obtain high-resolution (200-1000 Hz sampling rate) tri-dimensional measures of motion. The raw acceleration signal recorded using such sensors is a combination of a static component (determined by earth's gravitational pull) and a dynamic component (determined by the animal movement). Using a standard approach (Mathie et al. 2002) we filtered the raw acceleration signal using a low pass filter to separate these two components. One may think that recording mouse acceleration might be an inaccurate measure of motion because it would not detect movements that occur at constant velocity. However, unlike cars or other mechanical vehicles moving at a constant speed, animals rely on constant accelerations from their limbs to locomote, changing also their centre of mass in relation to the environment (Gleiss et al. 2011). Supporting this we found that the magnitude of the sum of the dynamic component of the three axis of acceleration (total dynamic acceleration or total body acceleration) was correlated with a simultaneous video based measure of motion (**Fig. 2.2a**, $r=0.74$, $p<0.05$). Furthermore, we found that the distribution of mices' total dynamic acceleration in the open field session was bimodal (**Fig. 2.2b**). We used the minimum value of acceleration between the two peaks of the bimodal distribution as a threshold to separate the distributions (**Fig. 2.2b**), and verified that values from

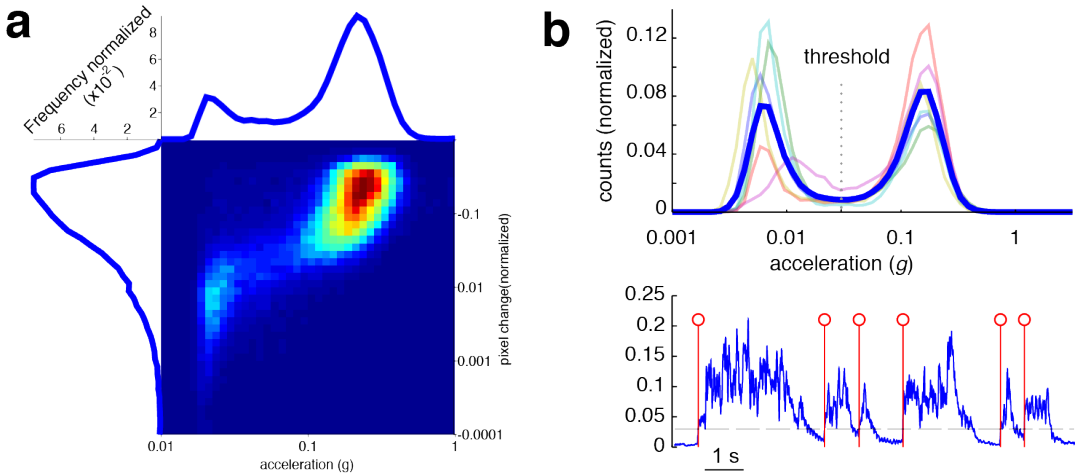

Figure 1.4 I Total body acceleration has a bimodal distribution

a, Bivariate histogram of log pixel change and log acceleration in the open field (n=13 sessions, from 3 mice). Notice the two clusters that emerge from this bivariate histogram (low acceleration/low pixel change cluster on the left and high acceleration/high pixel change cluster on the right). The acceleration histogram provides clear distinction between these two clusters. There is a high correlation between this video tracking measure and acceleration (r=0.74, n=62984 frames, p<0.05). **b**, Top; distribution of total dynamic acceleration in the open field. Blue thick line represents the mean distribution of all mice and the faded color lines represent the distribution for each mouse (obtained from a mean of 3 ± 2.2 one hour open field sessions per mouse). Bottom; the red lines represent examples of movement initiation trials determined using the threshold represented in the top panel overlaid on the total dynamic acceleration trace.

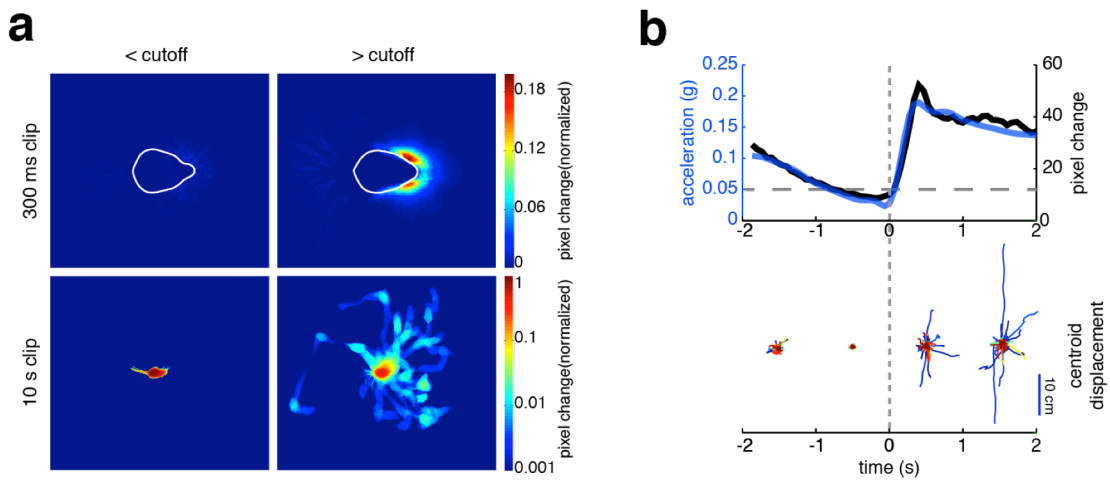

Figure 1.3 I Characterization of mouse spontaneous movement initiation using video and acceleration

a, Heat maps of mean pixel change of video clips with 300 ms and 10 s (top and bottom panels respectively) during which mice had acceleration lower (left panels) or higher than the threshold used to define immobility (right panels). **b**, Top; comparison between a video derived motion measure (pixel change) and total dynamic acceleration aligned to movement initiation determined using the acceleration threshold (n=454 initiations obtained from 3 mice during a total of 13 open field sessions, Pearson r=0.95, *P*< 0.0001). Bottom; representation of the movement of mice (based on center of mass) during each trial within the time intervals denoted on the x axis. The trajectories were aligned to the center of mass of the last frame of each 1 s interval. Different colors denote individual trials.

the low acceleration distribution corresponded to periods of immobility (with the possible exception of small and slow postural adjustments), while values from the high acceleration distribution corresponded to periods of overt mobility (**Fig. 2.3**). This allowed us to separate periods of immobility from periods of mobility, and to identify episodes of spontaneous movement initiation with great accuracy – crossings of the threshold preceded by at least 300 ms below the threshold (immobility) and followed by at least 300 ms above the threshold (mobility). To characterize these spontaneous movement initiations in more detail we used a combination of three variables obtained from the motion sensors: total body acceleration; the angular velocity of the axis most parallel to the dorsal-ventral axis of the mice and the gravitational acceleration of the same axis. While the total body acceleration provided us with a measure of movement initiation vigor, the angular velocity characterized the direction of the movement and the gravitational acceleration was sensitive to postural changes like rearing. We used the combination of these three variables to describe trajectories in the motion sensor space for each movement initiation (**Fig. 2.4**).

Transient activity of DAN's precedes movement initiation

Since motion sensors allowed us to accurately identify the transition between movement states (immobility to mobility) and to characterize their trajectories (including vigor and direction of movement), we could now investigate the activity of SNc DANs in relation to movement initiation. For this we used 16 channel movable electrode bundles coupled to a fiber optic cannula placed just above the SNc (**Fig. 2.5**). We implanted these bundles in six TH-Cre mice (Gong et al. 2007, line FI12) crossed with Ai32 mice (Madisen et al. 2012) to obtain expression of Channelrhodpsin2 (ChR2) in TH-positive neurons (**see methods for details**), and used the strategy of photoidentification (Lima et al. 2009) to identify which single units were dopaminergic (**Fig. 2.6**). We recorded 45 single units that were significantly activated by 10 ms pulses of blue light at 1 Hz. However, after analysing the average latency to activation and the relative increase in spike probability during light pulses, we only considered neurons with a latency ≤ 7 ms and an increase of 30% or more in spiking probability as photoidentified DANs (n=25 neurons, **Fig. 2.6, Fig. 2.7a, see methods for details**).

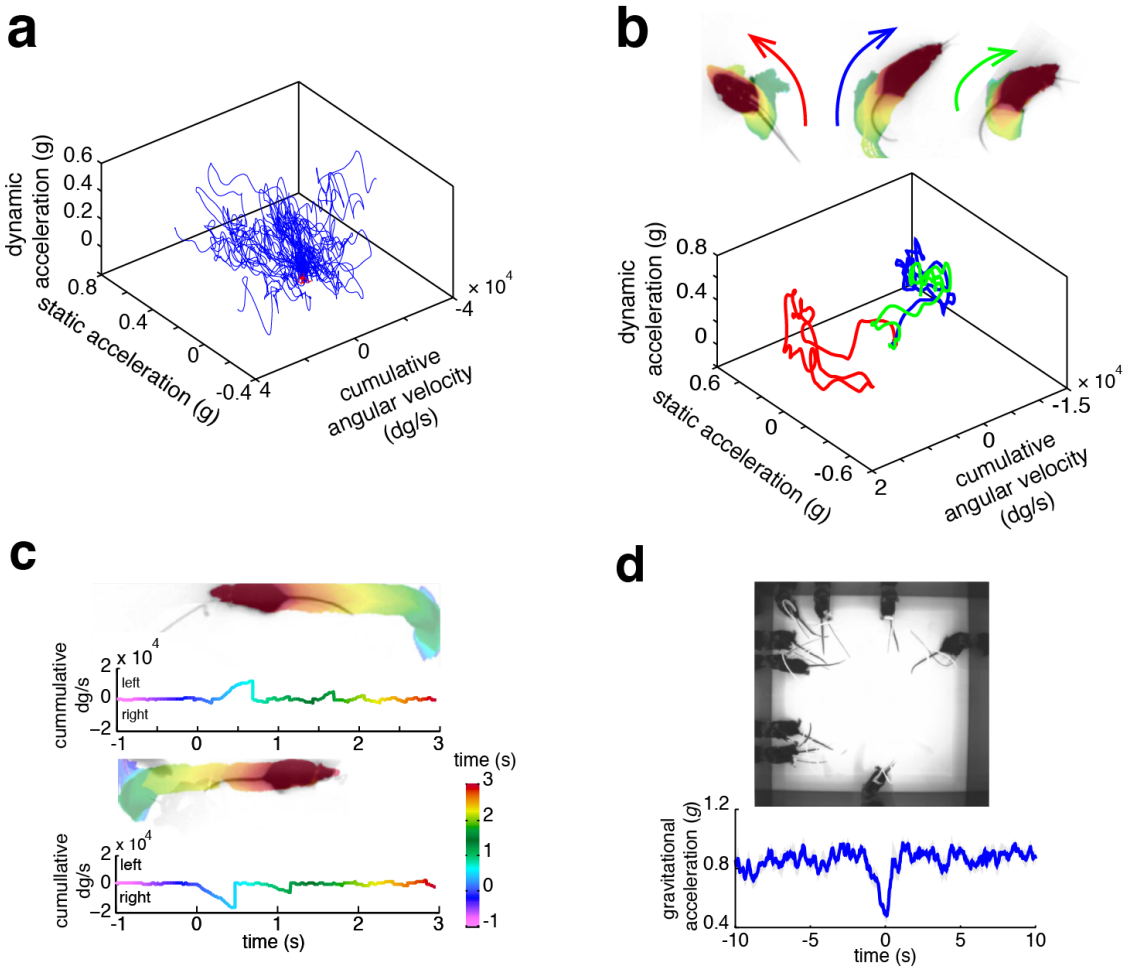

Figure 1.5 | Motion sensor variables and definition of movement initiation trajectories.

a, Example of 20 randomly selected trials of one session represented in a motion sensor 3d space determined by total dynamic acceleration, static acceleration and cumulative angular velocity of the sensor axis most parallel to mices' dorsal-ventral axis. The red portion of each trajectory represents the 300 ms of immobility before the initiation of movement and the blue portion represents the 1.5 s from movement initiation onward. **b**, Video frames time series of three examples of movement initiations (frames corresponding to the first 1.5 s after movement initiation) and their representation in the same motion sensor space shown in e. **c**, Example of the discrimination of the direction of movement by the angular velocity of the axis chosen to characterize initiations. The data is shown as angular velocity calculated cumulatively for consecutive bins with the same signal of the angular velocity. **d**, Detail of the axis of gravitational acceleration used to characterize initiations. The image shows 10 rearings overlapped and the plot below is the average gravitational acceleration aligned to the frames shown above (peak of the rearing).

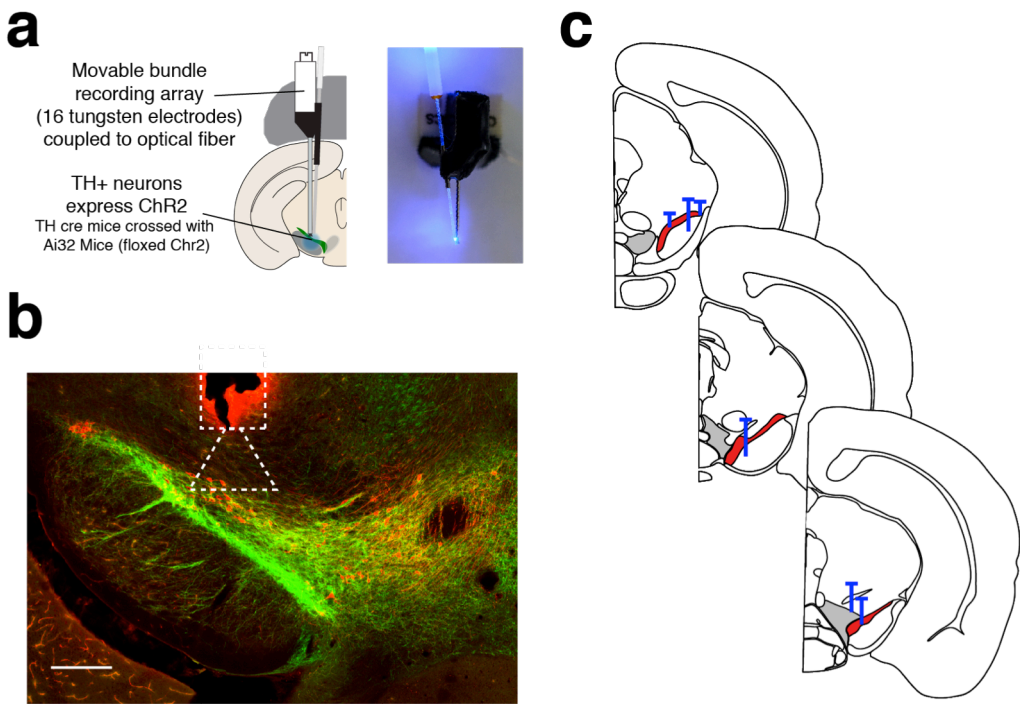

Figure 1.6 | Method used for external recordings of photoSNc DANs.

a, Schematics of the method used to record and photoidentify SNc DANs. Right; sixteen channel movable bundle electrode and fiber optic cannula passing the blue light used in photoidentification experiments. **b**, Photomicrograph of a midbrain slice of a TH Cre;Ai32 mouse denoting the right SNc and VTA. ChR2 in green and TH+ cells in red. Initial electrode position (dashed square) and distance travelled (dashed triangle). **c**, Optrode placement. Horizontal blue line denotes the cannula position and vertical line the distance travelled by the electrodes. Shaded gray area denotes VTA and red area denotes SNc.

We built peri-event time histograms (PETH) of these neurons activity aligned to spontaneous movement initiations (93.45 ± 35.99 mean spontaneous initiations per neuron recording), to examine whether these neurons were modulated or not by movement initiation. Movement initiation events were defined as described above (least 300 ms of immobility followed by at least 300 ms of mobility).

We found that the average activity of all the DANs recorded increased transiently before movement initiation (**Fig. 2.7b**). Consistently, we found that 80% of photoidentified DANs were significantly modulated by movement initiation and that the majority of these (65%) were positively modulated (**Fig 2.7c**). However we noticed that the PETHs of positively modulated neurons were heterogeneous. To better characterize the response of these neurons we compared the firing rate during 50 ms bins with the firing rate at baseline (-1.5 to -1 s in relation to movement onset) using a receiver operating characteristic (ROC) analysis. The area under the ROC curve

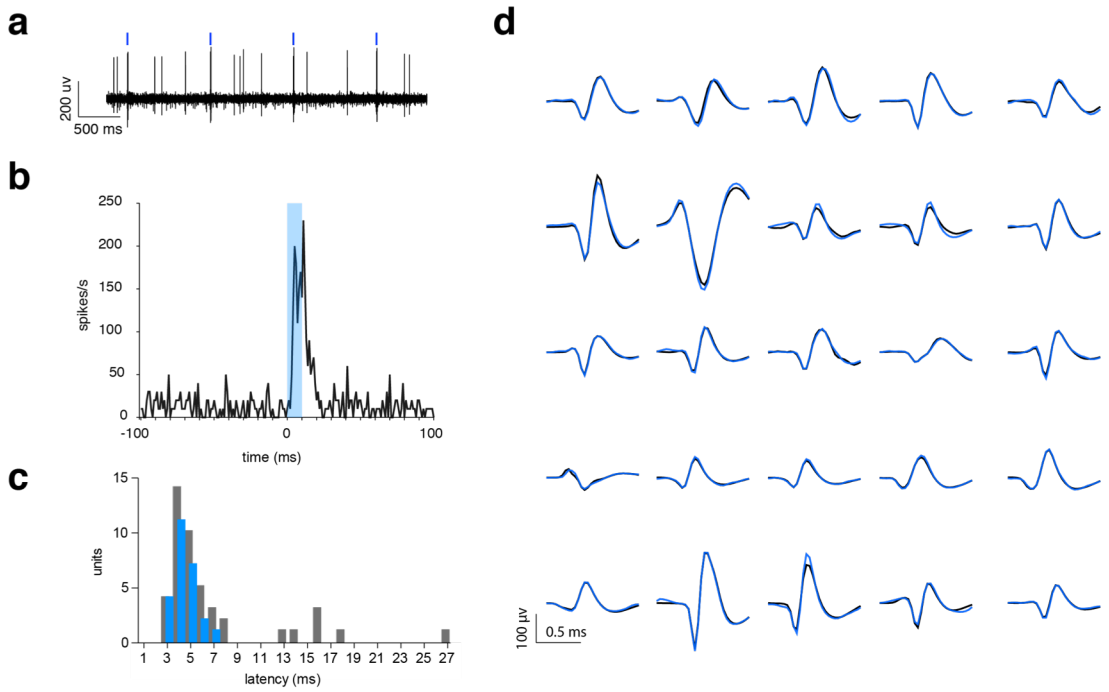

Figure 1.7 I Photoidentification of SNc DANs

a, Example of continuous recording of a photoidentified neuron. Small blue squares denote 10 ms light pulses of blue light that were delivered at 1Hz. **b**, PETH of the neuron in **a** aligned to blue light delivery (100 pulses). **c,** Histogram of latencies to modulation by light delivery. A threshold of 8 ms was used to define neurons as photoidentified (blue bars). Gray bars represent latencies of light modulated neurons that had latencies larger than 5 ms, thus not considered as photoidentified DANs. **c**, Mean spike traces for all photoidentified neurons. Black trace represents the mean for spikes obtained without light delivery and the blue trace represents the mean trace for spikes obtained during light delivery.

(auROC) was calculated for each time-bin, with values higher than 0.5 denoting an increased firing rate in relation to the baseline, and values lower than 0.5 denoting a decreased firing rate in relation to the baseline (**Fig. 2.7c**). We then used an affinity propagation algorithm (Frey & Dueck 2007a) on the traces that resulted from the ROC analysis (**Fig. 2.7d,e, see methods for details**). Besides segregating negatively modulated neurons from positively modulated neurons, positively modulated neurons were further separated in three different groups: Transiently active before the initiation of movement (cluster 1, n=6), transiently active before the initiation of movement and sustained inhibition after the initiation (cluster 2, n=2), and sustained increase in activity (cluster 3, n=5). Negatively modulated neurons were all clustered together (sustained decrease in activity, cluster 4, n=7) (**Fig. 2.7.c,d**). Interestingly, the latency for modulation preceded the initiation of movement for clusters of positively modulated neurons but not for the cluster of negatively modulated neurons (**Fig. 2.8**).

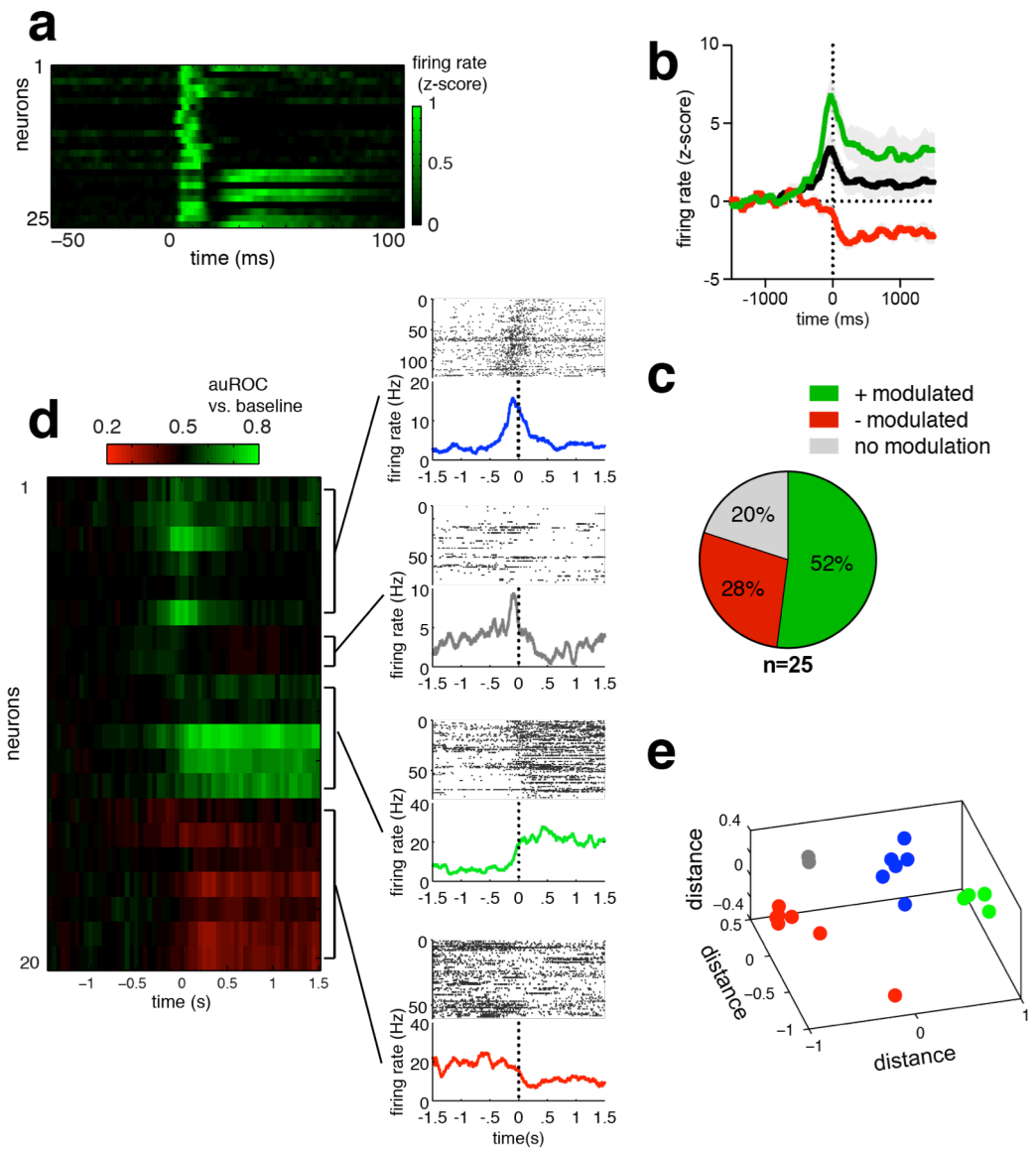

Figure 1.8 I External recordings of photoidentified SNc DANs during movement initiation.

a, Heat map representing the PETH of all photoidentified neurons, aligned to light delivery (n=25 neurons, median 3.5 neurons per mouse, 1-9 (min-max)). **b**, Mean trace for all neurons (including non-modulated, n=25, black), positively modulated neurons (n=13, green), and negatively modulated neurons (n=7, red) , aligned to movement initiation (93.45 ± 35.99 mean spontaneous initiations per neuron). Gray shadow denotes s.e.m. **c**, Proportion of modulated and non-modulated neurons. **d**, Left; responses from all modulated neurons aligned to movement initiation, sorted according to affinity propagation clustering (green increase from baseline, red decrease from baseline). Right; affinity clustering representative neuron for each cluster. **e**, Multidimensional scaling representation of the distance matrix used for affinity propagation clustering of modulated neurons. The colors correspond to the different clusters.

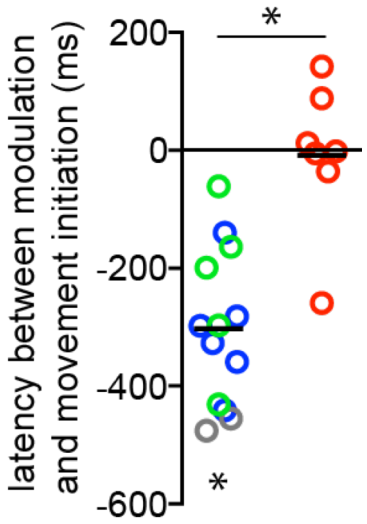

Figure 1.9 | Latency for modulated neurons

Latency of each neuron to be significant modulated referenced to movement initiation. A negative value indicates modulation preceding movement onset and positive indicates modulation after movement onset. Each neuron is colored according to the cluster it belongs to in Fig. 2.7. Negatively modulated neurons are on the right (red) and positively modulated neurons are on the left (other colors) of the plot. t-test vs. 0: positive neurons, $t(12)=8.28$, $P<0.0001$, negative neurons, $t(6)=0.18$, $P=0.86$; Pos. vs. Neg.: $t(18)=4.82$; $P=0.0001$).

To corroborate these findings we used a different technique also based on recording the activity of genetically identified DANs. We used a miniaturized epifluorescence microscope (Ghosh et al. 2011) to image calcium transients in genetically identified SNc DANs while mice were freely moving in the open field (**Fig. 2.9**) We implanted a gradient index (GRIN) lens (500 μm diameter, 8.2 mm) just above the SNc of three TH-Cre mice injected with an adeno-associated viral vector expressing GCaMP6f (Chen et al. 2013) in a Cre-dependent manner (AAV2/5.CAG.Flex.GCaMP6f).

When we aligned the fluorescence changes recorded through the GRIN lenses with movement initiation events, we observed that the activity of DANs was modulated by movement initiation in 50% of the neurons. Again, we found that the majority of modulated neurons were positively modulated by movement initiation.

The activity of individual DANs is not action-specific

We next examined whether the transient activity of individual DANs before action initiation was tuned to the initiation of specific actions or represented a more general signal before the initiation of all actions. As described above, we used a combination of three variables obtained from the motion sensors: Total body acceleration; the angular velocity of the axis most parallel to the dorsal-ventral axis of

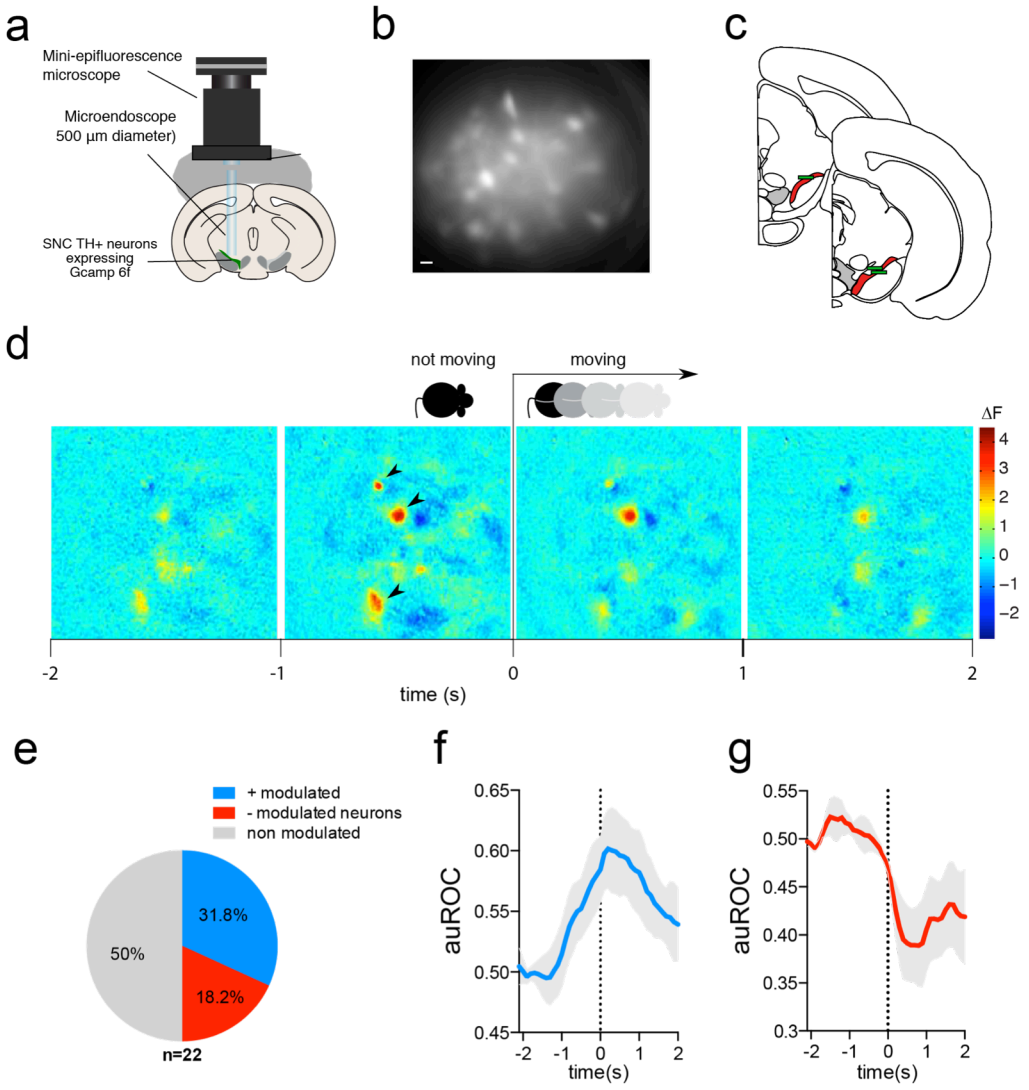

Figure 1.10 l SNc TH+ neurons calcium imaging during movement initiation.

a, Schematics of mini epifluorescence microscope and lens placement. **b**, Field of view of one mouse expressing GCaMP6f in SNc dopamine neurons (image is the projection of per pixel std of one FR8 session). **c,** Anatomical representation of lens placement. **d**, Example of the average pixel per pixel deltaF of one mouse aligned to movement initiation (n=46 trials). Black arrowheads denote three neurons which are significantly activated before movement initiation. **e**, Proportion of neurons modulated and non-modulated by movement initiation (n=22 neurons obtained from three mice). **f**, Mean trace of positively modulated neurons according to calcium imaging (solid line, n=7). Gray shadow denotes s.e.m. **g**, Mean trace of negatively modulated neurons according to calcium imaging (solid line, n=4). Gray shadow denotes s.e.m.

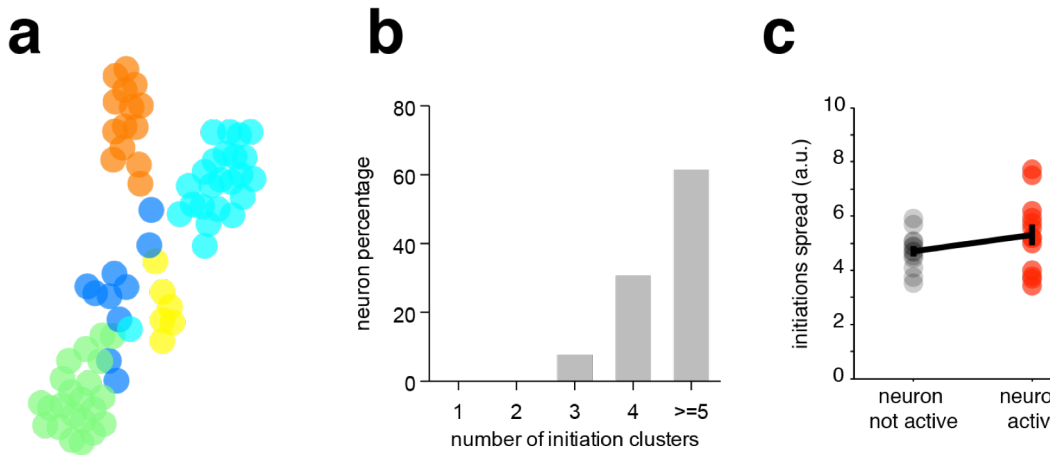

Figure 1.11 I Changes in activity of DAN's before movement initiation is not action specific

a, Representation of the initiations of one example session using t-SNE (Van Der Maaten et al. 2008) dimensionality reduction. Different colours represent different clusters of initiations determined using affinity propagation clustering. **b**, Number of initiation clusters in which each positively modulated neuron was significantly activated (n=13, 30.4% ± 0.19 of initiations were preceded by significant increase in neuron activity, see methods). **c**, Comparison of the spread of initiations (mean distance to every other initiation) between initiations not preceded by increased activity and initiations preceded by increased activity for positively modulated neurons.

the mice and the gravitational acceleration of the same axis to characterise each movement initiation. We used the combination of these three variables to describe trajectories in the motion sensor space for each movement initiation (**Fig. 2.4a,b**), and used affinity propagation to cluster different initiations. To perform this clustering analysis we created a vector for each initiation by concatenating the distribution of each of the three motion sensor variables during the first second of an initiation trajectory (**Fig. 2.10a, see methods for details**). We found that none of the positively modulated DANs were active only during one specific initiation cluster, but rather that most neurons were broadly tuned and responded before very different initiations (**Fig. 2.10b**). Furthermore, we found that initiation trajectories preceded by increased activity of each DAN were as variable as all other initiation trajectories (**Fig. 2.10c**). These data strongly indicate that each positively modulated DAN is active before the initiation of a wide range of movements, and hence not action-specific.

DAN activity before initiation is related to the vigor of future movements

Previous studies in patients with PD(Mazzoni et al. 2007) and animal models (Panigrahi et al. 2015) have shown that dopamine depletion leads to less vigorous movements. We therefore investigated whether the activity of DANs before movement

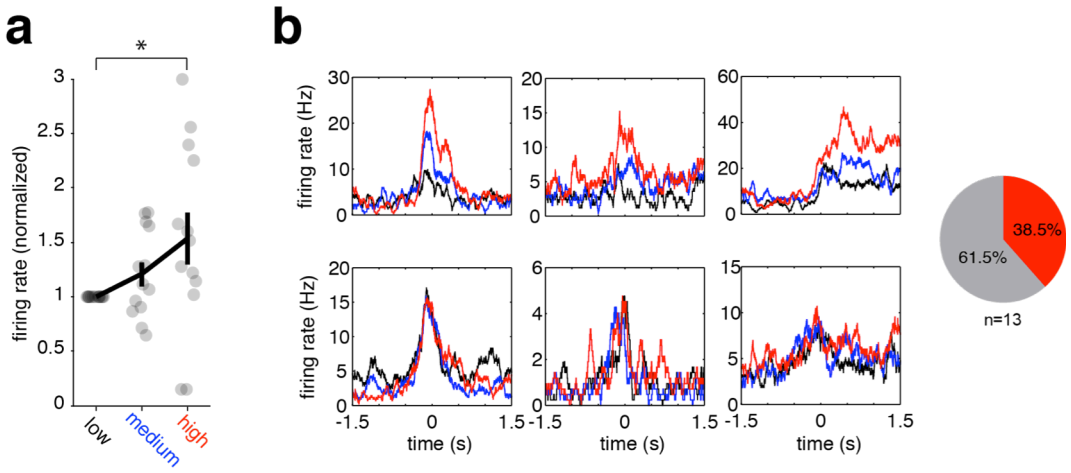

Figure 1.12 l Initiations preceded by increased activity of dopamine neurons are more vigorous.

a, Firing rate normalized (firing rate/firing rate for low acceleration trials) of positively modulated neurons for low, medium and high acceleration trials. Error bars denote S.E.M. **b**, examples of PETH of vigor-related neurons (top) and non-vigor related neurons aligned to movement initiation separated for high, medium and low acceleration initiations (red, blue and black respectively). The proportion of vigor related (red) and non-related neurons (gray) is quantified in the pie chart on the right.

* $P<0.05$

initiation encoded any information about the vigor of the movement about to be initiated. We used the mean acceleration during the first 500 ms of each spontaneous initiation as a measure of movement vigor, and separated trials into low acceleration trials (lower tertile), medium, and high acceleration trials (higher tertile). We verified that overall, the positive transients in dopamine activity 300 ms before movement initiation were significantly related to the vigor of future movement (**Fig. 2.11a**). When doing per trial analyses comparing all the lower vigor with the higher vigor initiations, we found that 38.5 % of the neurons had significantly higher activity before higher vigor movements (paired t-test comparing firing rate of low and high acceleration trials, $P < 0.05$, **Fig. 2.11b**).

METHODS

Animals

All experiments were approved by the Portuguese DGAV and Champalimaud Centre for the Unknown ethical committee and performed in accordance with European guidelines. TH-Cre male mice from the FI12 mouse line (Gong et al. 2007) between 3 and 5 months were used and TH-Cre:Ai32 (Madisen et al. 2012) between 2.5-6 months were used. TH-Cre: ROSA26R crossing were used to characterise the TH-cre FI12 line.

Recombinant adeno-associated viral vectors

The following Cre-dependent adeno-associated viral vector was used in the experiments shown in **Fig. 2.9**: AAV2/5.CAG.Flex.GCaMP6f.WPRE.SV40 (titre 1.19 × 10^{13}, University of Pennsylvania).

Optrodes and lens placement

Surgeries were performed using a stereotaxic system (Kopf). Mice were kept in deep anaesthesia using a mixture of Isofluorane and oxygen (1-3% Isofluorane at 1 l min-1). Before lowering the electrodes the bundle array was extended until it appeared at the edge of the cannula. Also, an optical fiber with 230 μm diameter and a NA of .39 (Thorlabs FMT 200 EMT) was fixed to the electrode cannula, allowing the fiber tip to rest on the side of the electrode cannula opening. Two small stainless steel screws (Antrin miniature Specialties #00-90x 1/16 SL Bind SST) were screwed into the skull of the mouse lateral to the holes used to introduce the electrodes. Before lowering the electrodes the ground wire was wrapped around these two screws. Using the tip of the bundle as reference the electrode was lowered at the following coordinates: -3.16 mm anteroposterior, 1.40 mm lateral from bregma and 4.20 mm deep from the brain surface. The space between the edge of the bone holes and the electrode was covered with cyanoacrylate and the electrode and screws were fixed in place by a cap built from dental cement.

The same stereotax system and anesthesia protocol was used for imaging experiments (**Fig. 2.9**). One μL of virus solution was injected in the right substantia nigra compacta at the following coordinates: -3.16 mm anteroposterior, 1.40 mm lateral from bregma

and 4.20 mm deep from the brain surface. The injection was done through a glass pipette using a Nanojet II (Drummond Scientific) with a rate of injection of 4.6 nl every 5 s. After the injection was finished the pipette was left in place for 10-15 min. The virus solution was kept at -80 ºC and thawed at room temperature just before the injection. A 500 μm diameter 8.2 mm long GRadient INdex (GRIN) lens (Part ID: GLP-0584, Inscopix) was implanted at the same coordinates as the injection. Before the lens was lowered, a blunt needle 28g was lowered to 3mm deep from the brain surface to facilitate the lowering of the GRIN lens. Then the GRIN lens was lowered (4.2 mm deep). The lens was fixed in place using cyanoacrilate and black dental cement (Ortho-Jet). One 1/16 inch stainless steel screw (Antrin miniatures) was attached to the skull to provide a scaffold to build a dental cement based cap that protected and fixed the lens to the skull.

Three weeks after this surgery the mouse was anesthetised and fixed with head bars. A baseplate (Part ID: BPC-2, Inscopix) attached to a mini epifluorescence microscope (nVista HD, Inscopix) was positioned above the GRIN lens. To position correctly the baseplate, brain tissue was imaged through the lens to find the appropriate focal plane using 20% of LED power, 5 Hz of frame rate and a digital gain of 4. Once the focal plane was set, the baseplate was cemented to the rest of the cap using the same dental cement. Imaging started 2-3 days after this final step.

Open field

We used a 39X39 cm open field with black walls (17.5 cm height) and white acrylic floor to assess mice's spontaneous movement. The open field was inside a sound attenuating chamber. Illumination was provided by white (2700 K) LED's (Dioder, Ikea) placed symmetrically on the floor and around the open field in a way that illumination of the open field was uniform and indirect (135 lx).

Acceleration and video recordings

In the experiments where photoidentified TH+ neurons were recorded, acceleration was recorded using a digital 9-axis inertial sensor with a sampling rate of 200 Hz (MPU-9150, Invensense, acceleration xyz, angular veleocity xyz, magnetometer xyz) assembled on a custom made PCB and connected to a computer via a custom made USB interface PCB (Champalimaud Foundation Hardware Platform). Magnetometer data was not used.

The experiments shown in Fig. 2.3 were done using an analogic 3-axis inertial sensor (acceleration xyz) was used with a sampling rate of 1000 Hz (LIS331AL, ST) assembled on a custom PCB (Champalimaud Foundation Hardware Platform), and the signals were fed to the analog inputs of a Cerebus recording system (Blackrock Microsystems).

Acceleration data obtained from these sensors aggregates acceleration from two sources: Acceleration generated from gravity and body acceleration. To separate these two components we processed data obtained from both types of inertial sensor using a custom matlab code. We used a standard approach (Mathie et al. 2002) that relies on filtering the 3-axis data using a Butterworth filter. In our analysis we used a median filter (7 bin wide) to remove noise peaks. Then we used a 1 Hz high pass 5th order Butterworth filter to remove the static (gravitational) component of the signal. Unless stated otherwise, in our analysis we used the sum of the 3 vectors of acceleration as a global measure of body acceleration.

Video recordings were obtained using a charge-coupled device camera (DFK 31BF03, Imaging Source) using and a custom-developed software in Labview (National Instruments) at a rate of 15 frames per second. This software allowed us to introduce signals to the video frames to sync acceleration, neural recordings and light delivery periods.

Extracellular recordings of photoidentifed SNc DAN's

Electrodes

We used a single-drive movable micro-bundle (sixteen 23μm tungsten electrodes) with an optic fiber guide cannula (Innovative neurophysiology, see Fig. 2.5a for schematics). The neural activity and the timestamps from the light stimulation were recorded using a Cerebus recording system (Blackrock Microsystems).

Optogenetic setup

Light from a free-launched 200-mW, 473-nm, diode-pumped, solid-state laser (Laserglow Technologies), controlled using an AOM (AA Optolectronic), was delivered after being captured by a collimator and split using a one-input to two-outputs rotary joint (Doric Lenses). Two hundred nm, .22 NA optical fiber patch cords were used to guide the light to the fibres implanted in the mice. Light intensity was measured before and during experiments using a similar fiber to the ones implanted and a Photodiode

Power Sensor (PD1000-S130C, Thorlabs). The power was adjusted at the tip of the fibre to be ~3 mW.

Recordings

Experiments were started one week after electrode placement. Everyday we sorted putative units using an online sorting algorithm (Central Software, Blackrock Microsystems) while the mouse was in its home cage. If putative single units were isolated, we would deliver a screening protocol consisting of a train of 100 blue light pulses with 10 ms width delivered at 1 Hz. Using a neurophysiology data analysis software (NeuroExplorer V4) we built PETH aligned to the train pulses. If any of the isolated units appeared to be modulated by the light train, the mouse was introduced in the open field and neurons were recorded for one hour. The stimulation protocol was run again at the end of the open field session for confirmation. At the end of the experiment the micro-bundle was advanced 50 μm to record next day. We used six mice in this experiments. During this experiment microbundles were moved on average 433 ± 93.1μm.

Units were resorted using an offline sorting algorithm (Offline Sorter V3, Plexon Inc.) to isolate single units based on waveform characteristics, inter-spike intervals and clustering. Single units together with the timestamps of the light stimulation provided by a pulse generator (Master 8, AMPI) were exported to MATLAB for analysis.

Criteria used to photoidentify DAN's:

Neural activity referenced to light pulse onset was averaged in 1-ms bins, and averaged across trials to construct a PETH, which was the basis for analysing amplitude and latency of light related firing activity. Distributions of the PETH from -900 to -10 ms before light onset were considered baseline activity. We then determined which bin, slid in 1 ms steps during an epoch spanning from light onset to 50 ms after, met the criteria for significant firing rate increase. A significant increase in firing rate was defined if at least 4 consecutive bins had firing rate larger than a threshold of 5 standard deviations above baseline activity. The latency to photoidentification was defined as the time between light onset and the first significant bin. Based on the distribution of latencies of significantly modulated neurons. in accordance with previous studies (Jin & Costa 2010; Cohen et al. 2012), we used a very short latency (≤7 m) combined with at least an increase in 30% of the firing rate during the light pulse and a

high correlation coefficient between spikes during light on and off (> 0.9) as criteria for positive photoidentification.

Criteria to identify neurons movement initiation

We built a PETH for each photoidentified single unit spanning from 1500 ms before and after movement initiation events. Neural activity was averaged in 100-ms bins, shifted by 1 ms (100 bin, centered on current bin). Distributions of the PETH from -1000 to -500 ms before light onset were considered baseline activity. We then determined which bin, slid in 1 ms steps during an epoch spanning from —500 ms to 500 ms after movement initiation, met the criteria for significant firing rate change. A significant change in firing rate was defined if at least 50 consecutive bins had firing rate higher or lower than a threshold of 2.56 standard deviations above or below baseline activity (99% CI). The latency to photoidentification was defined as the time between movement onset and the first of the 50 consecutive significant bins.

Area under the ROC curve analysis (auROC)

For this analysis we employed a method similar to the one described by Cohen et al (Cohen et al. 2012). We convolved the spike trains with a function similar to a post-synaptic potential. To produce the ROC curves, we compared the firing rate of each 50ms bin to the firing rates during baseline (-1500:-1000 ms before movement initiation) across trials. The area under the curve for each bin was calculated using trapezoidal numerical integration.

Identification of neuron types using affinity propagation clustering

We used the affinity propagation algorithm (Frey & Dueck 2007b) to look for subtypes of significantly modulated neurons. It is an efficient clustering algorithm that takes as inputs the similarities between pairs of observations in the dataset (in this case the AUC traces for each modulated neuron), and finds exemplars and the clusters around them by exchanging real-valued messages between data points. We used the MatLab (Mathworks) function made available by the authors at http://www.psi.toronto.edu/index.php?q=affinity%20propagation. We used the correlation between neuron AUC traces as the measure of similarity used by the algorithm. Also we used maxits=1000, convits=100; lam=0.9 and a preference equal to the median similarity of the dataset.

GCaMP6f imaging using Mini-epifluorescence microscope

Mice were briefly anaesthetised using a mixture of Isofluorane and oxygen (1% Isofluorane at 1 l min^{-1}) and the mini-epifluorescence microscope was attached to the baseplate. This was followed by a period of 20-30 min of recovery in his homecage before experiments started. Fluorescence images were acquired at 10 Hz and the LED power was set 10–20% (0.1–0.2 mW) with a gain of 4. Image acquisition parameters were set to the same values between sessions to be able to compare the activity recorded. Three GCaMP6f expressing TH-Cre mice were imaged while freely exploring an open field. The same mice and one more were also imaged during the FR8 task (see chapter 5).

Calcium image processing and analysis

GCaMP6f image processing and fluorescence trace extraction

All fluorescence movies were initial processed using the Mosaic Software (version 1.1.2, Inscopix). First all frames were spatially binned by a factor of 4. To correct the movie for translational movements and rotations, the frames were registered to a reference image consisting of an average of the all raw fluorescence movie. This was achieved by implementing the TurboReg registration engine (Thévenaz et al. 1998) within the mosaic software. The movie was cropped after registration to remove the post-registration black borders.

GCaMP6f fluorescence trace extraction

Although calcium imaging using miniscopes enables researchers to image neurons in freely moving mice, it is a challenge to adequately extract neuronal signals without background contamination. Because of this we implemented the Constrained non-negative matrix factorization for endoscopic data (CNMF-E) framework (Zhou et al. 2016; Klaus, A, Martins, GM, Paixão VB, Zhou, P, Paninski, L, Costa 2017). This recently described framework is an adaptation of the CNMF Algorithm (Pnevmatikakis et al. 2016). It can reliably deal with the large fluctuating background from multiple sources in the data, allowing the accurate source extraction of cellular signals. It includes four steps: (1) Initialize spatial and temporal components of single neurons without the direct estimation of the background; (2) estimate the background given the estimated neurons' spatiotemporal activity; (3) update the spatial and temporal components of all neurons while fixing the estimated background fluctuations; (4)

iteratively repeat step 2 and 3. We briefly describe the algorithm used in our work, and more details can be found in the preprint of the CNMF-E paper (Zhou et al. 2016) and in (Klaus, A, Martins, GM, Paixão VB, Zhou, P, Paninski, L, Costa 2017) In the initialization step, we first used a mean-subtracted 2D Gaussian kernel to filter the raw video data. The parameters of this kernel are selected to resemble the distribution of soma diameters (μ_{CNMF-E}=0, σ_{CNMF-E}=6.9 μm, maximum soma diameter d_{CNMF-E}=34.5 μm). Filtering the data with this kernel acts as a template matching to find all morphological shapes similar to a soma. In the filtered data, the background is approximately removed because it is almost flat within the spatial range of the kernel, and the kernel integrates to zero. In contrast, soma shapes are preserved and become more visible because they match the template shape. As a result, we can accurately extract each neuron's calcium activity from the fluorescence at its center pixels (so-called seed pixels) in the filtered data. Furthermore, we developed a method to detect seed pixels by choosing pixels with high local correlations and signal-to-noise ratio (SNR). Given a seed pixel, we initialize one neuron by estimating its temporal activity as the temporal trace of the pixel in the filtered data. To get its spatial component, we crop a small square with the size of 2 times larger than a cell body centered at the seed pixel from the raw data. Then we estimate the background fluctuation within the cropped area as the median in each frame. For each pixel within the selected square, we assume its fluctuations are from two sources: One is the initialized neuron and the other one is the background fluctuation. Since we have the temporal traces for all these two sources, we run linear regression to get the weights for each component and the weights corresponding to the neural activity lead to our initialization of the spatial footprints. Once we have both the spatial and temporal component of this neuron, we subtract its spatiotemporal activity from the raw video data and repeat the same procedure to initialize another neuron until the specified number of neurons has been detected or no more seed pixels can be found. This greedy initialization method is able to efficiently and accurately detect almost all neurons. In the next step, we estimate the background activity for each pixel individually. For each pixel, we first choose its neighbors with a distance larger than neuron size. Accordingly, these pixels do not share the same cellular activity but they share the same sources of the background. Then we use the projection of this pixel's temporal trace on a linear span of its neighbors' traces as its estimated background fluctuations. Finally, we subtract this estimated background from the raw video data and update all neuronal spatial and temporal components using alternating matrix factorization (Pnevmatikakis et al. 2016;

Zhou et al. 2016; Friedrich et al. 2016). Importantly, we include the temporal deconvolution in the step of updating temporal activity as well to denoise extracted calcium activity.

Criteria to identify GCaMP6f neurons modulated by movement initiation

We built a PETH for each neuron trace spanning from 3 s before and after movement initiation events. For this analysis we considered movement initiations defined as transitions between a period of at least 500ms below 0.05 *g* of body acceleration to a period of at least 500ms above 0.05 *g*. Distributions of the PETH from -3 to -1 s before movement onset were considered baseline activity. We then determined which bin, during an epoch spanning from -0.5 s to 0.5 s after movement initiation, met the criteria for significant ΔF/F0 change. A significant change in ΔF/F0 was defined if at least 2 consecutive bins had ΔF/F0 higher or lower than a threshold of 99 % above or below baseline ΔF/F0.

Anatomical verification

Animals were sacrificed after completion of the experiments. First, animals were anesthetized with isofluorane, followed by intraperitoneal injection of ketamine/xylaxine (~5 mg kg−1 xylazine; 100 mg kg−1 ketamine). Animals were then perfused with phosphate-buffered saline (PBS) 1X and 4% paraformaldehyde, and brains extracted for histological processing. Brains were kept in the 4% paraformaldehyde overnight and then transferred to PBS 1X solution. Brains were sectioned coronally in 50 µm slices (using a Leica vibratome VT1000S and kept in PBS solution before mounting or immunostaining treatment). Images were taken using a widefield fluorescence microscope (Zeiss AxioImager) and the tip of the longest cannula track found was used to determine the anatomical location of the electrodes which was represented in the corresponding Allen Brain Atlas (Lein et al. 2007) slice (**Fig. 2.5**).

To estimate the specificity of the TH-Cre line we crossed TH-Cre mice with ROSA26-EGFP mice. TH-Cre:ROSA26-EGFP mice express GFP in neurons expressing Cre recombinase. We used slices from one TH-Cre: ROSA26-EGFP mouse and used a tyrosine hydroxylase antibody (ImmunoStar) to label VTA and SNc DANs. We imaged the VTA and SNc in three different slices (~bregma -2.9; -3.3; -3.8) using a confocal microscope equipped with a Diode 405 nm, Argon multi line 458-488-514 nm and a DPSS 561 nm lasers (LSM710, Zeiss). We acquired Z stacks (354um × 354um × 5 µm; 5 µm interslice) in a tile that covered the VTA, SNc and areas 200um above and

below the SNc. We imported these images into the Stereo Investigator software (MBF Bioscience) and used a stereological approach to count labelled cells (TH+ and cre+) and evaluate co-localization, using a 100μmx100μm counting frame (**Fig 2.12**).

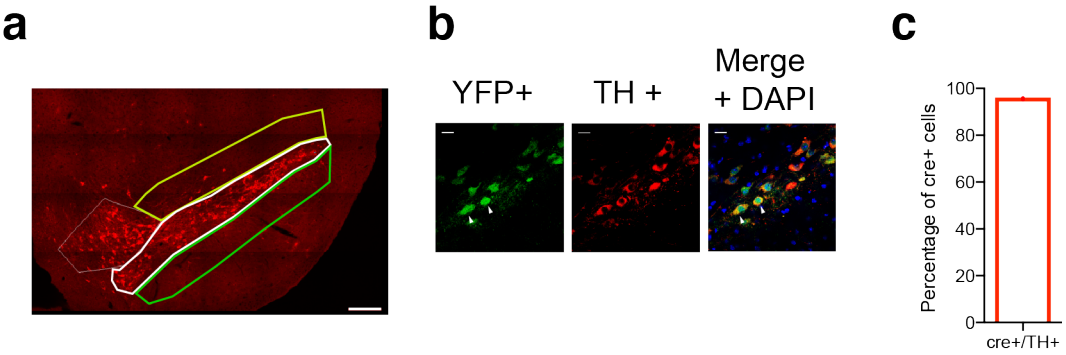

Figure 2.12| FI12 TH-cre mice characterization.

a, TH-Cre crossed with ROSA26R-YFP mice (expression of YFP in Cre+ cells). Left and middle, example of a midbrain slice of a TH-Cre X ROSA26R mouse with TH+ neurons labelled in red. White line delimits the SNc, and the yellow and green line delimit areas that cover a depth of 200 μm above and below the nigra respectively that were also targeted by stereological cell counts. **b**, Example of a SNc sampling field. Closed arrowheads denote examples of Cre+ cells that were TH+. Scale bar = 20μm **c**, Quantification of the specificity of the Cre line for tagging TH+ cells (median 95.3%, n= 3 slices; 117 counting frames).

Statistics

Statistical hypothesis testing was done at a 0.05 significance level (except for classification of neurons which was done at a 0.01 significance level as explained above). Parametric testing was used whenever possible to test differences between two or more means. Normality was tested using the Shapiro-Wilk test, while F-test (for unpaired t-tests) was used to assess equality of variance. If data was not normally distributed, we first tried to transform the data using the natural logarithm. If the distribution of the transformed data was still not normally distributed or there was a significant difference in variance, an alternative non-parametric test was used. Linear mixed models were used to check for main effects and interactions in experiments with repeated measures and more than one factor. The assumptions for linear mixed regressions were checked by careful inspection of the model residuals to check for normality and equality of variances. When main effects or interactions were significant, we did planned comparisons according to experimental design. Least Square Means (LSM) was used for planned comparisons when linear mixed models were significant. Statistical tests were done using Prism (GraphPad), Matlab (MathWorks) statistical toolbox, R (R core team 2015, v. 3.1.3, *lme* (Bates et al. 2015)).

Chapter 3 | INHIBITION OF DANS DECREASES THE PROBABILITY OF ACTION INITIATION AND THE VIGOR OF FUTURE MOVEMENTS

SUMMARY

In the previous chapter we showed that SNc DANs are transiently more active just before a movement is initiated and that the activity of some of these neurons relates to the vigor of future movements. In this chapter we used optogenetic inhibition of SNc DANs to interrogate the causality of this activity. We found that inhibition of these neurons led to a decrease in the movement of mice. However this decreased was due to a specific impairment in movement initiation, i.e. inhibition impaired the initiation of movement without affecting ongoing movements. Inhibition impaired movement initiation by lowering the probability of initiating movements, increasing the latency to initiate a movement and determining initiations with lower vigor.

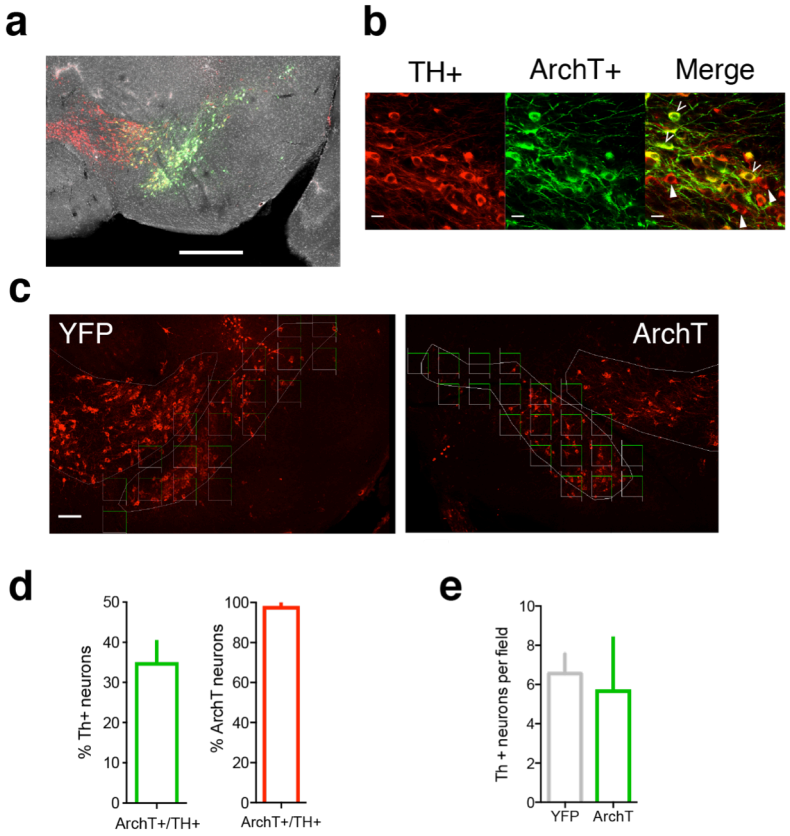

Figure 1.13 | Characterisation of ArchT infection

a, Representative merged image of VTA and SNc after 2 weeks of infection. ArchT + cells are labelled in green and TH+ cells are labelled in red and merged colors in yellow. ArchT + cells are mainly confined to SNc. scale bar=500 μm. **b**, Detail of a SNc region labelled for TH (red) and ArchT (green). Open arrowheads are examples of TH+ and ArchT + cells and closed arrowheads denote examples of TH+ and ArchT - cells. scale bar=20 μm. **c**, Examples of the slices and fields used to do the stereological count shown in e and g. scale bar=100 μm. **d**, Efficiency of ArchT virus infection (left). Specificity of ArchT virus infection (right). This was calculated by quantifying the whole SNc stereologically and not just the area closest to the infection (n=6 slices from two ArchT mice, 122 counting frames). **e**, Stereological quantification of the number of SNc TH+ cells in YFP and ArchT expressing mice at 2 weeks of infection (n=6 slices from two ArchT mice, 122 counting frames, YFP: n=6 slices from two YFP mice, 124 counting frames).

RESULTS

Optogenetic control of SNc DANs

To achieve temporally controlled inhibition of dopaminergic neuron activity, we used an AAV2/1 virus to express archaerhodopsin (ArchT, Han et al. 2011), in a Cre-dependent manner, in the SNc of TH-Cre mice (**Fig. 3.1**). Again, we used the same 16 channel movable electrode bundles coupled to a fiber optic cannula (**Fig.**

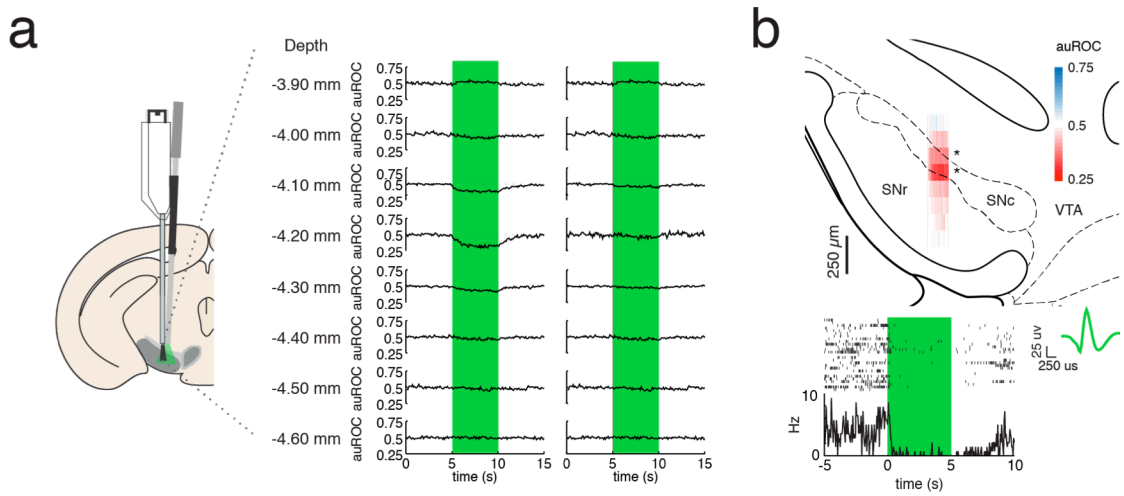

Figure 1.14 l ArchT can effectively inhibit SNc DANs

a, Mean unit activity aligned to light onset (less than 0.5 auROC indicates decrease from baseline and more than 0.5 auROC indicates increase from baseline) at different recording depths. The green rectangle signals the duration of light delivery. Left panel shows the mean of all units recorded and right panel shows the mean of all units except negatively modulated units. **b**, Top; anatomical representation of the average unit activity depending on recording depth and the location of the recording electrodes cannula (red decrease from baseline, blue increase from baseline). Bottom, example of a single unit inhibited by green light.

3.2) to confirm *in vivo* that ArchT was efficiently silencing SNc DANs. Neural activity was recorded daily and the electrodes were moved 50 μm at the end of each recording session. We were thus able to record neural activity from different depths (-3.90 mm to -4.60 mm from the brain surface), with neurons being recorded above, within and below the SNc. Using this strategy we were able to record from 140 units from 2 mice (24 single units and 116 multi-units). We found that 18.5% of these units were inhibited when green light (556 nm) was continuously delivered for 5 s. Only one of the recorded units (0.7%) was activated during light delivery. However, the percentage of cells inhibited was not homogeneous throughout all depths (χ^2 (4, 140) = 18.01, $P < .05$, test based on five levels of depth from -3.9 to -4.6 mm with 150 μm steps). In fact, when we investigated the mean activity of all units recorded at each depth, we found that the mean activity during light delivery changed depending on the depth, and it was only significantly different at the depths were the SNc is located (**Fig. 4a,b**), where the percentage of inhibited units reached 61.3%.

Inhibition of SNc DANs impairs movement

Using the same approach we expressed ArchT in the SNc of 11 TH-Cre mice and YFP in the SNc of a control group of 9 TH-Cre mice, and recorded their acceleration using a 3-axis accelerometer while they were freely moving in an open

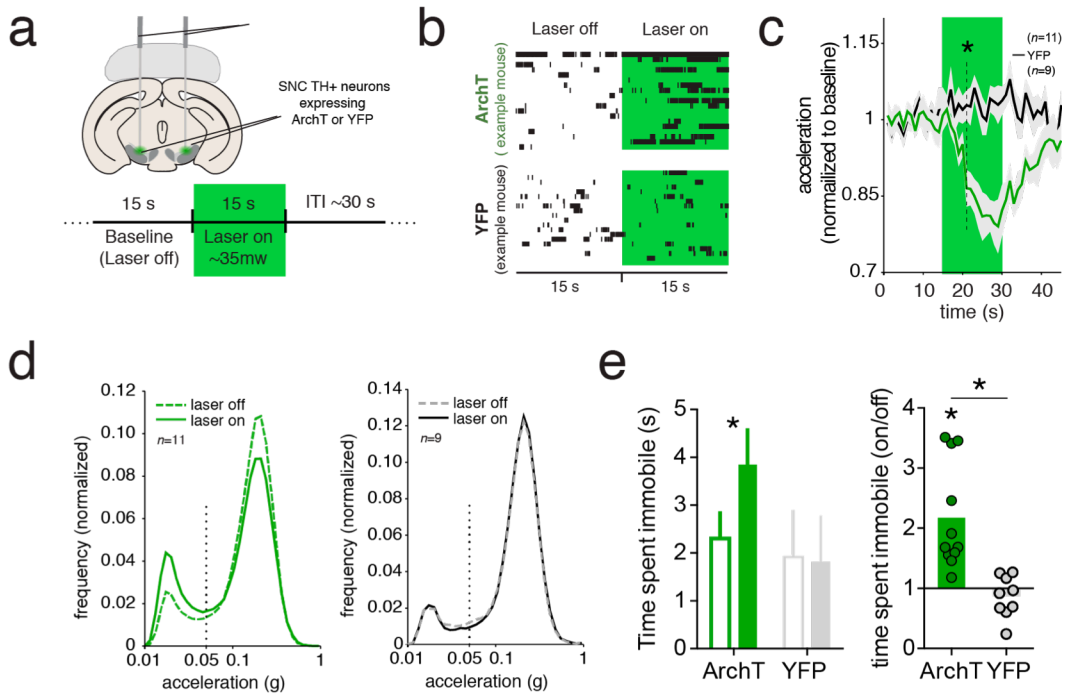

Figure 1.15 I Inhibition of SNc DANs impairs movement

a, Schematics showing fiber positioning and trial structure. **b**, Example of the periods of immobility during baseline and light delivery (green) for one ArchT and one YFP expressing mouse. Vertical lines denote bins of immobility. **c**, Acceleration of ArchT and YFP mice in the open field before, during (green rectangle) and after light delivery. Acceleration was normalised by dividing each bin by mean baseline acceleration (1-15 s). **d**, Distribution of acceleration in the open field during laser-on and -off for ArchT (left) and YFP (right) groups. Vertical dashed line denotes the threshold used to distinguish immobile from mobile state. **e**, Time spent immobile during laser-off and laser-on periods (left). Time spent immobile during laser-on normalised by the baseline value (right). Clear bars indicate laser-off and filled laser-on. Error bars and shaded areas denote s.e.m. * $P<0.05$

field. While mice were in the open field, there were unpredictable trials where green light was delivered continuously for 15 s (mean of 22 ± 3 trials group with a mean inter-trial interval of 64 ±2 8 s per mouse in the ArchT group and a mean of 23 ± 4 trials with a mean inter-trial interval of 65 ± 33 s per mouse in the YFP group). We found that inhibition of SNc DANs for 15 s led to a decrease in mean total body acceleration (**Fig. 3.3a-c**). This decrease did not seem to be due to a decrease in acceleration when the animals were moving, but rather to increased time spent immobile, since the change observed in acceleration distribution was mostly an increased probability of mice being below the immobility threshold, without changing the mode and variability around the high acceleration peak (**Fig. 3.3de**).

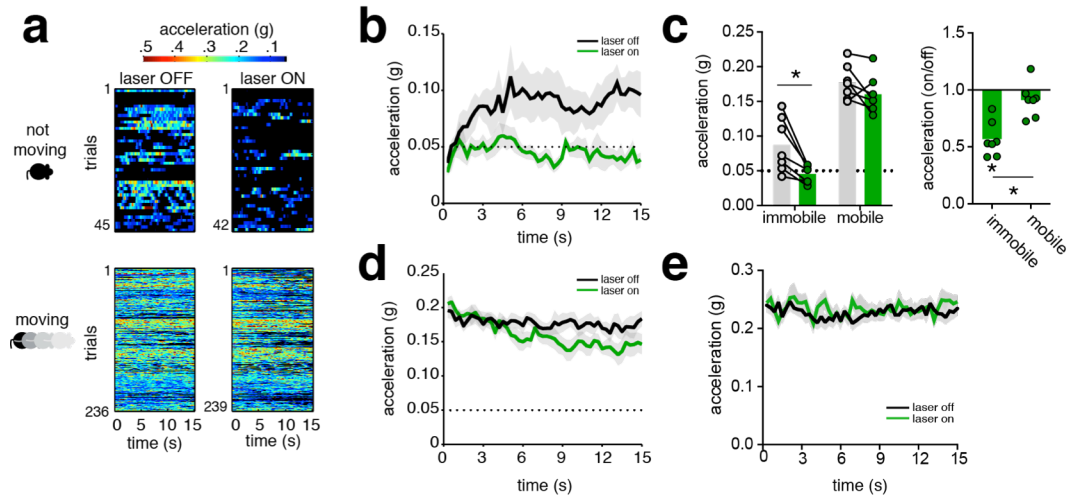

Figure 1.16 | Change in acceleration due to SNc DAN inhibition is state dependent.
a, Heat maps of acceleration data of all trials where the mouse was immobile (top) or mobile (bottom) prior to trial start, in laser off (left) and laser on (right) conditions (trials obtained from n=11 ArchT mice). **b**, Acceleration during laser-off and laser-on trials when ArchT mice were immobile before trial start (n=7 mice). **c**, Left, mean values of the data plotted in b and c. Gray bars represent laser-off data while green bars represent laser on data. Right, data shown in left panel normalized (laser-on/laser-off). **d**, Acceleration during laser-off and laser-on trials when ArchT mice were mobile before trial start (n=7 mice). Horizontal dotted line denotes the threshold used to classify acceleration state. **e**, Mean acceleration per mouse for trials where mice were already mobile when photoinhibition was triggered, and never stopped during the trial (n=10).

* $P<0.05$

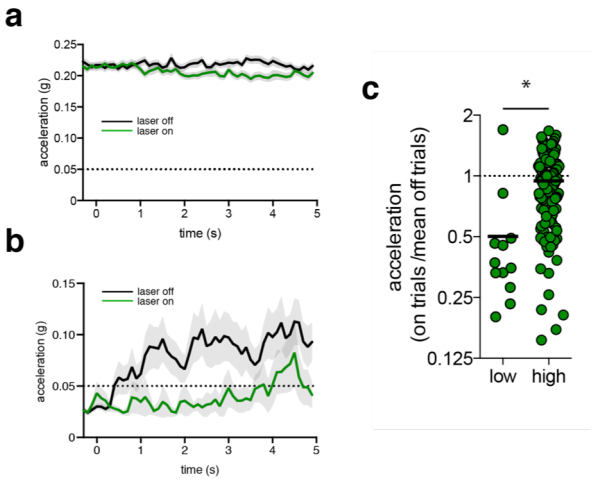

Figure 1.17 | Five-second inhibition of SNc TH+ neurons during mobile and immobile trials.
a, Acceleration during laser-off and brief laser-on trials (5 s inhibition) when ArchT mice were mobile before trial start (n=217 laser-on trials obtained from 5 ArchT mice, n=212 laser-off trials obtained from 11 ArchT mice). Horizontal dotted line denotes the threshold used to classify acceleration state. **b**, Acceleration during laser-off and brief laser-on trials (5 s inhibition) when ArchT mice were immobile before trial start (n=17 laser-on trials obtained from 5 ArchT mice, n=12 laser-off trials obtained from 5 ArchT mice). Horizontal dotted line denotes the threshold used to classify acceleration state. **c,** Acceleration during brief laser-on (5 s inhibition) normalized by mean laser-off acceleration for immobile and mobile states (n=17 laser-on immobile trials obtained from 5 ArchT mice, n=12 laser-off immobile trials obtained from 7 ArchT mice; n=217 laser-on mobile trials, n=212 laser-off mobile trials).

Inhibition of SNc DANs impairs movement by perturbing the initiation of movement

To investigate more specifically whether inhibiting SNc DANs affected movement initiation or impaired ongoing movement, we separated trials into immobile (inhibition started when mice were immobile), and mobile trials (inhibition started when mice were mobile, **Fig. 3.4**). Although mean acceleration decreased during inhibition there was an interaction between inhibition and the trial type (**Fig. 3.4b,d**, accel state*laser $F(1,6)=13.00$ $P=0.011$, see details in the extend statistical data table). To explore this interaction we compared mean acceleration between mobile and immobile trials, and found a significant impairment in movement initiation when SNc DANs were inhibited during immobility (**Fig. 3.4c**). The effect of inhibition was relatively rapid with a significant difference between light and no light after 2.4 s (**Fig. 3.4b**). Consistently, we also tested that 5 s of inhibition was sufficient to impair movement initiation (**Fig. 3.5**).

On the contrary, there was no significant change in mean acceleration when inhibition happened after movement onset (**Fig. 3.4c**). However, we observed a tendency for acceleration to decrease during inhibition of DANs for trials where mice were overtly moving before inhibition (**Fig. 3.4b**). This could be due to a decrease in the acceleration of ongoing movements, or to difficulties in movement initiation when animals happened to spontaneously stop in some of those trials. To disentangle these hypotheses we analyzed mobile trials further. We did not find a change in the vigor of movement when SNc DANs were inhibited after movement initiation but mice did not stop during the 15 s of inhibition (**Fig 3.4e**). Furthermore, in mobile trials where mice stopped during the 15 s (≥ 300 ms immobile), there was no difference in acceleration between laser-on and laser-off trials prior to the first stop. However, there was clear difficulty in movement initiation after the first stop (**Fig. 3.6a).** This was not observed in YFP controls **(Fig. 3.6b).**

We analysed in more detail the deficits in movement initiation when the inhibition was triggered while mice were immobile. We found there was a significant decrease in the probability of initiating movement during the 15 s of inhibition (**Fig. 3.7a**). Furthermore, even in trials where mice were able to initiate movements, the latency to initiate was significantly higher than in laser-off trials, and importantly, the initiated movements were less vigorous (**Fig. 3.7b,c**).

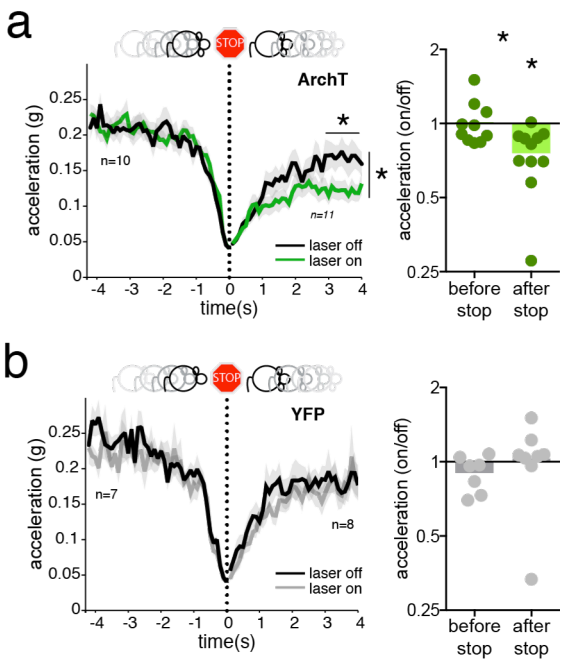

Figure 1.18 | Inhibition of SNc DANs impairs movement initiation without changing ongoing movement

a, Left; mobile trials aligned to the first stop. Right; normalized mean acceleration (laser-on/laser-off) before (-4:-3 s) and after (3:4 s) the first stop for ArchT mice. **b**, Same as in a for the YFP group. Error bars and shaded areas denote s.e.m. * *P*<0.05

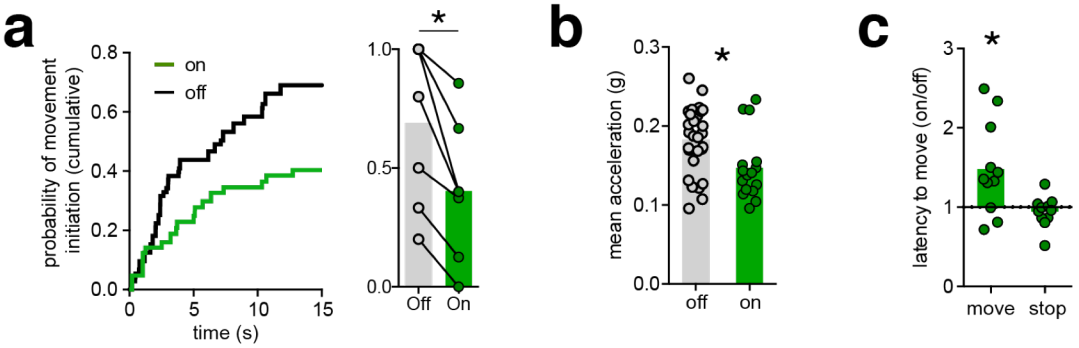

Figure 1.19 | SNc DAN inhibition decreases the probability of movement initiation and the vigor of future movements.

a, Left, mean cumulative probability of initiating movement for immobile trials, for laser on (green) and laser off (black) trials (n=7 ArchT mice). Right, mean probability to initiate movement per mouse for laser on and laser off trials (n=7 ArchT mice) **b**, Mean acceleration for initiations that occurred during immobile trials for laser on (green, n=16) and laser off trials (black, n=30 trials) of ArchT mice. **c,** Normalized mean latency to initiate movement or stop (laser on/laser off; n= 11 ArchT mice).

Taken together, these data indicate that DAN activity before movement initiation modulates the probability and vigor of future movements, but activity in these neurons does not appear to be critical for the maintenance and vigor of ongoing movements.

METHODS

Animals

All experiments were approved by the Portuguese DGAV and Champalimaud Centre for the Unknown ethical committee and performed in accordance with European guidelines. TH-Cre male mice from the FI12 mouse line (Gong et al. 2007) between 3 and 5 months were used.

Recombinant adeno-associated viral vectors

The following Cre-dependent adeno-associated viral vectors were used in these experiments:

AAV2/1.CAG.Flex.ArchT-GFP (titre 1.4 × 10^{12}, University of Pennsylvania); AVV2/1.EF1a.DIO.eYFP (titre 1.4 × 10^{13}, University of North Carolina).

Virus injections , fibers and electrode placement

Surgeries were performed using a stereotaxic system (Kopf). Mice were kept in deep anesthesia using a mixture of Isofluorane and oxygen (1-3% Isofluorane at 1 l min-1). 1.5 μL virus solution (ArchT or YFP) was injected bilaterally at 2.3 nl every 5 seconds bilaterally in the SNc at the following coordinates: -3.16 mm anteroposterior, 1.40 mm lateral from bregma and 4.20 mm deep from the brain surface. The injection was done through a glass pipette using a Nanojet II (Drummond Scientific) with a rate of injection of 4.6 nl every 5 s. After the injection was finished the pipette was left in place for 10-15 min. The virus solution was kept at -80 ºC and thawed at room temperature just before the injection. Using the same cranial holes, optical fibers with 230 μm diameter and a NA of .39 (Thorlabs FMT 200 EMT) were placed bilaterally at 3.9 mm deep from the brain surface. Optical fibers were built based on a published protocol (Sparta et al. 2012). To support the cap, two small stainless steel screws (Antrin miniature Specialties #00-90x 1/16 SL Bind SST) were screwed into the skull of the mouse lateral to the holes. A cap was built with dental cement around the fibers and screws. For the *in vivo* recordings to confirm ArchT inhibition, optrodes were lowered instead of fibers, at the same depth (electrodes were the same as described in the methods section on chapter 2).

Optogenetic setup

Light from a free launched 500-mW, 556-nm, diode-pumped, solid-state laser from CNI Lasers), controlled using an AOM (AA Optolectronic), was delivered after being captured by a collimator and split using a one-input to two-outputs rotary joint (Doric Lenses). Two hundred nm, .22 NA optical fiber patch cords were used to guide the light to the fibres implanted in the mice. Light intensity was measured before and during experiments using a similar fiber to the ones implanted and a Photodiode Power Sensor (PD1000-S130C, Thorlabs). The power was adjusted at the tip of the fibre to be ~35 mW.

Extracellular recordings to characterise the response of SNc neurons to light driven inhibition

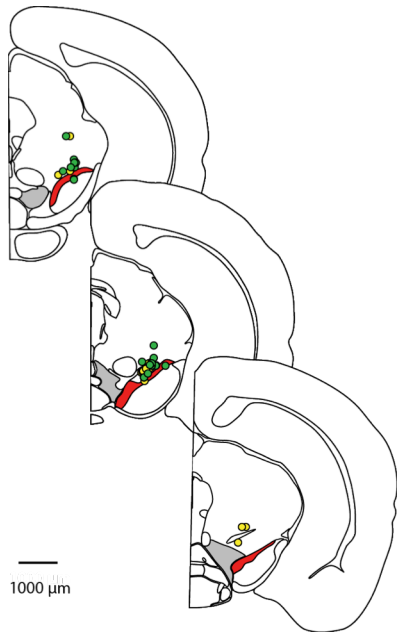

Figure 1.8 I Anatomical location of fiber tip in ArchT (green) and YFP mice (yellow)

We used the same setup and methodology described in Chapter 2 for the photoidentification experiments but instead of using blue light we used green light (see above for a description of the optogenetic setup). The mean auROC traces presented in figure 3.2a,b were calculated as described for the phototidentification experiments. The anatomical scheme depicted in figure 3.2 was based on the histologically determined position of the electrode cannula and the amount of electrode travel at each recording session. With the mouse in its home cage, we did 20-30 trials of 5 s inhibition separated while the mouse was freely moving. At the end of the experiment the micro-bundle was advanced 50 μm to record next day. We used two mice TH-Cre mice expressing ArchT in TH+ SNc neurons. Units were resorted using an offline sorting algorithm (Offline Sorter V3, Plexon Inc.) to isolate single units based on waveform characteristics, inter-spike intervals and clustering. Single units and multi-units together with the timestamps of light delivery provided by a pulse generator (Master 8, AMPI) were exported to MATLAB for analysis.

Open field

We used a 39X39 cm open field with black walls (17.5 cm height) and white acrylic floor to assess mices' spontaneous movement. The open field was inside a sound attenuating chamber. Illumination was provided by white (2700 K) LEDs (Dioder, Ikea) placed symmetrically on the floor and around the open field in a way that illumination of the open field was uniform and indirect (135 lx). Mice were introduced in the open field and green light was delivered continuously for periods of 15 (mean of 22 ± 3 trials with a mean inter trial interval (ITI) of 64 ± 28 s per mouse in the ArchT group and a mean of 23 ± 4 trials with a mean ITI of 65 ± 33 s per mouse in the YFP group).

An open field session was done the day before to habituate mice to the open field and to light delivery (with similar trial structure except for light duration which was 5 s). Data collected during this session is shown in **Fig 3.5.**

Anatomical verification of lens and fiber placement

Animals were sacrificed after completion of the experiments. First, animals were anaesthetized with isofluorane, followed by intraperitoneal injection of ketamine/xylaxine (~5 mg kg−1 xylazine; 100 mg kg−1 ketamine). Animals were then perfused with phosphate-buffered saline (PBS) 1X and 4% paraformaldehyde, and brains extracted for histological processing. Brains were kept in the 4% paraformaldehyde overnight and then transferred to PBS 1X solution. Brains were sectioned coronally in 50 µm slices (using a Leica vibratome VT1000S and kept in PBS solution before mounting or immunostaining treatment). Images were taken using a widefield fluorescence microscope (Zeiss AxioImager) and the tip of the longest fiber track was used to determine the anatomical location the implants. This location was represented in the corresponding Allen Brain Atlas (Lein et al. 2007) slice (**Fig. 3.8**).

EXTENDED STATISTICAL TESTING DATA TABLE

Figure	Sample size (n)	statistical test	values
3.2b	-3.9 mm (3); -4mm (22); -4.1mm (14); 4.2mm (6); -4.3mm (8); -4.4mm (10); -4.5mm (4); -4.6mm (5)	Kruskal-Wallis test; Dunn's multiple comparison test (all means vs mean -4.6mm)	H=18.22; *P*=0.011. -4.6 vs 3.9, p>0.99; -4.6 vs -4, *P*=0.078; **-4.6 vs -4.1, *P*=0.017**; **-4.6 vs -4.2 *P*=0.008**;-4.6 vs -4.3, *P*=0.67;4.6 vs -4.4, *P*=0.82; 4.6 vs -4.5, *P*>0.99;
3.3c	ArchT (11); YFP (9)	Two-way mixed ANOVA; planned comparisons between laser on and laser off using Fisher's LSD	**Main effect group F(1,18)=16.9, *P*<0.0001**; **main effect time F(14,252)=5.32, *P*=0.002**, **Interaction effect F(14,252)=5.46, *P*=0.0019**; Planned comparisons ArchT - YFP, ***P*<0.05 from 7 s to 15 s after laser onset.**
3.3e (left)	ArchT (11); YFP (9)	Two-way mixed ANOVA; planned comparisons between laser on and laser off using Fisher's LSD; Data was ln transformed to meet the normality assumption	Main effect group F(1,18)=2.18, *P*=0.16; **Main effect laser F(1,18)=5.29, *P*=0.03**; **Interaction effect F(1,18)=21.82, *P*=0.0002**; Planned comparisons: **Archt laser off - laser on *P*<0.0001**, YFP laser off - laser on *P* = 0,13
3.3e (right)	ArchT (11); YFP (9)	One sample Wilcoxon Signed Rank against 1 and Mann-Whitney test (ArchT vs. YFP)	Wilcoxon vs. 1:**ArchT, W=66, *P*=0.001**, YFP, W=-21 *P*=0,25 **ArchT vs. YFP: U=2; *P*<0.0001**
3.4c (left)	ArchT (7)	Two-way repeated measures ANOVA	Main effect **laser F(1,6)=23.8 *P*=0.003**, Main effect **acceleration state F(1,6)=98.2 *P*<0.0001**; Planned comparisons: **Low acceleration laser off - laser on, *P* = 0.014**, high acceleration laser off - laser on *P* = 0.215
3.4c (right)	ArchT (7)	One sample t-test against 1 and paired two sample t -test (ArchT low vs. ArchT high)	t-test vs. 1: ArchT low acceleration, t(6)=7.38, *P*=0.003, ArchT high acceleration,t(6)=1.54 *P*=0,173. **ArchT low vs. ArchT high: t(6)=3.52; *P*=0.012**
3.4b,d	ArchT (7)	Three-way repeated measures ANOVA (accel state, laser, time); data was Ln transformed for normality.	Main effects: **accel stateF(1,6)=77.83, *P*<0.001**; **laser F(1,6)=53.16, *P*<0.001**; time F(49,294)=1.28, *P*=0.31 Interactions: **accel state*laser F(1,6)=13.00 *P*=0.011;** laser*time F(49,294)=1.78, *P*=0.171, **accel state*time F(49,294)=3.062, *P*=0.034**; accel state*time*laser, F(49,294)=0.73, *P*=0.57
3.4e	ArchT (10)	Two-way repeated measures ANOVA	Main effect laser: F(1,9)=0.77, *P*=0.40; **Main effect time: F(49,441)=1.52, *P*=0.016**; interaction: F(49,441)=1.04, *P*=0.40).
3.5c	n=17 laser-on immobile trials obtained from 5 ArchT mice, n=12 laser-off immobile trials obtained from 7 ArchT mice; n=217 laser-on mobile trials, n=212 laser-off mobile trials		
3.6a (left)	ArchT before stop (10) ArchT after stop (11)	Linear mixed model with mouse as the random effect and laser state as fixed effect.	Before stop: Main effects: laser, F(10)=0.1881 *P*=0.67; time F(42,378)=37.7, <0.0001=; laser*time, F(42,378)=0.94, *P*=0.59. After stop: Main effects**: laser, F(10)=5.55 *P*=0.04**; time F(39,390)=19.95, *P*<0.0001; **laser*time, F(39,390)=2.33, *P*<0.0001.** Least square means was used for pairwise comparisons (on-off) at each time point. In the figure is shown by the horizontal line the point in time were these comparisons were consecutively significant.
3.6a (right)	ArchT before(10); ArchT after (11);	One sample t-test against 1. linear mixed model comparing mean acceleration before (-4 to -3s) vs mean acceleration after (3-4s). Linear mixed model with mouse as the random effect and laser state as fixed effect.	t-test vs. 1: ArchT before stop (data was transformed (log) for normality), t(9)=0.087, *P*=0,93; **ArchT after stop, t(10)=3.98, *P*=0.003.** before vs after: **χ^2(1)=10.392; *P*=0.0013**
3.6b (left)	YFP before stop (7) YFP after stop (8)	Linear mixed model with mouse as the random effect and laser state as fixed effect.	Before stop: Main effects: laser, F(6)=1.72 *P*=0.23; time F(42,252)=22.3, <0.0001=; laser*time, F(42,252)=0.82, *P*=0.78.

			After stop: Main effects: laser, F(7)=1.74 *P*=0.23; time F(39,278)=13.6, *P*<0.0001; laser*time, F(39,278)=0.51, *P*=0.99.
3.6b (right)	YFP before stop (7) YFP after stop (8)	One sample t-test against 1. linear mixed model comparing mean acceleration before (-4 to -3s) vs mean acceleration after (3-4s). Linear mixed model with laser state nested within mouse as the random effect and laser state as fixed effect.	t-test vs. 1: YFP before stop, t(6)=1.76, *P*=0.13; ArchT after stop, t(7)=0.26, *P*=0.80. before vs after: $\chi^2(1)=1.052$; *P*=0.31
3.7a	ArchT (7)	paired t -test (ArchT on vs. ArchT off)	**t(6)=4.46; *P*=0.004**
3.7b	trials laser off (28), trials laser on (16), obtained from 7 ArchT mice.	Linear mixed model with mouse as the random effect and laser state as fixed effect.	**$\chi^2(1)=6.58$; *P*=0.01**
3.7c	ArchT (n=11)	One sample t-test against 1	**Latency to move: t=2.75, *P*=0.02**; latency to stop: t(1,10)=0.99, *P*=0.35

Chapter 4 | ACTIVATION OF DOPAMINE NEURONS PROMOTES MOVEMENT INITIATION AND INVIGORATES INITIATED MOVEMENTS

SUMMARY

In the previous chapter we showed that inhibition of SNc dopamine neurons impaired movement initiation without affecting ongoing movements. This supports a causal role for the increase in activity preceding movement initiation that we observed in most SNc. However, being able to activate these neurons depending on the motion state (mobile or immobile) is necessary for a complete interrogation of the causal role of these neurons in movement initiation.

Here we take again advantage of the high temporal resolution of optogenetics to activate SNc dopamine neurons and evaluate the impact of this activation in spontaneous movement of mice in an open field. In light of the results reported in the previous chapter, we again look into changes in movement in different motion states (mobile vs. immobile). Here we use a strategy similar to the one we employed in the last chapter, using random trials of activation and a post hoc separation of movement states, but also a closed loop strategy where mice acceleration is monitored online and SNc dopamine neurons activation is triggered when mice are in different movement states.

In accordance with the previous chapter we found that transient activation of these neurons not only promoted movement initiation by increasing the probability of moving when mice were immobile and decreasing the latency to initiate a movement, but also promoted the initiation of more vigorous movements.

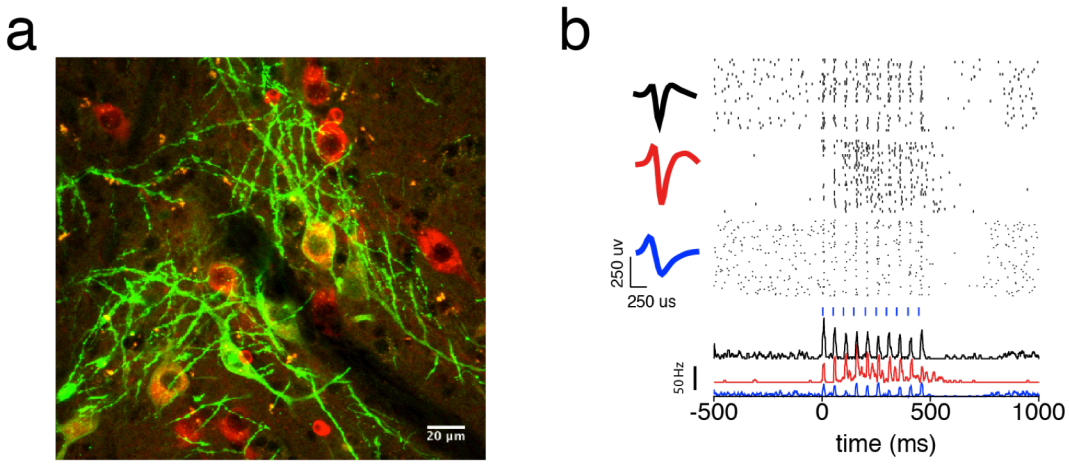

Figure 1.20 I Transient activation of dopamine neurons using optogenetics,

a, Photomicrograph showing substantia nigra dopamine neurons (red, TH immunostaining). Some of the dopamine neurons are expressing ChR2 (green, GFP fluorescent tag). **b,** Example of three SNc dopamine neurons (single units) expressing ChR2, following 10 pulses at 20 Hz. Vertical black lines represent spikes and the traces in the bottom correspond to the PETH for each neuron.

RESULTS

Activation of dopamine neurons promotes movement initiation

We investigated whether brief activation of dopamine neurons would be sufficient to promote movement initiation. To test this hypothesis, we expressed ChR2 in SNc dopamine neurons using the same Cre-dependent strategy described in chapter 2 (local injection of AAV2/1 viruses containing DIO ChR2-YFP in seven mice and control DIO EYFP in five mice; **Fig. 4.1a**). Using the same approach described in previous chapters, we did external recordings in the SNc with mice freely moving to confirm that we could in fact drive dopamine neurons using this strategy (**Fig. 4.1b**)

While mice were exploring an open field, we transiently activated SNc dopamine neurons (10 pulses at 20 Hz). We defined no laser trials as trials aligned to 6 seconds before laser pulses started, which served as internal controls. Next, we separated trials as we described in chapter 3 into mobile and immobile trials (mean of 23.4 ±7.81 trials Chr2 mobile on, 22.7 ±7.95 Chr2 mobile off, 8.43±6.81 trials Chr2 immobile on, 7.85±5.81 Chr2 immobile off, 18.6±5.12 YFP mobile on, 18.8±4.92 YFP mobile off, 16.4±5.17 YFP immobile on, 16.2±5.22 YFP immobile off).

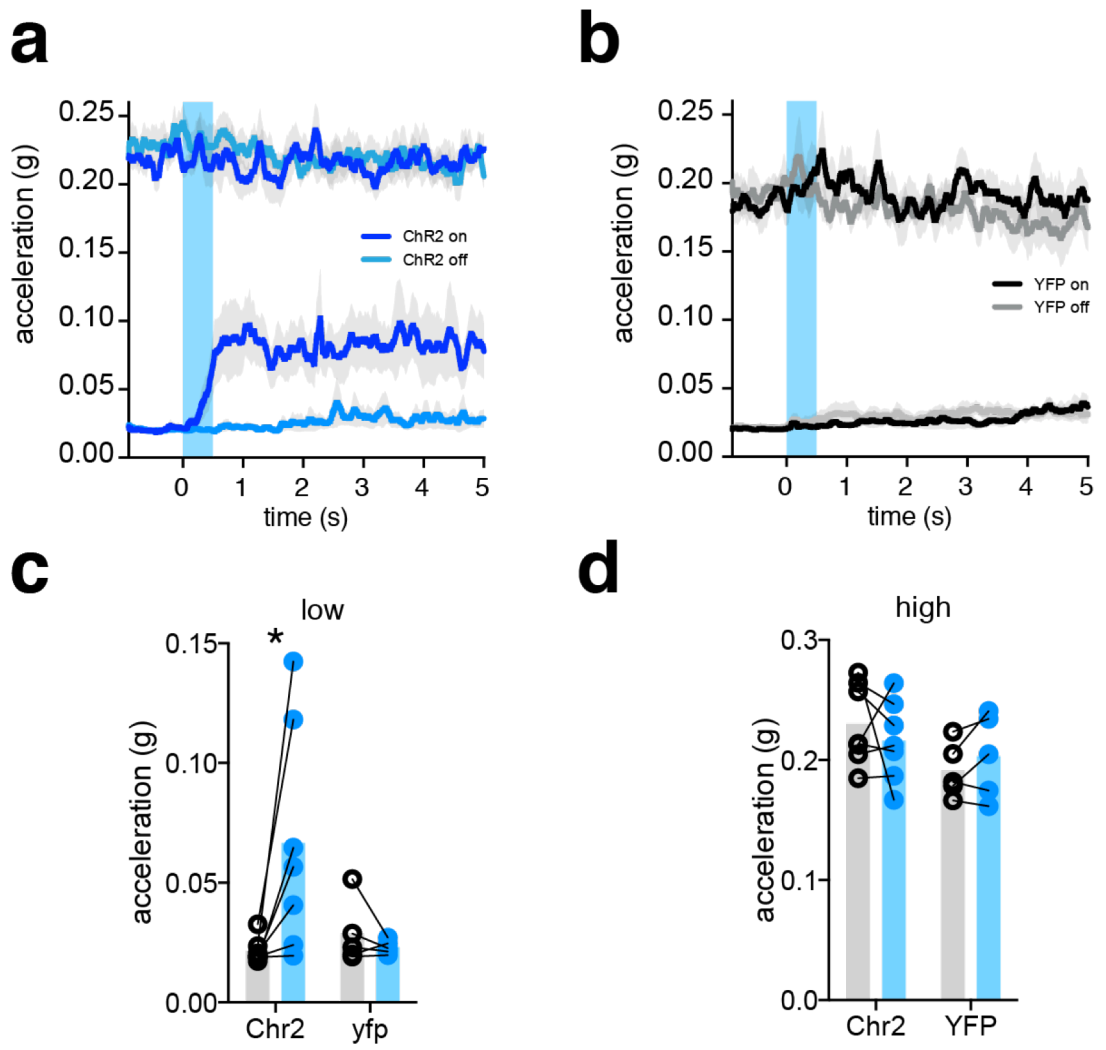

Figure 1.21 | Transient activation of SNc dopamine neurons promotes movement in a state dependent manner.

a, Mean acceleration during laser-off and laser-on trials, depending on the acceleration state before the trial for ChR2 mice. **b,** Same as in a for YFP mice. **c**, mean acceleration from 0 to 1s for trials where animals were immobile before the laser trigger. **b** mean acceleration from 0 to 1s for trials where animals were moving before the laser trigger. Grey bars indicate laser-off and filled laser-on. Grey shaded areas represent S.E.M., * P<0.05

We found that this brief activation of SNc dopamine neurons when mice were immobile was sufficient to promote movement initiation, while the same activation pattern when mice were overtly moving did not affect ongoing acceleration (**Fig. 4.2**). No significant differences were found in the YFP group.

To further dissect this, we performed an online closed loop experiment in which mice received stimulation if they were immobile for at least 900ms, but only in 50% of the trials (mean of 20,6± 8.68 Chr2-off trials, 16.6 ±3.5 ChR2-on trials, 18.4 ±3.2 YFP-off trials, 19.2±2.49 YFP-on trials). We set an inter-trial interval of at least 30 s (**Fig 4.3**). Trials where light was not delivered were used as an internal control (laser-off trials). The rationale was that this experiment would disambiguate between the

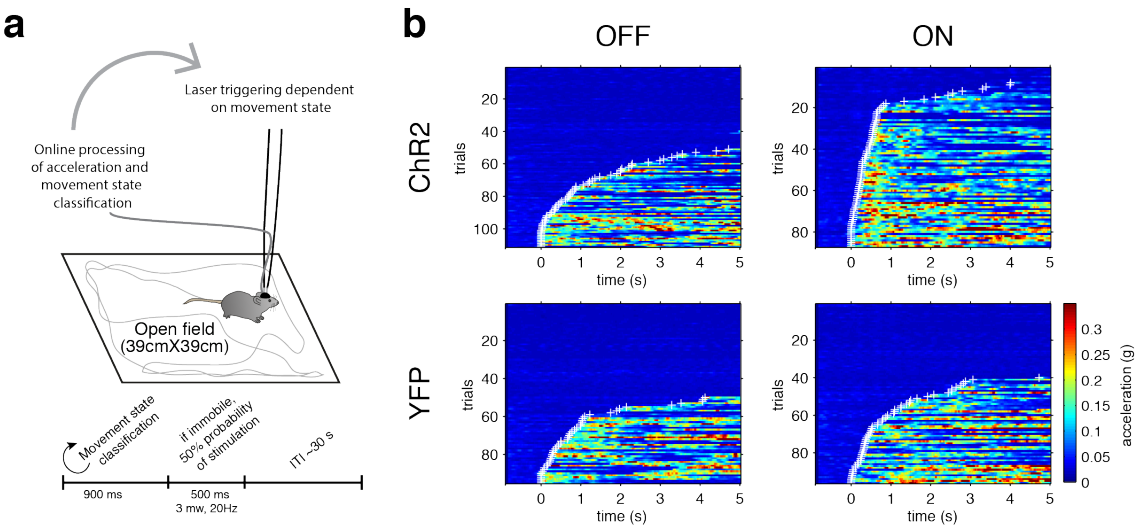

Figure 1.22 | Closed loop acceleration state based stimulation

a, Set-up for closed loop experiment. Acceleration was monitored and movement state of mice was classified online. SNc dopamine neurons stimulation was triggered automatically only when the mice were immobile (in 50% of the trials). To have isolated trials of stimulation, there was an inter-trial interval of at least 30s. **b**, experimental setup for closed loop experiments. e, Heat maps of acceleration data of all trials for both ChR2 and YFP groups. Laser-trigger criteria was reached at time 0. White crosses signal the onset of movement for a given trial. Blue light was delivered from 0 to 0.5s in laser-on trials (right panels).

reinforcing effects of dopamine and the movement promoting effects of dopamine; a reinforcement effect should result in increased stopping with a corresponding decrease in the interval between immobility episodes. Also, in this way we would be in more control regarding the number of trials we could obtain for the immobile state.

Again, we found that brief activation of SNc dopamine neurons in laser-on trials resulted in increased mean acceleration (**Fig. 4.4a**), with no effect in laser-off trials compared to YFP controls. The acceleration during the first second following the closed loop trigger was higher during laser-on than during laser-off trials in the ChR2 group (**Fig. 4.4b**). Moreover, the latency to initiate movement when SNc dopamine neurons were briefly activated was almost three times shorter than in laser-off trials (**Fig. 4.4c**). Also, the percentage of trials in which movement was initiated during the first second was higher during laser-on than during laser-off trials (**Fig. 4.4d**). This result is not easily explainable by reinforcement effects, because SNc dopamine neuron stimulation when animals were immobile did not result in an increased frequency of immobility episodes (interval between immobility periods: ChR2, 254.5±116.5 s; YFP, 150.5±65.8 s; t=1.74, *P*=0.12). Although the previous results argue for an increase probability of movement initiation, they do not clarify whether dopamine activation promotes the initiation of more vigorous movements. For this we calculated the maximum acceleration during the first second after movement initiation for trials in which mice

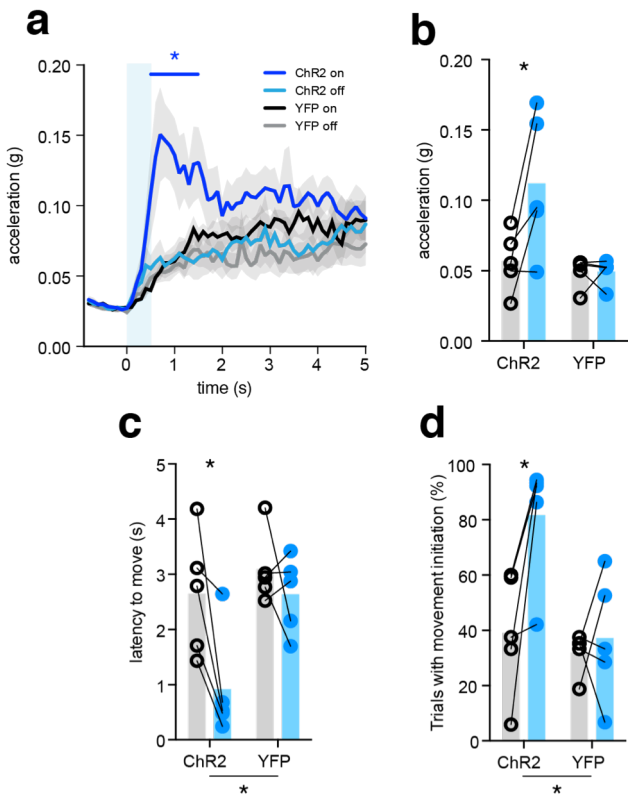

Figure 1.23 l Closed loop triggered SNc dopamine neurons activation promotes movement initiaition

a, Mean acceleration for ChR2 and YFP groups during laser-on and laser-off closed loop trials. Light blue area indicates laser-on period, n= 5 mice per group. **b**, mean acceleration from 0 to 1s depending on laser state and group. **c**, Latency to initiate movement depending on laser state and group. **d**, Percentage of trials per mouse with movement initiation between 0 and 1s depending on laser state and group. Grey bars indicate laser-off and blue bars laser-on. Grey shaded areas represent S.E.M., * P<0.05

eventually started to move, and compared between laser-on and laser-off trials (**Fig. 4.5**). We found that in fact movements initiated during laser-on trials were more vigorous than movements spontaneously initiated during laser-off trials, for mice expressing ChR2.

In summary, the results of ChR2 experiments were the opposite of what was obtained in ArchT experiments. Brief activation of SNc dopamine neurons was sufficient to promote and invigorate spontaneous self-paced movement initiations.

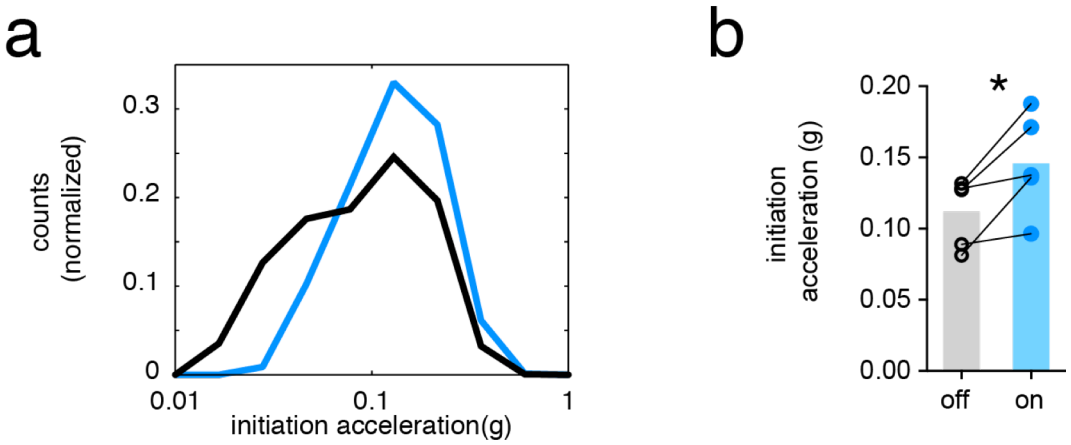

Figure 1.24 l Brief activation of SNc dopamine neurons promotes more vigorous initiations

a, mean distribution of acceleration during the first second after movement initiation for laser-on and laser off (n=5 ChR2 mice). **b**, mean acceleration during the first second of movement initiation during laser off and laser on trials (n=5 ChR2 mice). Clear bars indicate laser-off and blue bars laser-on, error S.E.M., * P<0.05

METHODS

Animals

All experiments were approved by the Portuguese DGAV and Champalimaud Centre for the Unknown ethical committee and performed in accordance with european guidelines. TH-Cre male mice from the FI12 mouse line(Gong et al. 2007) between 3 and 5 months were used.

Recombinant adeno-associated viral vectors

The following Cre-dependent adeno-associated viral vectors were used in these experiments:

AAV2/1.ChR2-eYFP (titre 1.4 × 10^{13}; University of North Carolina); AVV2/1. EF1a.DIO.eYFP (titre 1.4 × 10^{13}, University of North Carolina.

Virus injections , fibres and electrode placement

Surgeries were performed using a stereotaxic system (Kopf). Mice were kept in deep anaesthesia using a mixture of Isofluorane and oxygen (1-3% Isofluorane at 1 l min-1). 1.5 μL virus solution (ChR2 or YFP) was injected bilaterally at 4.6nl every 5 seconds bilaterally in the SNc at the following coordinates: -3.16 mm anteroposterior, 1.40 mm lateral from bregma and 4.20 mm deep from the brain surface. The injection was done through a glass pipette using a Nanojet II (Drummond Scientific) with a rate of injection of 4.6 nl every 5 s. After the injection was finished the pipette was left in place for 10-15 min. The virus solution was kept at -80 ºC and thawed at room temperature just before the injection. Using the same cranial holes, optical fibers with 230 μm diameter and a NA of .39 (Thorlabs FMT 200 EMT) were placed bilaterally at 3.9 mm deep from the brain surface. Optical fibers were built based on a published protocol(Sparta et al. 2012). To support the cap, two small stainless steel screws (Antrin miniature Specialties #00-90x 1/16 SL Bind SST) were screwed into the skull of the mouse lateral to the holes. A cap was built with dental cement around the fibers and screws. For the in vivo recordings to confirm ChR2 activation, optrodes were lowered instead of fibers, at the same depth (electrodes were the same as described in the methods section on chapter 2).

Optogenetic setup

Light from a free-launched 200-mW, 473-nm, diode-pumped, solid-state laser (Laserglow Technologies), controlled using an AOM (AA Optolectronic), was delivered after being captured by a collimator and split using a one-input to two-outputs rotary joint (Doric Lenses). Two hundred nm, .22 NA optical fiber patch cords were used to guide the light to the fibres implanted in the mice. Light intensity was measured before and during experiments using a similar fiber to the ones implanted and a Photodiode Power Sensor (PD1000-S130C, Thorlabs). The power was adjusted at the tip of the fibre to be ~3 mW.

Extracellular recordings to characterise the response of SNc neurons to light driven activation

We used the same setup and methodology described in chapter 2 for the photoidentification experiments. With the mouse in is home cage, we did 30-70 trials of 500 ms of 10 ms pules at 20 Hz frequency while the mouse was freely moving. At the end of the experiment the micro-bundle was advanced 50 μm to record next day. We used two mice Th-Cre mice expressing ChR2 in TH+ SNc neurons. Units were resorted using an offline sorting algorithm (Offline Sorter V3, Plexon Inc.) to isolate single units based on waveform characteristics, inter-spike intervals and clustering. Single units and multi-units together with the timestamps of light delivery provided by a pulse generator (Master 8, AMPI) were exported to MATLAB for analysis. In **Fig. 4.1** we are showing three examples of single units responding to the light with a latency < 6 ms.

Open field

We used a 39X39 cm open field with black walls (17.5 cm height) and white acrylic floor to assess mice's spontaneous movement. The open field was inside a sound attenuating chamber. Illumination was provided by white (2700 K) LED's (Dioder, Ikea) placed symmetrically on the floor and around the open field in a way that illumination of the open field was uniform and indirect (135 lx). Mice were introduced in the open field and a train of blue laser light (10 ms pulses at 20 Hz, during 0.5 sec) was delivered with a variable interval: after 90 s there was a 33% probability that the light was delivered and this was repeated every 10 seconds until light was delivered.

Open field - Closed loop experiment

In closed loop experiments the same light pulse train was used but it was delivered depending on the acceleration state of the mouse in the following way: Mice acceleration was monitored online by feeding the analog accelerometer data through a Cerebus recording system (Blackrock Microsystems) into Matlab (Mathworks) using Blackrock's Matlab interface (CBMEX). Using a custom matlab code we processed accelerometer data as described above. We monitored mice acceleration using bins of 300 ms and when mice reached 900 ms below the threshold used to identify immobility, light was delivered with a 50% probability. There was a minimum of 30 s between trials.

Statistics

Statistical hypothesis testing was done at a 0.05 significance level (except for classification of neurons which was done at a 0.01 significance level as explained above). Parametric testing was used whenever possible to test differences between two or more means. Normality was tested using the Shapiro-Wilk test, while F-test (for unpaired t-tests) was used to assess equality of variance. If data was not normally distributed, we first tried to transform the data using the natural logarithm. If the distribution of the transformed data was still not normally distributed or there was a significant difference in variance, an alternative non-parametric test was used. Lnear mixed models were used to check for main effects and interactions in experiments with repeated measures and more than one factor. The assumptions for linear mixed regressions were checked by careful inspection of the model residuals to check for normality and equality of variances. When main effects or interactions were significant, we did planned comparisons according to experimental design. Least Square Means (LSM) was used for planned comparisons when linear mixed models were significant. Statistical tests were done

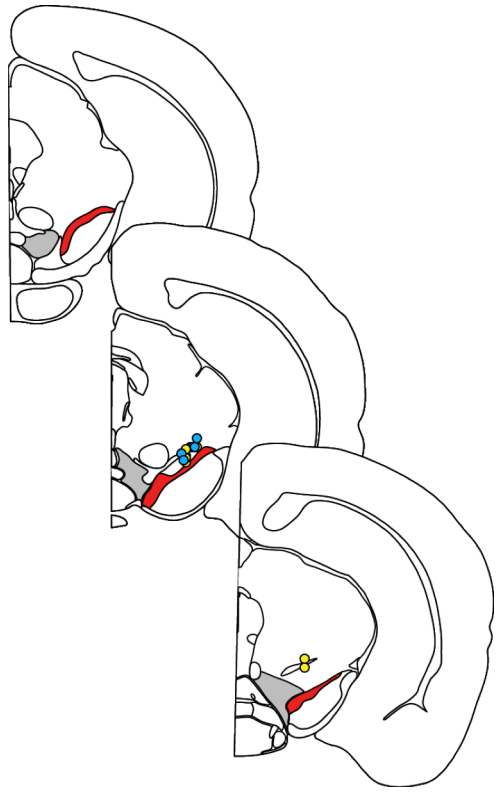

Figure 1.25 I Anatomical location of fiber tip in ChR2 (blue) and YFP mice (yellow)

using Prism (GraphPad), Matlab (MathWorks) statistical toolbox, R (R core team 2015, v. 3.1.3, *lme* (Bates et al. 2015)).

Anatomical verification of lens and fiber placement

Animals were sacrificed after completion of the experiments. First, animals were anaesthetized with isofluorane, followed by intraperitoneal injection of ketamine/xylaxine (~5 mg kg−1 xylazine; 100 mg kg−1 ketamine). Animals were then perfused with Phosphate-buffered saline (PBS) 1X and 4% histological processing. Brains were kept in the 4% paraformaldehyde overnight and then transferred to PBS 1X solution. Brains were sectioned coronally in 50 µm slices (using a Leica vibratome VT1000S and kept in PBS solution before mounting or immunostaining treatment). Images were taken using a widefield fluorescence microscope (Zeiss AxioImager) and the tip of the longest fibre track was used to determine the anatomical location of the implants. This location was represented in the corresponding Allen Brain Atlas(Lein et al. 2007) slice (**Fig. 3.6**).

EXTENDED STATISTICAL TESTING DATA TABLE

Figure	Sample size (n)	statistical test	values
4.2c	ChR2(7); YFP(5)	Linear mixed model with mouse as the random effect and laser state and group as fixed effect.	Main effects: Group, F(1,10)=1.86 *P*=0.20; **Laser F(1,10)= 9.58, P=0.013**; **Group*laser, F(1,10)=11.63, *P*=0.007**. Planned comparisons: **CHr2 laser off - laser on *P*=0.001**, YFP laser off - laser on *P* = 0,55
4.2d	ChR2(7); YFP(5)	Linear mixed model with mouse as the random effect and laser state and group as fixed effect.	Main effects: Group, F(1,10)=2.98 *P*=0.12; Laser F(1,10)= 0.075, P=0.79; Group*laser, F(1,10)=1.31, *P*=028. Planned comparisons: CHr2 laser off - laser on, *P*=0.37; YFP laser off - laser on *P* = 0,50
4.4a	ChR2(5); YFP(5)	Linear mixed model with mouse as the random effect and laser state and time as fixed effects.	ChR2: Main effects: **laser, F(1,4)=7.86 *P*=0.049, time F(49,392)=3.52, *P*<0.0001; laser*time, F(49,392)=2.46, *P*<0.0001.** Least square means was used for pairwise comparisons (on-off) at each time point. In the figure is shown by the horizontal line the point in time were these comparisons were consecutively significant. YFP: Main effects: laser, F(1,4)=1.96 *P*=0.23; time F(49,392)=8.38, *P*<0.0001; laser*time, F(49,392)=1.25, *P*=0.13.
4.4b	ChR2(5); YFP(5)	Linear mixed model with laser state nested within mouse as the random effect and laser state and group as fixed effects.	Main effects: **laser, F(1,8)=7.88 *P*=0.023, group F(1,8)=5.83, *P*=0.042; laser*group, F(1,8)=7.77, *P*=0.024.** Planned comparisons: **CHr2 laser off - laser on *P*=0.0042**, YFP laser off - laser on *P* = 0,99
4.4c	ChR2(5); YFP(5)	Linear mixed model with laser state nested within mouse as the random effect and laser state and group as fixed effects.	Main effects: **laser, F(1,8)=9.33 *P*=0.0157, group F(1,8)=6.43, *P*=0.035; laser*group, F(1,8)=3.19, *P*=0.11.** Planned comparisons: **CHr2 laser off - laser on *P*=0.009**, YFP laser off - laser on *P* = 0,40
4.4d	ChR2(5); YFP(5)	Linear mixed model with laser state nested within mouse as the random effect and laser state and group as fixed effects.	Main effects: **laser, F(1,8)=7.49 *P*=0.026, group F(1,8)=8.343, *P*=0.020; laser*group, F(1,8)=4.58, *P*=0.065.** Planned comparisons: **CHr2 laser off - laser on *P*=0.009**, YFP laser off - laser on *P* = 0,68
4.5b	ChR2(5)	Paired t-test	**T(4)=3.19, *P*=0.033**

Chapter 5 | Activity of SNc DANs modulates the initiation but not the execution of an action sequence

Summary

In the previous chapters we showed that most DANs increased their activity before movement initiation and in some cases this activity predicted the vigor of the initiated movement. In accordance, inhibition of DANs impaired movement initiations while activation promoted and invigorated them. Interestingly, neither activation nor inhibition changed movements already ongoing.

In this chapter, we explore the role of SNc DANs in self-paced action sequences. In these experiments mice learned to press a lever eight times to get access to a reward. In light of our previous findings we wanted to know whether SNc DANs had a specific role in the initiation of the whole sequence, or each element of the sequence. If each movement in a sequence becomes concatenated or chunked into sequences of movements, then DAN activity before a sequence would modulate sequence initiation but activity during the sequence would not modulate the execution of the concatenated movements.

First we recorded SNc DAN activity during early and late training of the action sequence. At the end of training there were more significantly modulated neurons to the first press than to the other presses in the sequence. In fact the number of first press related neurons was similar to the number of reward related neurons, although these two populations were mostly non-overlapping.

To understand whether this press related activity had a causal role, we inhibited SNc DANs in two different moments of the action sequence: before the first lever press and after the first lever press. We found that inhibition of SNc DANs before the first lever press led to an increased latency to initiate the action sequence, while inhibition after the first press did not affect the execution of the action sequence.

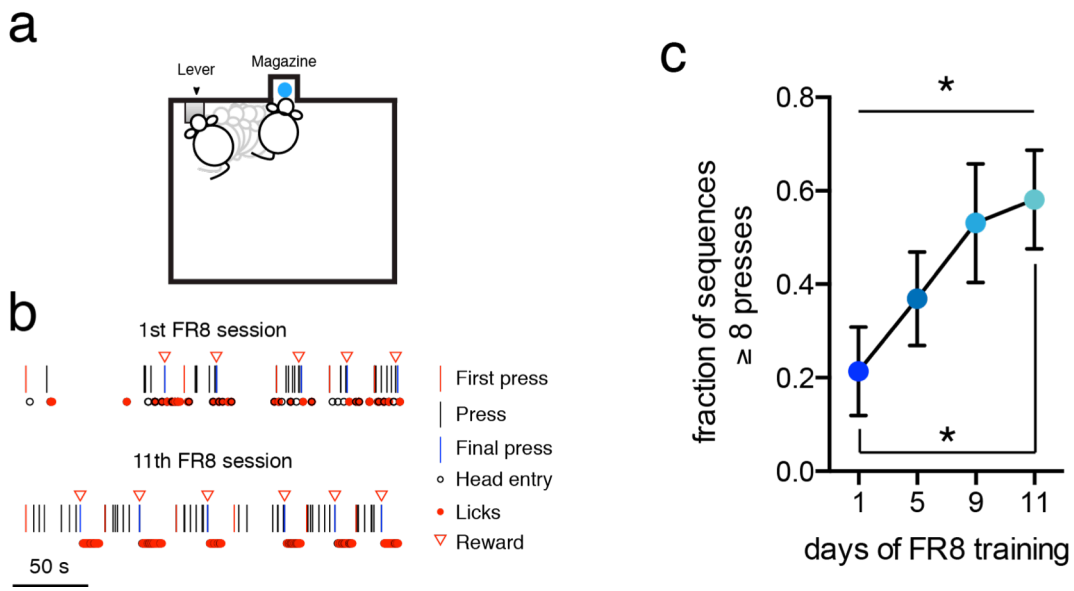

Figure 1.26 | Mice are able to learn an action sequence

a, Schematics of the operant box mice were trained in. The lever is presented left of the reward delivery magazine. **b**, Example of a mouse's behavior inside the operant box on the first day and last day of training. **c**, Fraction of sequences (breaking sequences when mice lick) per day of training (n=6).

RESULTS

SNc DANs are transiently active before the initiation of action sequences

The results presented in previous chapters highlight a specific role for transient dopamine activity in gating self-paced movement initiation but not for modulating ongoing movements. Based on these findings, one prediction would be that if individual spontaneous movements are concatenated or chunked into sequences of movements, then DAN activity before a sequence would modulate sequence initiation but activity during the sequence would not modulate the execution of the concatenated movements. This is in accordance with previous studies showing that DAN activity related to action initiation/termination emerges during action sequence learning (Jin & Costa 2010; Wassum et al. 2012). To test this prediction, we trained mice in a self-paced operant task in which eight lever presses led to a sucrose 20% solution reward (fixed ratio eight task, FR8), without any explicit stimuli signalling the availability of reward (Jin & Costa 2010) (**Fig. 5.1**). First mice

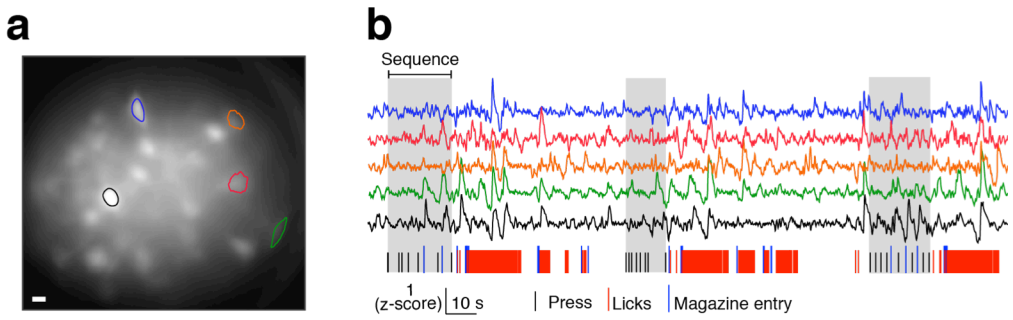

Figure 1.27 I Imaging SNc DANs while mice perform the FR8 task

a, Example of a field of view of a Th-Cre mouse expressing GCaMP6f in the SNc. Horizontal white bar denotes 20 μm. Pixel intensity represents the standard deviation of that pixel during the recorded session. Colored contours indicate the ROIs used to obtain the same color traces in b. **b**, Example of traces obtained using the CNMF-E algorithm and task related behaviors for one session. Color of traces matches the ROIs shown in a.

learned to press the lever once to obtain the sucrose reward. When they were able to achieve the reinforcement schedule was changed to FR8 where mice had to press the lever 8 times to get access to a sucrose reward. Because mice already learned how to press the lever, they were able to obtain rewards even in the first session of FR8. However, their behaviour in the first sessions was not structured into sequences and lever presses were often interrupted by head entries and licks (**Fig. 5.1b**). As training progressed the fraction of sequences with 8 or more presses increased (**Fig. 5.1c**). Also, with training, mice developed a predictable path from the magazine to the lever (i.e. it became highly probable that a mouse went from the magazine to the lever right after consuming the reward).

To investigate the relation between DAN activity and the learned action sequence, we used the same strategy and mice described in Chapter 2 to image SNc DANs (**Fig 2.9**). We implanted a gradient index (GRIN) lens (500 μm diameter, 8.2 mm) just above the SNc of four Th-Cre mice and at the same time injected an adeno-associated viral vector to express GCaMP6f (Chen et al. 2013) in a Cre-dependent manner (Atasoy et al. 2008) (AAV2/5.CAG.Flex.GCaMP6f). We then used a miniaturized epifluorescence microscope (Ghosh et al. 2011) to image calcium transients in genetically identified SNc DANs while mice were performing the FR8 task (**Fig. 5.2**). We created peri-event time histograms (PETHs) using normalized fluorescence (z-score of ΔF) traces aligned to six different events during the sequence (first, second, third, third to final, second to final and final press of each sequence).

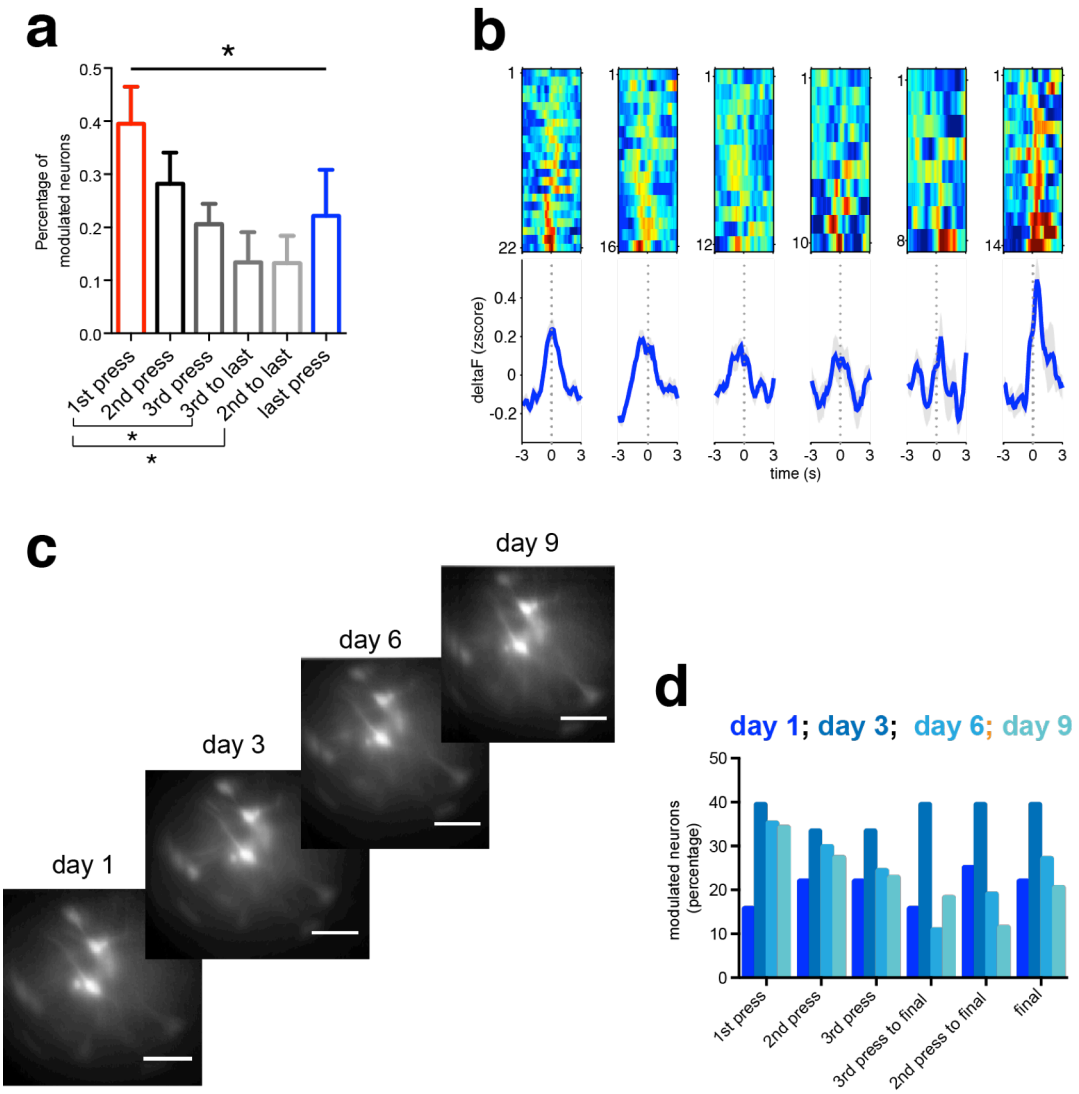

Figure 1.28 I SNc press related neurons at the end of training and during training

a, Percentage of neurons modulated by the different presses within a sequence at the end of training. **b**, Heat map of the PETH of positively modulated neurons for each press event (top panel) and the average of these PETHs (bottom panel), at the end of training. Gray shadow denotes s.e.m. **c,** Field of view of one of the GCaMP6 expressing mice across different training days spanning from the beginning to the end of training. **d**, Percentage of neurons significantly modulated by the sequence lever presses across training.

We quantified positively modulated neurons for each of the sequence events that were significantly different (≥ 3σ) from baseline (-5 to -2 s before first press, **see also methods for details**). We also quantified neurons positively modulated by reward that were significantly different (≥ 3σ) from baseline (-5 to -2 s before first lick, **see also methods for details**). Similarly to previous findings (Jin & Costa 2010), we found that the proportion of modulated neurons was different between press events, with the highest proportion (39%) of neurons being modulated by the first press (**Fig. 5.3a,b**). One advantage of this imaging technique is that it allows the tracking of neurons over

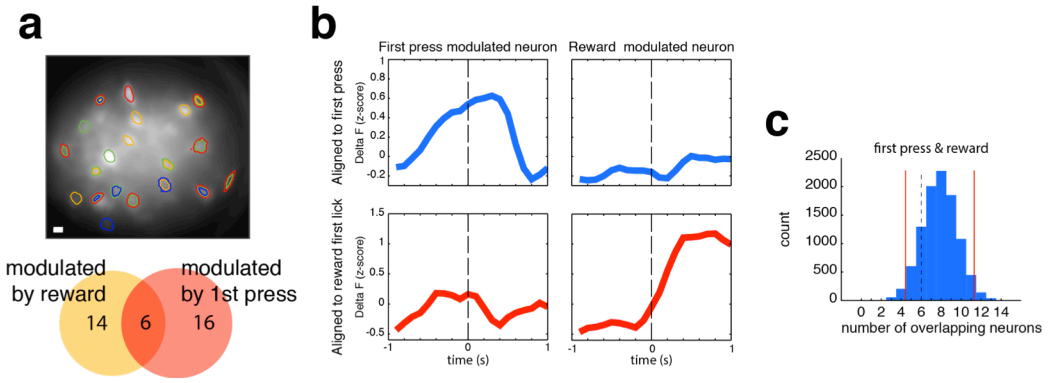

Figure 1.29 | Relation between first press related neurons and reward related neurons

a, Example of the map of significantly modulated ROIs for one mouse. Red, green and blue represent ROIs modulated by the first, middle and last press correspondingly. Orange ROIs correspond to neurons modulated by reward. Bottom, Venn diagram representing the overlap of reward related and first press related neurons. **b**, Example of a neuron modulated by first press but not reward (left plots) and a neuron related to reward but not first press (right plots), aligned to first press (blue) and reward consumption (red). **c**, Monte Carlo simulation (10000 samples) to determine a distribution of the number of overlapping neurons for first press and reward assuming a random assignment. Red lines denote a 95% confidence interval. Dashed line represents the number of overlapping neurons found in our experiment.

different experimental days. In three of the mice used in this experiment, we recorded the activity of SNc neurons throughout training (**Fig. 5.3c,d**). By doing so we could compare the proportion of positively modulated neurons for each press. Interestingly, the higher proportion of neurons related to first press that we saw late in training was not apparent early in training (**Fig. 5.3d)**. We also quantified the proportion of neurons positively modulated by reward consumption (aligning traces to the first lick with reward available). We found a similar percentage of neurons modulated by first press and reward (34.7 ± 16% reward neurons and 39.5 ± 14% first press neurons, **Fig. 5.4a,b**). Importantly, the overlap of reward with first press neurons was not significantly different of that expected by chance with most neurons being either just first press related or reward related (**Fig. 5.4c**).

Inhibiting the activity of DANs impairs action sequence initiation

As we described in the beginning, with training mice adopted a predictable path between the magazine and the lever. This meant that the initiation of an action sequence became predictable. To be able to detect when mice initiated the approach to the lever, we placed an infrared beam right next to the magazine, at the beginning of the path between the magazine and lever. This allowed us to detect when mice were going to initiate a new sequence (breaking the IRB after consuming a reward) and quantify the latency to initiate a sequence (time between IRB break and first lever

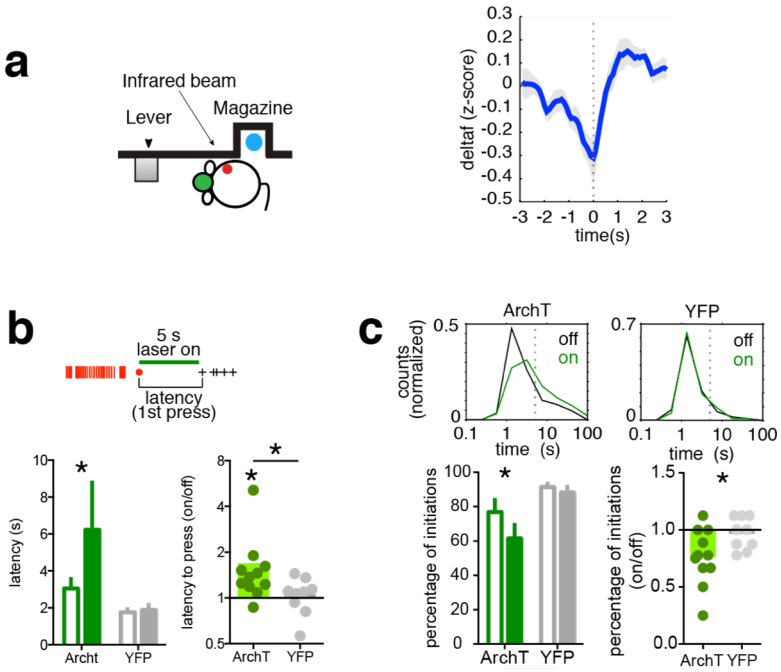

Figure 1.30 l Inhibition of SNc impair action initiation

a, First lever press neurons aligned to the moment when mice cross from the magazine in direction of the lever, before the first lever press. This is the same event that triggers DAN inhibition in the ArchT experiments (n=22 neurons). **b**, Latency to initiate lever press sequence for laser-off trails and trials with inhibition starting just before sequence initiation for both ArchT (n=11) and YFP (n=9) groups. Right plot shows the mean latency to sequence initiation during laser-on trials normalized by the latency during laser-off trials. **c**, Left, distribution of latencies for laser-on and laser-off trials, for the ArchT and YFP groups. Right, percentage of late initiations (latency >5 s) for laser-off trails and trials with inhibition starting just before sequence initiation for both ArchT (n=11) and YFP (n=9) groups.

press). Next we tested whether SNc DAN activity was necessary for appropriate sequence initiation and execution. To achieve this we used the same strategy described in chapter 3 to express an inhibitory opsin (ArchT) in SNc DANs. We trained these mice expressing ArchT (n=11) in the FR8 task and late in training they developed predictable sequence initiations and trajectories after reward consumption (Tecuapetla et al. 2016). In one experiment we assessed whether SNc DANs were relevant for appropriate sequence initiation by starting inhibition of these neurons when mice broke the IRB while going from the magazine to the lever and after reward consumption. Using the data acquired in the previous experiment we aligned the activity of first press related neurons to the moment mice broke the IRB and found that the increase in activity happened after this event (**Fig. 5.5a**). This suggests that inhibition initiated on breaking the IRB could avoid the increase in activity related to the first press of the sequence.

In a second experiment we triggered the inhibition of SNc DANs after mice performed the first lever press to assess the role of these neurons in the execution of the sequence. In both experiments inhibition lasted for 5 s and we compared a block of 9

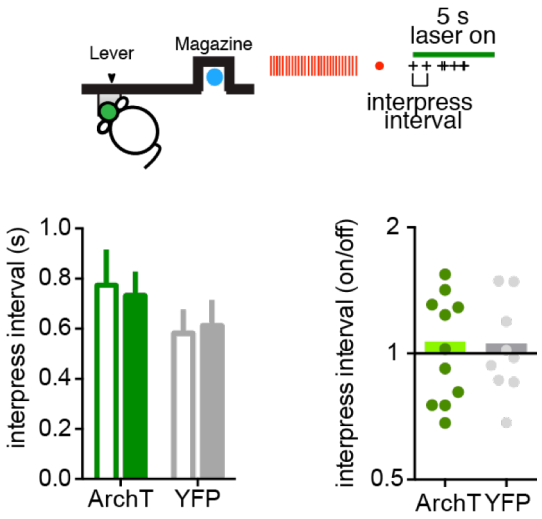

Figure 1.31 | Inhibition of SNc DANs does not impair sequence execution

Left; press rate in trials with no light delivery and trials with light delivery starting after the first press for both ArchT (n=11) and YFP (n=9) groups. Right; mean press rate during laser-on trials normalised by mean press rate during laser-off trials.

sequences with inhibition (laser-on block) with a previous block without inhibition (laser-off block) during the same session. Also, a YFP group (n=9, no inhibitory opsin) was used to control for unspecific light effects. Inhibition during 5 s before the first lever press resulted in a significant increase in the latency to initiate the action sequence when compared to laser-off trials (**Fig. 5.5b**). Moreover, the proportion of trials with latencies longer than 5 s was also significantly increased (**Fig. 5.5c**). However, the sequence inter-press interval was not perturbed during a 5sd inhibition triggered by the first press (**Fig. 5.6**). No effects were observed in YFP controls (**Fig. 5.5, 5.6**). These findings were replicated using DAT IRES-Cre mice using a different inhibitory opsin (Jaws, Chuong et al. 2014) and inhibiting pseudorandomly 30% of the trials (**Fig. 5.7, see methods for details**).

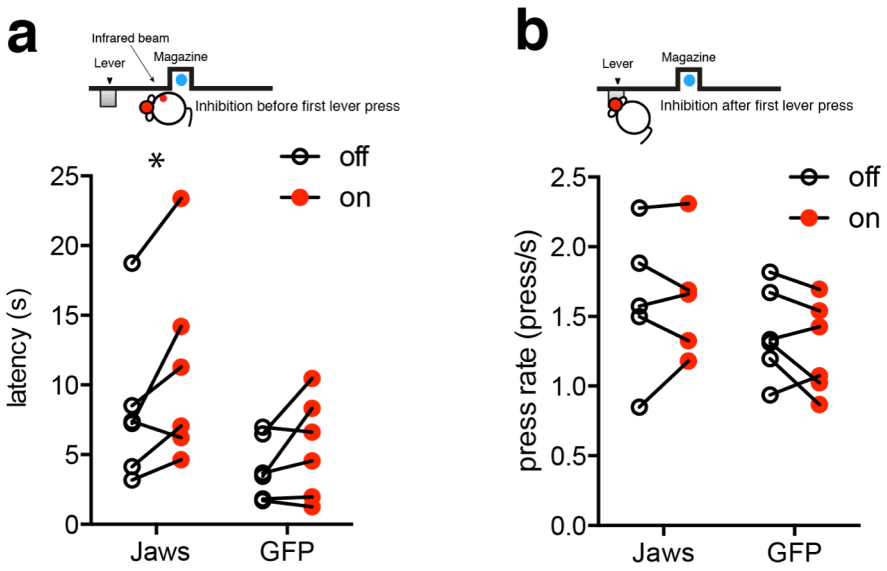

Figure 1.32 | FR8 inhibition experiment using Jaws in DAT-Cre mice

We replicated the result obtained in the FR8 task with ArchT, using Jaws opsin (see methods for details of the experiment). **a**, Latency to initiate a lever press sequence for laser-off trails and trials with inhibition starting before sequence initiation for both Jaws (n=6) and GFP (n=6) groups. **b**, Press rate in trials with no light delivery and trials with light delivery triggered by the first press for both Jaws (n=6) and GFP (n=6) groups.

METHODS

Animals

All experiments were approved by the Portuguese DGAV and Champalimaud Centre for the Unknown ethical committee and performed in accordance with European guidelines. TH-Cre male mice from the FI12 mouse line (Gong et al. 2007) between 3 and 5 months.

Recombinant adeno-associated viral vectors

The following Cre-dependent adeno-associated viral vectors were used in the experiments:
AAV2/5.CAG.Flex.GCaMP6f.WPRE.SV40 (titre 1.19 × 10^{13}, University of Pennsylvania); AAV2/1.CAG.Flex.ArchT-GFP (titre 1.4 × 10^{12}, University of Pennsylvania); AVV2/1.EF1a.DIO.eYFP (titre 1.4 × 10^{13}, University of North Carolina); AAV8/hSyn.Flex.Jaws-GFP (titre 4.2 × 1012, University of North Carolina); rAAV8/hSyn.DIO.eGFP, (titre 4.9 × 1012, University of North Carolina).

Virus injections, lens and fiber placement

Surgeries were performed using a stereotaxic system (Kopf). Mice were kept in deep anestheia using a mixture of Isofluorane and oxygen (1-3% Isofluorane at 1 l min^{-1}).
For imaging experiments 1 μL of virus solution was injected in the right substantia nigra compacta at the following coordinates: -3.16 mm anteroposterior, 1.40 mm lateral from bregma and 4.20 mm deep from the brain surface. The injection was done through a glass pipette using a Nanojet II (Drummond Scientific) with a rate of injection of 4.6 nl every 5 s. After the injection was finished the pipette was left in place for 10-15 min. The virus solution was kept at -80 ºC and thawed at room temperature just before the injection. A 500 μm diameter 8.2 mm long GRadient INdex (GRIN) lens (Part ID: GLP-0584, Inscopix) was implanted at the same coordinates as the injection. Before the lens was lowered, a blunt needle 28 g was lowered to 3 mm deep from the brain surface to facilitate the lowering of the GRIN lens. Then the GRIN lens was lowered (4.2 mm

deep). The lens was fixed in place using cyanoacrilate and black dental cement (Ortho-Jet). One 1/16 inch stainless steel screw (Antrin miniatures) was attached to the skull to provide a scaffold to build a dental cement based cap that protected and fixed the lens to the skull.

Three weeks after this surgery the mouse was anesthetized and fixed with head bars. A baseplate (Part ID: BPC-2, Inscopix) attached to a mini epifluorescence microscope (nVista HD, Inscopix) was positioned above the GRIN lens. To position correctly the baseplate, brain tissue was imaged through the lens to find the appropriate focal plane using 20% of LED power, 5 Hz of frame rate and a digital gain of 4. Once the focal plane was set, the baseplate was cemented to the rest of the cap using the same dental cement. Imaging started 2-3 days after this final step.

For optogenetic experiments, the surgical set-up and method was used. 1.5 μL virus solution (ArchT or YFP) was injected bilaterally at 2.3 nl every 5 s bilaterally in the SNc at the following coordinates: -3.16 mm anteroposterior, 1.40 mm lateral from bregma and 4.20 mm deep from the brain surface. The injection was done through a glass pipette using a Nanojet II (Drummond Scientific) with a rate of injection of 4.6 nl every 5 s. After the injection was finished the pipette was left in place for 10-15 min. The virus solution was kept at -80 ºC and thawed at room temperature just before the injection. Using the same cranial holes, optical fibers with 230 μm diameter and a NA of .39 (Thorlabs FMT 200 EMT) were placed bilaterally at 3.9 mm deep from the brain surface. Optical fibers were built based on a published protocol (Sparta et al. 2012). To support the cap, two small stainless steel screws (Antrin miniature Specialties #00-90x 1/16 SL Bind SST) were screwed into the skull of the mouse lateral to the holes. A cap was built with dental cement around the fibers and screws. For the Jaws experiment, the same procedure was followed except that it was injected1 μL of virus (Jaws or and optical fibers with 400 μm diameter and a NA of .5 (Thorlabs FP400URT) were implanted at the same depth.

Optogenetic setup

For ArchT experiments, light from a free launched 500-mW, 556-nm, diode-pumped, solid-state laser from CNI Lasers), controlled using an AOM (AA Optolectronic), was delivered after being captured by a collimator and split using a one-input to two-outputs rotary joint (Doric Lenses). Two hundred nm, .22 NA optical fiber patch cords were used to guide the light to the fibres implanted in the mice.

For the Jaws group and corresponding controls we used a red LED (~100 mW max output, ~625 nm, Prizmatix). The light was captured by a large diameter optical fibre (1mm) which connected to a one-input to one-output rotary joint. A branched 500μm optical fibre was then used to connect to the fibers implanted in the mice.

Light intensity was measured before and during experiments using a fiber similar to the ones implanted and a power meter (PD1000-S130C, Thorlabs). The power was adjusted at the tip of the fiber to be ~35 mW for ArchT experiments and ~9 mW in Jaws experiments.

Light intensity was measured before and during experiments using a similar fiber to the ones implanted and a Photodiode Power Sensor (PD1000-S130C, Thorlabs). The power was adjusted at the tip of the fibre to be ~35 mW.

FR8 operant task

Behaviour training and testing took place in operant chambers as described previously (Jin & Costa 2010). Briefly, each chamber (23 cm L × 20cm W × 19.5 cm H) was housed within a sound attenuating box (Med-Associates, St. Albans, VT) and equipped with one retractable lever on the left side of the food magazine and a house light (3 W, 24 V) mounted on the left lateral wall. Sucrose solution (10 %) was delivered into a metal cup in the magazine through a syringe pump (20 μL per reward). Magazine entries were recorded using an infrared beam and licks using a contact lickometer. Mice were placed on food restriction throughout training, and fed daily after the training sessions with ~2 g of regular food to allow them to maintain a body weight of around 85 % of their baseline weight.

Training started with a 30 min magazine training session in which the reinforcer was delivered on a random time schedule, on average every 60 s (30 reinforcers). The following day lever-pressing training started with continuous reinforcement (CRF), in which animals obtained a reinforcer after each lever press. The session began with the illumination of the house light and insertion of the lever, and ended with the retraction of the lever and the offset of the house light. In the first day of CRF the sessions lasted 45 min or until mice received five reinforcers, the second day of CRF lasted 45 min or until mice received 15 reinforcers, and the last day of CRF lasted 45 min or until mice received 30 reinforcers. This last CRF session was repeated if mice failed to obtain 30 rewards within the time limit. After CRF, animals started to be trained (day 1) on a fixed ratio schedule in which eight presses earn a reinforcer (FR8), without any stimulus

signalling when eight presses were completed or when the reinforcer was delivered; this training continued for 12-14 days.

All timestamps of lever presses, magazine entries and licks for each animal were recorded with a 10 ms resolution. The same training chamber was used during imaging and optogenetic experiments.

Calcium image processing and analysis

GCaMP6f image processing and fluorescence trace extraction

All fluorescence movies were initial processed using the Mosaic Software (version 1.1.2, Inscopix). First all frames were spatially binned by a factor of 4. To correct the movie for translational movements and rotations, the frames were registered to a reference image consisting of an average of the all raw fluorescence movie. This was achieved by implementing the TurboReg registration engine (Thévenaz et al. 1998) within the mosaic software. The movie was cropped after registration to remove the post-registration black borders.

GCaMP6f fluorescence trace extraction

Although calcium imaging using miniscopes enables researchers to image neurons in freely moving mice, it is a challenge to adequately extract neuronal signals without background contamination. Because of this we implemented the Constrained non-negative matrix factorization for endoscopic data (CNMF-E) framework (Zhou et al. 2016). This recently described framework is an adaptation of the CNMF Algorithm (Pnevmatikakis et al. 2016). It can reliably deal with the large fluctuating background from multiple sources in the data, allowing the accurate source extraction of cellular signals. It includes four steps: (1) initialize spatial and temporal components of single neurons without the direct estimation of the background; (2) estimate the background given the estimated neurons' spatiotemporal activity; (3) update the spatial and temporal components of all neurons while fixing the estimated background fluctuations; (4) iteratively repeat step 2 and 3. We briefly describe the algorithm used in our work, which is based on the work developed by others (more details can be found in the preprint of the CNMF-E paper (Zhou et al. 2016) and in (Klaus et al 2017)). In the initialization step, we first used a mean-subtracted 2D Gaussian kernel to filter the raw

video data. The parameters of this kernel are selected to resemble the distribution of soma diameters ($\mu_{CNMF\text{-}E}$=0, $\sigma_{CNMF\text{-}E}$=6.9 µm, maximum soma diameter $d_{CNMF\text{-}E}$=34.5 µm).

Filtering the data with this kernel acts as a template matching to find all morphological shapes similar to a soma. In the filtered data, the background is approximately removed because it is almost flat within the spatial range of the kernel, and the kernel integrates to zero. In contrast, soma shapes are preserved and become more visible because they match the template shape. As a result, we can accurately extract each neuron's calcium activity from the fluorescence at its center pixels (so-called seed pixels) in the filtered data. Furthermore, we used a method to detect seed pixels by choosing pixels with high local correlations and signal-to-noise ratio (SNR). Given a seed pixel, we initialize one neuron by estimating its temporal activity as the temporal trace of the pixel in the filtered data. To get its spatial component, we crop a small square with the size of 2 times larger than a cell body centered at the seed pixel from the raw data. Then we estimate the background fluctuation within the cropped area as the median in each frame. For each pixel within the selected square, we assume its fluctuations are from two sources: one is the initialized neuron and the other one is the background fluctuation. Since we have the temporal traces for all these two sources, we run linear regression to get the weights for each component and the weights corresponding to the neural activity lead to our initialization of the spatial footprints. Once we have both the spatial and temporal component of this neuron, we subtract its spatiotemporal activity from the raw video data and repeat the same procedure to initialize another neuron until the specified number of neurons has been detected or no more seed pixels can be found. This greedy initialization method is able to efficiently and accurately detect almost all neurons. In the next step, we estimate the background activity for each pixel individually. For each pixel, we first choose its neighbors with a distance larger than neuron size. Accordingly, these pixels do not share the same cellular activity but they share the same sources of the background. Then we use the projection of this pixel's temporal trace on a linear span of its neighbors' traces as its estimated background fluctuations. Finally, we subtract this estimated background from the raw video data and update all neuronal spatial and temporal components using alternating matrix factorization (Pnevmatikakis et al. 2016; Zhou et al. 2016; Friedrich, Zhou, and Paninski 2016).

Criteria to identify lever press related GCaMP6f neurons

We constructed a PETH for each neuron trace spanning from -3 to 3 s from lever press onset for the first, second, third, third to final, second to final and final press, and also for the first lick of reward. Distributions of the PETH from -5 to -3 s before first lever press were considered baseline activity for all press related activity and distributions from -5 to -3 s before the first lick of reward PETH was considered as baseline for reward related activity. We then searched each PETH during an epoch spanning from -0.5 s to 0.5 s for bins that would be significantly different from the baseline. A significant change in fluorescence was defined as at least 3 consecutive bins had fluorescence higher than a threshold of 99 % above baseline ΔF/F0.

Inhibition during FR8 task

The same groups of ArchT and YFP mice used in the open field inhibition experiment were trained to perform the FR8 task. Optogenetic experiments were started at the end of the FR8 training. We used two different light delivery schedules: Continuous light delivery for 5 s before the first lever press in a sequence; and continuous light delivery for 5 s after the first lever press in a sequence. For the first condition we made the triggering of the light contingent on the breaking of an infrared beam (IRB) positioned just next to the magazine, on the side of the lever. This way mice coming from consuming the reward would break the IRB before they started the next sequence. Sessions were divided into two blocks: A first block of 15 trials without light delivery; and a second block of 10 trials with light delivery. The last 10 trials with no light delivery were used to compare with the 10 trials with light delivery. In a few trials the mouse failed to break the IRB before starting the action sequence. These trials were discarded and not included in the analysis. We used the median latency to first lever press and mean interpress interval within the first 5 s of the sequence to compare laser-on with laser-off trials for each group. Sessions with no light delivery were interspersed between sessions with light delivery and a first session with light delivery was used just to habituate the mice to the delivery of light and it was not analysed. The same methodology was used in Jaws experiments with the exception that instead of light-on and light-off blocks there was a 30% probability of switching on the laser on each trial and data was collected in three consecutive sessions for each experimental condition (inhibition before initiation and inhibition after first press).

Anatomical verification of lens and fiber placement

Animals were sacrificed after completion of the experiments. First, animals were anaesthetized with isofluorane, followed by intraperitoneal injection of ketamine/xylaxine (~5 mg kg−1 xylazine; 100 mg kg−1 ketamine). Animals were then perfused with phosphate-buffered saline (PBS) 1X and 4% paraformaldehyde, and brains extracted for histological processing. Brains were kept in the 4% paraformaldehyde overnight and then transferred to PBS 1X solution. Brains were sectioned coronally in 50 µm slices (using a Leica vibratome VT1000S and kept in PBS solution before mounting or immunostaining treatment). Images were taken using a widefield fluorescence microscope (Zeiss AxioImager) and the tip of the longest fibre or lens track was used to determine the anatomical location these implants. This location was represented in the corresponding Allen Brain Atlas (Lein et al. 2007) slice (**Fig. 2.9 & 3.7**).

EXTENDED STATISTICAL TESTING DATA TABLE

Figure	Sample size (n)	statistical test	values
5.1c	4 GCaMP TH-Cre mice + 2 YFP TH-Cre mice	Friedman test	**F=11.60; *P*=0.003**; Dunn's multiple comparisons between first lever and the rest: Day 1 vs. 5, *P*>0.99; 1 vs. 9, *P*=0.076; **1 vs. 11, *P*=0.0052**;
5.3a	GCaMP6 TH-Cre mice(4)	Friedman test	**F=12.33; *P*=0.031**; Dunn's multiple comparisons between first lever and the rest: 1st vs. 2nd, *P*>0.99; 1st vs. 3rd, *P*=0.12; **1st vs. 3rd to last, *P*=0.031**; **1st vs. 2nd to last, *P*= 0.031**; 1st vs. last, *P*=0.29
5.5b (left)	ArchT(11), YFP(9)	Linear mixed model with laser state nested within mouse as random effect and laser state and group as fixed effects. Data was ln transformed to achieve residual normality.	Main effects: **laser, F(1,18)=6.97, *P*=0.017**; **group F(1,18)=4.79, *P*=0.042**; **laser*group, F(1,18)=4.62, *P*=0.046.** Planned comparisons: **CHr2 laser off - laser on *P*=0.0032**, YFP laser off - laser on *P* = 0,86
5.5b (right)	ArchT(11), YFP(9)	One sample Wilcoxon Signed Rank against 1 and Mann-Whitney test (ArchT vs. YFP)	Wilcoxon vs. 1: **ArchT, W=62, *P*=0.003**, YFP, W=15, *P*=0.43 **ArchT. vs.YFP: U=19; *P*=0.02**
5.5c (bottom left)	ArchT(11), YFP(9)	Linear mixed model with laser state nested within mouse as random effect and laser state and group as fixed effects.	Main effects: **laser, F(1,18)=10.42, *P*=0.0047**; **group F(1,18)=4.54, *P*=0.047**; laser*group, F(1,18)=3.87, *P*=0.0647**.** Planned comparisons: **CHr2 laser off - laser on *P*=0.0016**, YFP laser off - laser on *P* = 0,49
5.5c (bottom right)	ArchT(11), YFP(9)	One sample t-test against 1 and independent samples t -test (Welch corrected)	t-test vs. 1: **ArchT, t(10)=3.17, *P*=0.01**, YFP, t(8)=0.18, *P*=0.70 **ArchT. vs.YFP: t(16.5)=2.32; *P*=0.034**
5.6 (left)	ArchT(11), YFP(9)	Linear mixed model with laser state nested within mouse as random effect and laser state and group as fixed effects.	Main effects: laser, F(1,18)=0.034, *P*=0.86; group F(1,18)=1.04, *P*=0.32; laser*group**,** F(1,18)=0.44, *P*=0.51**.**
5.6 (right)	ArchT(11), YFP(9)	One sample t-test against 1 and independent samples t -test (Welch corrected)	t-test vs. 1: ArchT, t(10)=0.73, *P*=0.48, YFP, t(8)=0.60, *P*=0.57 ArchT. vs.YFP: t(17.69)=0.090; *P*=0.92

Chapter 6 | Discussion

One must stop conducting research before one has finished. Otherwise, one will never stop and never finish.

Barbara Tuchman

What is the role of dopamine neurons in movement initiation? In different forms, this question as attracted the attention of researchers over the past 30 years. However, as we described in the introduction, the answer to this question is still unclear. One reason for this is the fact that much of the focus of research regarding DANs switched to understanding the role of dopamine neurons in reward error prediction. The reigning dichotomy that has dominated the field in the last decades states that movement related functions of dopamine are due to their tonic activity, while their role in reward error prediction is due to their phasic activity. What is different now? Why should one revisit this question? Neuroscience like other fields of science is ever evolving. In the last few years new methods emerged that allow a new approach into this question. For example, the development of new transgenic mice lines that enable genetic tagging of neural populations. This paired with the optogenetic methods that were emerging when this work started allowed for a new way to identify SNc DANs, record their activity and interrogate their role by manipulating their activity with a high temporal resolution.

Using these techniques we uncovered that most SNc DANs are significantly modulated by spontaneous movement initiation. However neuron modulation is heterogeneous with some neurons being negatively modulated while the majority are positively modulated. Although positively modulated neurons have a diverse profile they all increase firing before the initiation of movement while almost all negatively modulated neurons decrease their firing rate very close to or after movement initiation. This suggested that activation of dopaminergic neurons could have a causal role in spontaneous movement initiation. With our optogenetic experiments we showed that in fact SNc DAN activity modulates self-paced movement initiation and that a brief activation of SNc DANs is sufficient to promote movement initiation. We also showed that SNc DAN activity modulates the initiation of a learned action sequence.

Importantly, our precisely-timed and state-dependent optogenetic manipulations in both open field and operant behaviour experiments did not change ongoing spontaneous movements or ongoing learned action sequence performance respectively.

Transient increase in SNc DAN activity precedes the initiation of movements

In this study we found that most SNc DANs are significantly modulated by spontaneous movement initiation in a fast time scale. Although this finding may not seem surprising given the movement initiation impairments found in PD (Berardelli et al. 2001), it contradicts the current view that movement regulation happens only through slow tonic changes in the firing rate of SNc DANs (Niv et al. 2005; Schultz 2007). As we mentioned in the introduction, this current theory is fuelled by the fact that previous experiments did not show a clear relationship between the activity of DANs and movement on a fast time scale (Howe et al. 2013) or because this response seemed very mild when compared with the response related to rewards (Schultz & Romo 1990). To be precise, it is not that researchers did not see a relation between SNc DAN activity changes and movement initiation. Even in the early experiments with external recordings of putative dopamine neurons carried out by Schultz and Romo (Schultz et al. 1983; Schultz & Romo 1990; Romo & Schultz 1990), it was apparent that some SNc DANs were positively modulated by self-paced movement initiation. However, only a minority of these neurons were activated before movements were initiated. Also the magnitude of this modulation was much lower that the one reported during the same tasks when monkeys touched a food reward or as a response to a signal predicting the food reward. At that point it was already apparent, not only because of PD but also because of the effect of striatal dopamine depletions in animal models, that dopamine release in the striatum was necessary for movement. Thus their interpretation was that the non-modulated spontaneous activity of SNc DANs exerted a permissive effect on the activity of other neurons, MSNs or cortical neurons projecting to the striatum. However they did recognize that at that time it was not possible to understand whether the mild changes in activity preceding movement initiation were relevant or not (Romo & Schultz 1990). This was technically unapproachable with the methods available then.

Why are our results different? There are striking methodological differences between our work and previous studies. Much of the previous work using extracellular recordings of putative SNc DANs relied on the identification of DANs based on

physiological properties such as firing rate and wave shape and length (read our note in the introduction). Although neurons identified using these criteria in the SNc have been shown to be dopaminergic by juxtacellular labelling (Brown et al. 2009), it is less clear that the opposite has been shown, i.e. that all neurons that do not fit these criteria are not DANs. Also the studies on which these criteria have been based and many other studies that used these criteria to identify putative DANs, recorded the activity of neurons while animals were anesthetized (B S Bunney et al. 1973; Grace & Bunney 1983; Brown et al. 2009). This could have led to a bias in the identification of a subgroup of DANs in detriment of others. These problems are more apparent in the VTA, where it became obvious that the standard criteria were identifying both dopaminergic and non-dopaminergic cells (Ungless et al. 2004). When using an optogenetic approach (expression of ChR2 in SNc exclusively in dopaminergic or GABAergic neurons using a Cre recombinase approach), it was found that the waveform size was in fact not different between photoidentified dopaminergic and GABAergic neurons in the VTA with the authors concluding that many identified DANs would have been missed if previous criteria were used (Cohen et al. 2012). Our use of a similar genetically based tagging of DANs corresponds to the state of the art method for identifying specific neuron populations. It is possible that this allowed us to record neurons that would have been missed if we had employed external recordings using electrophysiological and pharmacology based criteria (Ungless & Grace 2012). Another important aspect related to DAN identification is that after the description of these neurons' response to reward, some authors started using the transient response to unpredictable reward as one of the criteria to identify putative DANs (Nomoto et al. 2010). It seems that this is in fact an important bias because it has been found that independently of originating in the VTA or the SNc, DANs that project to the dorsal-medial striatum do not respond to unpredictable reward but show transient responses depending on the direction of the action being selected (Parker et al. 2016). Once more, the method we used for identifying DANs does not suffer from this bias. In voltammetry studies, a similar bias is present, since fast cycling voltammetry studies have been mostly circumscribed to the ventral-medial striatum, where reward related projections seem to predominate and action/movement related neurons do not (Parker et al. 2016; Howe & Dombeck 2016).

However, the precision of our strategy to identify neurons depends on the specificity of the Cre line we used. In fact, TH-cre lines specificity has been questioned in a recent paper (Lammel et al. 2015). Nevertheless, it is important to underline that the authors

focused their analyses and criticism on the lack of specificity in the VTA and mainly on the more medial portion of the VTA, an area that we did not record from. These authors reported higher specificity of TH-cre lines for the SNc, which we confirmed by crossing our TH-cre line with a floxed reporter line (**Fig. 2.12**). Taking into consideration that we found a high specificity (95.3%) with such a strategy and also a high proportion of neurons modulated by initiation, our results cannot be accounted for by a specificity problem of our TH-cre line.

Chronic recording and photoidentification of single units in the SNc of freely moving mice is in our hands a challenging low yield technique. Although we used a genetic approach that enables the production of ChR2 in DANs in the SNc, we were only able to record 25 photoidentified units. The challenge lay in the fact that we could only use single units that had been successfully modulated by light with a very short latency and high probability. We think that this difficulty is not a particularity of our approach in the lab. For example, in one of the first seminal studies using photoidentification to identify DANs, the authors isolated only 26 neurons. This happened even though they used microdrives with 6 tetrodes coupled to a fiber and were recording in the VTA (Cohen et al. 2012). Nevertheless, based on the rational we presented above, we think that there is a net-gain in this trade-off (genetic identification/ low neuron number).

Another aspect that may contribute to the differences between our work and the work of others is the way we have defined movement initiation. To pin point when a movement starts is not as trivial as one may think. Also, a high temporal resolution was necessary for the proper alignment of movement initiation to electrophysiology data. Our use of inertial sensors not only provided us with a clear threshold to separate immobility from mobility, but it also made it possible with a high temporal resolution. A comparison with a video based analysis revealed that there was not such a clear bimodal separation when using video based measures (**Fig. 2.2**). Also it would have been very challenging, if not impossible, to use video measures with a resolution as high as the motion sensor resolution (200Hz) to image an open field. Also, because we placed the motion sensor on the head of mice, we could pick up head movements without locomotion as movement initiations, while this would have been much more difficult to discern if using only video based tracking of movement. In the early work by Schultz and Romo (Schultz & Romo 1990; Romo & Schultz 1990), they used electromyographic (EMG) recordings to decide when movement was initiated. This may explain the discrepancy between the latency of modulation of DANs that they reported

(most modulated neurons were changing activity with or after movement initiation), since EMG changes would be already apparent during the isometric contractions. This could be seen as evidence that increased DAN activity does not have a causal role in movement initiation. However, the manipulations we did do support a causal role for activity of DANs in movement initiation. It could be that in fact the initial isometric or small postural adjustments preceding the overt initiation of movement are not influenced by the activity of dopaminergic neurons.

We did not see only neurons positively modulated by movement initiation. In fact 28% of the modulated neurons were negatively modulated. This is perhaps an unexpected finding, since there is a tendency to regard SNc neurons as a homogeneous population. While this thesis was being developed and using a different strategy, other authors have also found a heterogeneous representation of movement initiation in midbrain DANs (Dodson et al. 2016). Using juxtacellular recordings in awake, head-fixed mice on top of a running wheel, they reported that SNc DANs were mostly inhibited at movement onset (similar to the inhibition cluster we showed in **Fig. 2.7**). However, they also reported that almost a third of SNc neurons increased firing rate before movement initiation (4/15 neurons). Interestingly, they reported that anatomically distinct groups of midbrain DANshad different profiles. More than one-third of DANs in the lateral VTA (5/14 neurons) and almost all DANs in substantia nigra pars lateralis (4/5 neurons) increased their firing rate just before the initiation of movement, without the decrease in firing rate after movement onset that was evident in SNc neurons. The discrepancy between the proportion of positively modulated and negatively SNc modulated neurons we described and the proportions described in this study could be due to significant methodological differences. Although these authors used juxtacellular labelling to identify whether the neurons were dopaminergic or not, they could have been biased to record from neurons with the classical DAN electrophysiology profile. Because they were moving the electrode and recording one neuron at a time, using a very challenging technique, it is possible that they have invested more in neurons that matched the typical DANs properties (Ungless & Grace 2012). Also, most of their analyses rely on short movement initiations (<1 s), described as mice adjusting their position on the running wheel. On the other hand, just like we reported, the decrease in firing rate happened at or after movement onset, even though they used EMG to detect when movement was initiated. These authors did not use acute manipulations of these neurons to test whether the firing rate changes in different anatomical subtypes of midbrain DANs had a causal role in movement initiation. It is important to note that

even in the classical recordings by Schultz and Romo (Schultz et al. 1983) heterogeneity in the modulation of the SNc neurons was already reported. However both positive modulation and negative modulation happened mostly at or after EMG determined onset of movement.

In recent years there were other studies with recordings of putative midbrain DANs showing movement initiation or acceleration related activity (Jin & Costa 2010; Puryear et al. 2010; Wang & Tsien 2011; Barter et al. 2015). The first of these papers was developed in our laboratory and the work developed in this thesis was in fact a follow-up of this discovery. Jin and Costa (Jin & Costa 2010) showed that approximately half of the putative SNc DANs they recorded were transiently active before the initiation and at the termination of an action sequence. However, at the time they were not able to test whether this transient increase in firing rate had a causal role in action initiation. Also, it was unclear whether this increase in activity was only task related or part of a more general mechanism related to movement initiation. We will discuss this work more extensively later while discussing our FR8 findings. Similarly, others have found that putative DANs in the VTA are transiently active at the initiation and termination of mice voluntary run bouts (Wang & Tsien 2011). We have built on these findings by showing that genetically identified SNc DANs are modulated by both spontaneous non-rewarded and task related rewarded movements. This will be further discussed below. Also we uncovered that this modulation is heterogeneous in spontaneous movements with some neurons presenting with transient increases in firing rate that preceded spontaneous movement initiation, defying both the idea that this population of neurons is homogeneous and only affects movement in a slow time scale. Moreover, as we will also discuss below, we have built on these findings by manipulating the activity of these neurons using optogenetics, thus probing whether DANs have a causal role in movement initiation.

DAN activity before initiation is related to the vigor of future movements

As we mentioned in the introduction, previous works have pointed to a role of SNc DANs in the regulation of movement vigor (Mazzoni et al. 2007; Panigrahi et al. 2015). Here we have found that the pre-movement activity of 38% of the neurons positively modulated by movement initiation correlated with the vigor of the movement about to be initiated. A correlation between putative DANs and kinematics of head movements

(acceleration and velocity) was also reported by Barter *et al* (Barter et al. 2015). Nevertheless there are several differences between their report and our findings. For example, the analysis of movement was restricted to the head of the mouse (the mouse was standing on a platform with restriction of the movements they could perform). Also, all movement was captured in the context of a task were rewards or punishments were delivered. Moreover, they did not analyze separately activity related to movement initiation. Also these authors relied on identification of DANs based on electrophysiology properties and not genetica identification of DANs raising doubts regarding the specificity of the recordings. It was shown recently that progressive loss of SNc DANs leads to a progressive reduction of the vigor of movements and a change in their neural representation in the striatum (Panigrahi et al. 2015). However, this interesting finding did not clarify how DANs contributed to the regulation of movement vigor. For example, although the vigor of movement is lower in patients with PD (Mazzoni et al. 2007) and in this mouse model with progressive depletion of DANs, it remains unclear whether this effect is due to the low levels of dopamine before the movement is selected, during the performance of the movement or both. Our electrophysiology results suggested that transient activity of some SNc DANs before movement is initiated could be modulating movement vigor. However this was a correlative observation and not evidence of causality. Our optogenetic manipulation experiments revealed that in fact the activity of SNc DANs regulates not only the probability of movement initiation but also the vigor of future movements.

Optogenetic manipulation of SNc DAN activity modulates movement initiation and movement vigor in a state dependent manner

When we inhibited SNc DANs, movements were not only less likely to be initiated but were also less vigorous when initiated. Conversely, brief activation of SNc DANs increased the probability of movements being initiated and initiated movements were more vigorous. This result combined with our electrophysiology findings argue against the current view that movement is modulated solely through tonic firing of SNc DANs. During the development of this thesis other groups reported similar findings: Transient activation of SNc DANs was shown to increase the speed of head movements in mice standing on a high platform (Barter et al. 2015). Others showed that transient activation of DAN terminals in the dorsal striatum was sufficient to promote movement initiation (Howe & Dombeck 2016). However, these results did not clarify whether the modulation of movement by DANs was specific or not for movement initiation.

Moreover, results regarding the effect of inhibition of SNc DANs in movement were not reported in these studies[3]. One study did report a decrease in movement in the open field when VTA neurons were optogenetically inhibited (Tan et al. 2012), while another study failed to find this effect (Tye et al. 2012).

With the closed-loop stimulation design we tested the effect of brief stimulation of SNc DANs in a more controlled way. For example, the state of acceleration before movement initiation was more consistent from trial to trial and between groups. It also enabled us to show that there was not a reinforcing effect because the intertrial interval was not shorter for the ChR2 mice. In other words, ChR2 mice were not stopping more often in sessions were stimulation happened during immobility. In fact there was a tendency for ChR2 mice to have longer intertrial intervals than control mice.

Our optogenetic manipulations allowed us to go further and dissect the importance of the activity of these neurons at different movement states. Taken together our data shows that the modulation of movement vigor by SNc DANs is state dependent, i.e. changing the activity of DANs affects the probability and vigor of future movements but it does not affect ongoing movements. This result could seem incongruent with the observation that some photoidentified DANs maintained increased activity after movement initiation. However, these results are compatible with a peculiar finding recently published. Howe *et al* (Howe & Dombeck 2016), while imaging the terminals of DANs in the striatum of head fixed mice, found that spontaneous movement initiation was preceded by transient activity of DANs. Curiously, peaks of acceleration during ongoing locomotion were followed by transient activity of the same terminals instead of being preceded. In light of this finding, it does make sense that DAN manipulation has a different effect depending if it happens before movement is started or during movement. However it still remains unclear what could be the role of these transients of DAN terminals following peaks of acceleration. It could be that they have a sensorimotor integration function or that they might be relevant for other features of movement besides acceleration (e.g. posture, muscle tone etc.), features that would not be well characterized by the inertial sensors we used.

The fact that inhibiting SNc DANs did not promote movement initiation is in agreement with the observation that negatively modulated neurons decrease their activity mostly at the moment of initiation or after. Thus the significance of this modulation is still unclear.

[3] Howe *et al* did try to inhibit DAN terminals and SNc DANs using hallorhodopsin but failed to produce a significant result which the authors attributed to technical difficulties.

It could be tempting to propose that some SNc DANs could increase their activity to promote certain types of movement initiation while others at the same time would decrease their activity to avoid the interference of other movements. However, we found that positively modulated neurons were increasing their activity for different types of initiation. To put it another way, movement initiations preceded by increased dopamine activity were not more similar to each other. Also, it has been shown that SNc DANs projecting to the striatum have widely spread axonal arborizations (Matsuda et al. 2009). These two observations argue against a role of SNc DANs to act as selectors or inhibitors of specific movements. On the other hand, the functional heterogeneity we found is also not compatible with a simple bulk signaling of SNc DANs.

Although optogenetics is a powerful technique to probe causality it is not without caveats. In the case of our experiments we could not activate or inhibit the functional subtypes of DANs found. Furthermore, when we are activating optogenetically neurons we are producing an artificial pattern, probably coupling the firing of neurons that would not fire concomitantly. In the case of inhibition experiments one could also argue that they impose an artificial pattern because SNc DANs generally have spontaneous baseline activity while the inhibition would silence at least some of the neurons completely. However, even with the limitations we just described, the methodology we used corresponds to the state of the art for causal manipulations for neurons in deep nucleus. Future work should focus on understanding whether the functional subtypes of neurons we described can be segregated (e.g. receive different projections, project to different structures or have different genetic identities). This could provide a way of manipulating specific subtypes of neurons and clarify further what is the role of each of the subtypes described here.

SNc DANs become preferentially active before the initiation of action sequences

The results in the open field highlight a specific role for transient dopamine activity in gating self-paced movement initiation but not in modulating ongoing movements. Although obtained in a different context, these results are in accordance with previous work in the lab where it was shown that SNc DANs through training become transiently

active at the start of an action sequence (Jin & Costa 2010). Nevertheless, the causal role of this transient activity preceding sequence initiation was still unclear.

In this thesis we replicated their results using calcium imaging instead of external recordings with the advantage of being able to record several genetically identified DANs at the same time, while tracking neurons throughout training.

Similarly to previous findings (Jin & Costa 2010), we found that the proportion of modulated neurons was different between press events with the highest proportion of neurons being modulated by the first press (**Fig. 5.3**). This higher proportion of neurons related to first press was not apparent early in training, and seemed to develop with sequence learning (Fig. 5.4, Jin & Costa 2010).

With our optogenetic approach we were able to go further and demonstrate a specific role for SNc dopamine activity for self-paced initiation of a learned action sequence. Similarly to what we saw in the open field, we were able to perturb the initiation of the action sequence when inhibition was started before the first press but failed to change the execution of the sequence when inhibition was started after the first press. However, we did not test whether a brief activation was sufficient to promote movement initiation or decrease the latency to initiate in the context of this task. Also, in this task there was not time limit for mice to perform the eight lever presses. Thus mice could solve the task with different levels of vigor. So we could not test whether the lack of an effect in the performance of the sequence was dependent or not on the vigor of the sequence. An experiment where mice would be required to perform at a lower vigor on a lever and at higher vigor on the other could answer this question. We did not show an analysis of sequence performance for sequences that were preceded by SNc DAN inhibition. We did try to analyse these sequences and compare them with sequences not preceded by inhibition. However we had a low sampling problem because of the increased number of sequence initiations aborted (**Fig. 5.5**) and the small number of presses performed within the inhibition period and thus decided not to include it in this thesis.

Bridging motor activation properties of SNc DANs and their role in reward-based learning has remained a challenge. It was recently reported that acceleration modulated terminals mainly originated from SNc neurons and that reward responsive terminals mainly originated from VTA neurons (Howe & Dombeck 2016). However we found a similar percentage of neurons in the SNc modulated by initiation or reward,

with less than one third of action initiation neurons also being modulated by reward. This discrepancy might be due to methodological differences (e.g. head fixed vs freely moving different behavioural tasks), to mechanisms of local control of dopamine release at terminals or even anatomical segregation of the projections arising from these different neuron types. In support of this, it was found recently that while midbrain neurons (VTA and medial SNc) that project to the nucleus accumbens respond preferentially to reward and reward related cues while the ones that project to the dorsomedial striatum respond more strongly before a contralateral lever press.

This work together with our findings argues for the existence of functional subpopulations of SNc neurons (reward responding and initiation modulators). This distinction might be driven by differential inputs into these SNc neurons. Supporting this, it was recently shown that manipulation of PPN cholinergic inputs into the ventral SNc affects locomotion but does not condition mice in a conditioned place preference paradigm (Xiao et al. 2016). Future experiments should aim to clarify whether such functional subpopulations can be identify based on anatomical or genetic characteristics. This could allow for a selective manipulation of these sub-populations and a better understanding of the circuits underlying movement initiation and reward based learning.

Conclusions

We found that a large proportion of SNc DANs, non-overlapping with reward-responsive DANs, increased their activity before self-paced movement initiation. This movement-related DAN activity is not action-specific, and is related to the vigor of the movements to be initiated. Consistently, inhibition of DANs when animals were immobile impaired the probability of movement initiation, and the vigor of future movements. Conversely, brief activation of DANs when animals were immobile increased the probability of movement and the vigor of future movements. Dopamine activity manipulations after movement initiation did not affect ongoing movements. Similar findings were observed for the initiation and execution of learned action sequences.

These data suggest that the gating of self-paced initiation happens by permissive effects of dopamine on downstream striatal circuits that would receive information about which plans to execute from other inputs. This argues for a model in which dopamine modulates the excitability of striatal medium spiny neurons, which are also

critical for self-paced action initiation (Kravitz et al. 2010; Tecuapetla et al. 2016), by gating action-specific glutamatergic inputs from motor and pre-motor cortices and thalamus. Furthermore, although our results show that transient changes in the activity of SNc DANs are relevant for gating and invigorating self-paced movement, we do not claim that this gating occurs exclusively through transient changes in DAN activity. There is extensive literature showing modulation of self-paced movement initiation by sustained changes in the levels of striatal dopamine (Costa et al. 2006; Hnasko et al. 2006; Panigrahi et al. 2015). We hypothesize that transient changes can function as a fast system working on top of tonic release to adjust the concentration of striatal dopamine thus increasing the probability (and vigor) of initiation of movements planned at that exact time. More sustained changes in DAN activity could represent states in which the "gate" would be more permissive, increase the probability of action initiation during longer periods of time, therefore promoting movement (Spielewoy et al. 2000). This would translate into the exploration of different actions that in other states would be less probable, thus generating not only more movements but also a more variable motor repertoire leading to the exploration of new actions.

Our results also showed that SNc DANs can be reward responsive but also movement initiation related, and that these neurons are largely non-overlapping, which suggests the existence of sub-populations of SNc DANs putatively regulated by different inputs.

Dopamine depletion in PD is chronic. Studies of the role of dopamine in movement in chronic models of depletion are very valuable, but have limited our understanding of the dynamic role of SNc DAN activity in downstream circuits. Not surprisingly, current treatments are focused mainly on increasing dopaminergic effects in a sustained way, with potential undesired effects. Our work, by highlighting the relevance of transient activity of these neurons before self-paced movement initiation suggests that it could be beneficial to pursue treatments aimed at providing transient modulations of basal ganglia circuitry when patients initiate movements, e.g. via closed-loop deep brain stimulation (Rosin et al. 2011) triggered by activity in cortical areas related to motor planning.

REFERENCES

Albin, R.L., Young, A.B. & Penney, J.B., 1989. The functional anatomy of basal ganglia disorders. *Trends in Neurosciences*, 12(10), pp.366–375.

Atasoy, D. et al., 2008. A FLEX switch targets Channelrhodopsin-2 to multiple cell types for imaging and long-range circuit mapping. *J Neurosci*, 28(28), pp.7025–7030.

Barter, J.W. et al., 2015. Beyond reward prediction errors: the role of dopamine in movement kinematics. *Front Integr Neurosci*, 9, p.39.

Bates, D. et al., 2015. Fitting linear mixed-effects models using lme4. *Journal of Statistical Software*, 67(1), pp.1–48. Available at: http://cran.r-project.org/package=lme4%5Cnhttp://www.jstatsoft.org/index.php/jss/article/view/v067i01/v67i01.pdf.

Berardelli, A. et al., 2001. Pathophysiology of bradykinesia in Parkinson's disease. *Brain*, 124(Pt 11), pp.2131–2146.

Birkmayer, W. & Hornykiewicz, O., 1961. [The L-3,4-dioxyphenylalanine (DOPA)-effect in Parkinson-akinesia]. *Wien Klin Wochenschr*, 73, pp.787–788.

Björklund, A. & Dunnett, S.B., 2007. Dopamine neuron systems in the brain: an update. *Trends in neurosciences*, 30(5), pp.194–202.

Bromberg-Martin, E.S., Matsumoto, M. & Hikosaka, O., 2010. Dopamine in motivational control: rewarding, aversive, and alerting. *Neuron*, 68(5), pp.815–834.

Brown, M.T.C. et al., 2009. Activity of neurochemically heterogeneous dopaminergic neurons in the substantia nigra during spontaneous and driven changes in brain state. *Journal of Neuroscience*, 29(9), pp.2915–2925.

Bunney, B.S. et al., 1973. Dopaminergic neurons: effect of antipsychotic drugs and amphetamine on single cell activity. *The Journal of pharmacology and experimental therapeutics*, 185(3), pp.560–71. Available at: http://www.ncbi.nlm.nih.gov/pubmed/4576427 [Accessed February 7, 2016].

Bunney, B.S. et al., 1973. Dopaminergic neurons: effect of antipsychotic drugs on single cell activity. *J. Pharmacol. Exp. Ther.*, 185(3), pp.560–571. Available at: http://jpet.aspetjournals.org/content/185/3/560.short.

Carlsson, A. et al., 1958. On the presence of 3-hydroxytyramine in brain. *Science*, 127(3296), p.471.

Chen, T.-W. et al., 2013. Ultrasensitive fluorescent proteins for imaging neuronal activity. *Nature*, 499(7458), pp.295–300.

Chuong, A.S. et al., 2014. Noninvasive optical inhibition with a red-shifted microbial rhodopsin. *Nature Neuroscience*, 17(8), pp.1123–1129. Available at: http://www.ncbi.nlm.nih.gov/pubmed/24997763 [Accessed April 7, 2017].

Cohen, J.Y. et al., 2012. Neuron-type-specific signals for reward and punishment in the ventral tegmental area. *Nature*, 482(7383), pp.85–88.

Costa, R.M. et al., 2006. Rapid Alterations in Corticostriatal Ensemble Coordination during Acute Dopamine-Dependent Motor Dysfunction. *Neuron*, 52(2), pp.359–369.

Cui, G. et al., 2013. Concurrent activation of striatal direct and indirect pathways during action initiation. *Nature*, 494(7436), pp.238–242.

Dodson, P.D. et al., 2016. Representation of spontaneous movement by dopaminergic neurons is cell-type selective and disrupted in parkinsonism. *Proceedings of the National Academy of Sciences*, 113(15), p.201515941. Available at: http://www.pnas.org/content/113/15/E2180.abstract.

Ehringer, H. & Hornykiewicz, O., 1960. [Distribution of noradrenaline and dopamine (3-hydroxytyramine) in the human brain and their behavior in diseases of the extrapyramidal system]. *Klin Wochenschr*, 38, pp.1236–1239.

Foix, C. & Nicolesco, J., 1925. *Les noyaux gris centraux et la r{é}gion m{é}senc{é}phalo-sous-optique: suivi d'un appendice sur l'anatomie pathologique de la maladie de Parkinson*, Massons.

Frey, B.J. & Dueck, D., 2007a. Clustering by Passing Messages Between Data Points. *Science*, 315(5814).

Frey, B.J. & Dueck, D., 2007b. Clustering by Passing Messages Between Data Points. *Science*, 315(5814), pp.972–976. Available at: http://www.sciencemag.org/cgi/doi/10.1126/science.1136800.

Friedrich, J., Zhou, P. & Paninski, L., 2016. Fast Active Set Methods for Online Deconvolution of Calcium Imaging Data. *arXiv*, (Nips), pp.1–13. Available at: http://arxiv.org/abs/1609.00639.

Gerfen, C.R. et al., 1990. D1 and D2 dopamine receptor-regulated gene expression of striatonigral and striatopallidal neurons. *Science*, 250(4986), pp.1429–1432.

Gerfen, C.R. & Surmeier, D.J., 2011. Modulation of striatal projection systems by dopamine. *Annu Rev Neurosci*, 34, pp.441–466.

German, D.C. et al., 1989. Midbrain dopaminergic cell loss in Parkinson's disease: computer visualization. *Annals of neurology*, 26(4), pp.507–14. Available at: http://www.ncbi.nlm.nih.gov/pubmed/2817827.

Ghosh, K.K. et al., 2011. Miniaturized integration of a fluorescence microscope. *Nat Methods*, 8(10), pp.871–878.

Gleiss, A.C., Wilson, R.P. & Shepard, E.L.C., 2011. Making overall dynamic body acceleration work: on the theory of acceleration as a proxy for energy expenditure. *Methods in Ecology and Evolution*, 2(1), pp.23–33. Available at: http://doi.wiley.com/10.1111/j.2041-210X.2010.00057.x.

Gong, S. et al., 2003. A gene expression atlas of the central nervous system based on bacterial artificial chromosomes. *Nature*, 425(6961), pp.917–25. Available at: http://www.ncbi.nlm.nih.gov/pubmed/14586460.

Gong, S. et al., 2007. Targeting Cre recombinase to specific neuron populations with bacterial artificial chromosome constructs. *J Neurosci*, 27(37), pp.9817–9823.

Grace, A.A. & Bunney, B.S., 1983. Intracellular and extracellular electrophysiology of nigral dopaminergic neurons-1. Identification and characterization. *Neuroscience*, 10(2).

Guyenet, P.G. & Aghajanian, G.K., 1978. Antidromic identification of dopaminergic and other output neurons of the rat substantia nigra. *Brain Research*, 150(1), pp.69–84.

Han, X. et al., 2011. A high-light sensitivity optical neural silencer: development and application to optogenetic control of non-human primate cortex. *Frontiers in systems neuroscience*, 5, p.18. Available at: http://www.pubmedcentral.nih.gov/articlerender.fcgi?artid=3082132&tool=pmcentrez&rendertype=abstract [Accessed April 16, 2016].

Hassler, R., 1938. Zur Pathologie der Paralysis agitans und des postenzephalitischen Parkinsonismus. *J Psychol Neurol*, 48, pp.387–476.

Hnasko, T.S. et al., 2006. Cre recombinase-mediated restoration of nigrostriatal dopamine in dopamine-deficient mice reverses hypophagia and bradykinesia. *Proceedings of the National Academy of Sciences of the United States of America*, 103(23), pp.8858–8863.

Hornykiewicz, O., 1963. [The tropical localization and content of noradrenalin and dopamine (3-hydroxytyramine) in the substantia nigra of normal persons and patients with Parkinson's disease]. *Wien Klin Wochenschr*, 75, pp.309–312.

Hornykiewicz, O., 2006. The discovery of dopamine deficiency in the parkinsonian brain. *J Neural Transm Suppl*, (70), pp.9–15.

Howe, M.W. et al., 2013. Prolonged dopamine signalling in striatum signals proximity and value of distant rewards. *Nature*, 500(7464), pp.575–9. Available at: http://dx.doi.org/10.1038/nature12475%5Cnhttp://www.nature.com.ezp-prod1.hul.harvard.edu/nature/journal/v500/n7464/full/nature12475.html%5Cnhttp://www.pubmedcentral.nih.gov/articlerender.fcgi?artid=3927840&tool=pmcentrez&rendertype=abstract.

Howe, M.W. & Dombeck, D.A., 2016. Rapid signalling in distinct dopaminergic axons during locomotion and reward. *Nature*, 535(7613), pp.505–510. Available at: http://dx.doi.org/10.1038/nature18942 [Accessed December 26, 2016].

Jin, X. & Costa, R.M., 2010. Start/stop signals emerge in nigrostriatal circuits during sequence learning. *Nature*, 466(7305), pp.457–462.

Jin, X., Tecuapetla, F. & Costa, R.M., 2014. Basal ganglia subcircuits distinctively encode the parsing and concatenation of action sequences. *Nat Neurosci*, 17(3), pp.423–430.

Klaus, A, Martins, GM, Paixão VB, Zhou, P, Paninski, L, Costa, R., 2017. The spatiotemporal organization of the striatum encodes action space. *Neuron, In Press*.

Kravitz, A. V. et al., 2010. Regulation of parkinsonian motor behaviours by opt... [Nature. 2010] - PubMed result. *Nature*, 466(7306), pp.622–6. Available at: http://www.ncbi.nlm.nih.gov/pubmed/20613723.

Lammel, S. et al., 2015. Diversity of transgenic mouse models for selective targeting of

midbrain dopamine neurons. *Neuron*, 85(2), pp.429–438.

Lein, E.S. et al., 2007. Genome-wide atlas of gene expression in the adult mouse brain. *Nature*, 445(7124), pp.168–176.

Lima, S.Q. et al., 2009. PINP: a new method of tagging neuronal populations for identification during in vivo electrophysiological recording. *PLoS One*, 4(7), p.e6099.

Van Der Maaten, L., Hinton, G. & van der Maaten, G.H., 2008. *Visualizing Data using t-SNE*,

Madisen, L. et al., 2012. A toolbox of Cre-dependent optogenetic transgenic mice for light-induced activation and silencing. *Nat Neurosci*, 15(5), pp.793–802.

Mahon, S. et al., 2006. Distinct patterns of striatal medium spiny neuron activity during the natural sleep-wake cycle. *The Journal of neuroscience : the official journal of the Society for Neuroscience*, 26(48), pp.12587–12595.

Mathie, M.J. et al., 2002. Determining activity using a triaxial accelerometer. In *Proc. 2nd Joint EMBS-BMES Conf*. pp. 2481–2482.

Matsuda, W. et al., 2009. Single nigrostriatal dopaminergic neurons form widely spread and highly dense axonal arborizations in the neostriatum. *J Neurosci*, 29(2), pp.444–453.

Matsumoto, M. & Hikosaka, O., 2009. Two types of dopamine neuron distinctly convey positive and negative motivational signals. *Nature*, 459(7248), pp.837–41. Available at: http://www.pubmedcentral.nih.gov/articlerender.fcgi?artid=2739096&tool=pmcentrez&rendertype=abstract.

Mazzoni, P., Hristova, A. & Krakauer, J.W., 2007. Why don't we move faster? Parkinson's disease, movement vigor, and implicit motivation. *J Neurosci*, 27(27), pp.7105–7116.

Muzerengi, S. & Clarke, C.E., 2015. Initial drug treatment in Parkinson's disease. *BMJ*, 351, p.h4669.

Niv, Y., Daw, N.D. & Dayan, P., 2005. How fast to work: Response vigor, motivation and tonic dopamine. *Advances in Neural Information Processing Systems 18 (NIPS 2005)*, pp.1019–1026. Available at: http://papers.nips.cc/paper/2842-how-fast-to-work-response-vigor-motivation-and-tonic-dopamine.pdf.

Nomoto, K. et al., 2010. Temporally extended dopamine responses to perceptually demanding reward-predictive stimuli. *J Neurosci*, 30(32), pp.10692–10702. Available at: http://www.ncbi.nlm.nih.gov/pubmed/20702700%5Cnhttp://www.jneurosci.org/content/30/32/10692.full.pdf.

Palmiter, R.D., 2008. Dopamine signaling in the dorsal striatum is essential for motivated behaviors: Lessons from dopamine-deficient mice. In *Annals of the New York Academy of Sciences*. pp. 35–46.

Panigrahi, B. et al., 2015. Dopamine Is Required for the Neural Representation and Control of Movement Vigor. *Cell*, 162(6), pp.1418–1430.

Parker, N.F. et al., 2016. Reward and choice encoding in terminals of midbrain dopamine neurons depends on striatal target. *Nature Neuroscience*, 19(6), pp.845–854. Available at: http://www.nature.com/doifinder/10.1038/nn.4287%5Cnhttp://www.ncbi.nlm.nih.gov/pubmed/27110917%5Cnhttp://www.nature.com/doifinder/10.1038/nn.4287.

Pnevmatikakis, E.A. et al., 2016. Simultaneous Denoising, Deconvolution, and Demixing of Calcium Imaging Data. *Neuron*, 89(2), p.299.

Puryear, C.B., Kim, M.J. & Mizumori, S.J.Y., 2010. Conjunctive encoding of movement and reward by ventral tegmental area neurons in the freely navigating rodent. *Behav Neurosci*, 124(2), pp.234–247.

Rescorla, R. a & Wagner, a R., 1972. A theory of Pavlovian conditioning: Variations in the effectiveness of reinforcement and nonreinforcement. *Classical Conditioning II Current Research and Theory*, 21(6), pp.64–99. Available at: http://homepage.mac.com/sanagnos/rescorlawagner1972.pdf.

Romo, R. & Schultz, W., 1990. Dopamine neurons of the monkey midbrain: contingencies of responses to active touch during self-initiated arm movements. *Journal of neurophysiology*, 63(3), pp.592–606. Available at: http://www.ncbi.nlm.nih.gov/pubmed/2329363.

Rosin, B. et al., 2011. Closed-loop deep brain stimulation is superior in ameliorating parkinsonism. *Neuron*, 72(2), pp.370–384.

Salamone, J.D. et al., 1991. Haloperidol and nucleus accumbens dopamine depletion suppress lever pressing for food but increase free food consumption in a novel food choice procedure. *Psychopharmacology*, 104(4), pp.515–21. Available at: http://www.ncbi.nlm.nih.gov/pubmed/1780422 [Accessed April 8, 2017].

Salamone, J.D. & Correa, M., 2012. The Mysterious Motivational Functions of Mesolimbic Dopamine. *Neuron*, 76(3), pp.470–485.

Schultz, W., 1997. A neural substrate of prediction and reward. *Science*, 275, pp.1593–1599.

Schultz, W., 2010. Dopamine signals for reward value and risk: basic and recent data. *Behavioral and brain functions : BBF*, 6, p.24.

Schultz, W., 2007. Multiple dopamine functions at different time courses. *Annu Rev Neurosci*, 30, pp.259–288.

Schultz, W., 1998. Predictive reward signal of dopamine neurons. *Journal of neurophysiology*, 80(1), pp.1–27.

Schultz, W., 1986. Responses of midbrain dopamine neurons to behavioral trigger stimuli in the monkey. *Journal of Neurophysiology*, 56(5), pp.1439–1461.

Schultz, W., Dayan, P. & Montague, P.R., 1997. A neural substrate of prediction and reward. *Science*, 275, pp.1593–1599.

Schultz, W. & Romo, R., 1990. Dopamine neurons of the monkey midbrain: contingencies of responses to stimuli eliciting immediate behavioral reactions. *Journal of Neurophysiology*, 63(3), pp.607–624. Available at: http://www.ncbi.nlm.nih.gov/entrez/query.fcgi?cmd=Retrieve&db=PubMed&dopt=

Citation&list_uids=2329364.

Schultz, W., Ruffieux, A. & Aebischer, P., 1983. The activity of pars compacta neurons of the monkey substantia nigra in relation to motor activation. *Experimental Brain Research*, 51(3), pp.377–387.

Sparta, D.R. et al., 2012. Construction of implantable optical fibers for long-term optogenetic manipulation of neural circuits. *Nature protocols*, 7(1), pp.12–23. Available at: http://dx.doi.org/10.1038/nprot.2011.413.

Spielewoy, C. et al., 2000. Behavioural disturbances associated with hyperdopaminergia in dopamine-transporter knockout mice. *Behavioural pharmacology*, 11(3–4), pp.279–290.

Steinfels, G.F., Heym, J. & Jacobs, B.L., 1981. Single unit activity of dopaminergic neurons in freely moving cats. *Life Sciences*, 29(14), pp.1435–1442. Available at: http://www.sciencedirect.com/science/article/pii/0024320581900072 [Accessed February 21, 2016].

Surmeier, D.J. et al., 2007. D1 and D2 dopamine-receptor modulation of striatal glutamatergic signaling in striatal medium spiny neurons. *Trends in Neurosciences*, 30(5), pp.228–235.

Sutton, R.S. & Barto, A.G., 1981. Toward a modern theory of adaptive networks: expectation and prediction. *Psychological review*, 88(2), pp.135–70. Available at: http://www.ncbi.nlm.nih.gov/pubmed/7291377.

Syed, E.C.J. et al., 2015. Action initiation shapes mesolimbic dopamine encoding of future rewards. *Nature neuroscience*, (December), pp.1–6. Available at: http://www.nature.com/doifinder/10.1038/nn.4187%5Cnhttp://www.ncbi.nlm.nih.gov/pubmed/26642087.

Tan, K.R. et al., 2012. GABA Neurons of the VTA Drive Conditioned Place Aversion. *Neuron*, 73(6), pp.1173–1183.

Tecuapetla, F. et al., 2016. Complementary Contributions of Striatal Projection Pathways to Action Initiation and Execution. *Cell*, 166(3), pp.703–715.

Thévenaz, P., Ruttimann, U.E. & Unser, M., 1998. A pyramid approach to subpixel registration based on intensity. *IEEE Trans Image Process*, 7(1), pp.27–41.

Trulson, M.E., 1985. Simultaneous recording of substantia nigra neurons and voltammetric release of dopamine in the caudate of behaving cats. *Brain Research Bulletin*, 15(2), pp.221–223.

Trulson, M.E., Preussler, D.W. & Howell, G.A., 1981. Activity of substantia nigra units across the sleep-waking cycle in freely moving cats. *Neuroscience Letters*, 26(2), pp.183–188. Available at: http://www.sciencedirect.com/science/article/pii/0304394081903463 [Accessed February 22, 2016].

Tye, K.M. et al., 2012. Dopamine neurons modulate neural encoding and expression of depression-related behaviour. *Nature*, 493(7433), pp.537–541. Available at: http://www.nature.com/doifinder/10.1038/nature11740.

Ungless, M.A. & Grace, A.A., 2012. Are you or aren't you? Challenges associated with

physiologically identifying dopamine neurons. *Trends in Neurosciences*, 35(7), pp.422–430.

Ungless, M.A., Magill, P.J. & Bolam, J.P., 2004. Uniform inhibition of dopamine neurons in the ventral tegmental area by aversive stimuli. *Science (New York, N.Y.)*, 303(5666), pp.2040–2. Available at: http://www.ncbi.nlm.nih.gov/pubmed/15044807.

Wang, D. V. & Tsien, J.Z., 2011. Conjunctive processing of locomotor signals by the ventral tegmental area neuronal population. *PLoS ONE*, 6(1).

Wassum, K.M., Ostlund, S.B. & Maidment, N.T., 2012. Phasic Mesolimbic Dopamine Signaling Precedes and Predicts Performance of a Self-Initiated Action Sequence Task. *Biological Psychiatry*, 71(10), pp.846–854.

Wise, R.A., 2004. Dopamine, learning and motivation. *Nature reviews. Neuroscience*, 5(June), pp.483–494.

Xiao, C. et al., 2016. Cholinergic Mesopontine Signals Govern Locomotion and Reward through Dissociable Midbrain Pathways. *Neuron*, 90(2), pp.333–347.

Yohn, S.E. et al., 2016. Blockade of uptake for dopamine, but not norepinephrine or 5-HT, increases selection of high effort instrumental activity: Implications for treatment of effort-related motivational symptoms in psychopathology. *Neuropharmacology*, 109, pp.270–280. Available at: http://www.ncbi.nlm.nih.gov/pubmed/27329556 [Accessed April 8, 2017].

Zhou, P. et al., 2016. Efficient and accurate extraction of in vivo calcium signals from microendoscopic video data. Available at: http://arxiv.org/abs/1605.07266 [Accessed March 4, 2017].

Zweifel, L.S. et al., 2009. Disruption of NMDAR-dependent burst firing by dopamine neurons provides selective assessment of phasic dopamine-dependent behavior. *Proceedings of the National Academy of Sciences*, 106(18), pp.7281–7288. Available at: http://www.pnas.org/cgi/doi/10.1073/pnas.0813415106%5Cnhttp://www.pnas.org/content/106/18/7281.short%5Cnpapers2://publication/doi/10.1073/pnas.0813415106.